

Direction des bibliothèques

AVIS

Ce document a été numérisé par la Division de la gestion des documents et des archives de l'Université de Montréal.

L'auteur a autorisé l'Université de Montréal à reproduire et diffuser, en totalité ou en partie, par quelque moyen que ce soit et sur quelque support que ce soit, et exclusivement à des fins non lucratives d'enseignement et de recherche, des copies de ce mémoire ou de cette thèse.

L'auteur et les coauteurs le cas échéant conservent la propriété du droit d'auteur et des droits moraux qui protègent ce document. Ni la thèse ou le mémoire, ni des extraits substantiels de ce document, ne doivent être imprimés ou autrement reproduits sans l'autorisation de l'auteur.

Afin de se conformer à la Loi canadienne sur la protection des renseignements personnels, quelques formulaires secondaires, coordonnées ou signatures intégrées au texte ont pu être enlevés de ce document. Bien que cela ait pu affecter la pagination, il n'y a aucun contenu manquant.

NOTICE

This document was digitized by the Records Management & Archives Division of Université de Montréal.

The author of this thesis or dissertation has granted a nonexclusive license allowing Université de Montréal to reproduce and publish the document, in part or in whole, and in any format, solely for noncommercial educational and research purposes.

The author and co-authors if applicable retain copyright ownership and moral rights in this document. Neither the whole thesis or dissertation, nor substantial extracts from it, may be printed or otherwise reproduced without the author's permission.

In compliance with the Canadian Privacy Act some supporting forms, contact information or signatures may have been removed from the document. While this may affect the document page count, it does not represent any loss of content from the document.

Université de Montréal

Polymeric Nanoparticles: From Microporosity and Drug Release Kinetics to Cellular Interactions

par
Shilpa Sant

Faculté de Pharmacie

Thèse présentée à la Faculté des études supérieures
en vue de l'obtention du grade de Philosophiae Doctor
en Sciences Pharmaceutiques
Option Technologie pharmaceutique

August, 2007



© Shilpa Sant, 2007

Université de Montréal
Faculté des études supérieures

Cette thèse intitulée:

Polymeric Nanoparticles: From Microporosity and Drug Release Kinetics to Cellular
Interactions

Présentée par:

Shilpa Sant

a été évaluée par un jury composé des personnes suivantes :

Prof. Fahima Nekka, Président-rapporteur

Prof. Patrice Hildgen, Directeur de recherche

Prof. Suzanne Giasson, Membre du jury

Prof. Abdelwahab Omri, Examineur externe

Prof. Fahima Nekka, représentant du doyen de la FES



Résumé

Les polymères biodégradables façonnés sous forme de nanoparticules (NPs) ont été très étudiés pour leur capacité à libérer une grande variété de médicaments, protéines et peptides de façon contrôlée sur des périodes de plusieurs semaines à plusieurs mois. Plusieurs facteurs, tels que les propriétés physico-chimiques des médicaments et des polymères ainsi que la structure interne de la matrice polymérique de la particule, influencent la libération du médicament.

La taille nanométrique des NPs limite l'étude de leur structure microporeuse. Ainsi l'importance des micropores n'a pas été prise en considération par le passé du fait qu'aucune méthode de mesure n'était disponible. Cependant les pores de tailles nanométriques augmentent de façon significative le ratio surface interne / volume, qui a son tour affecte l'hydratation des polymères, la perméabilité et conséquemment la dégradation du polymère qui à l'origine insoluble dans l'eau, est transformé en fragments solubles. Il est donc d'une grande importance de mieux comprendre la structure interne microporeuse afin de mieux prédire la libération des médicaments des NPs.

Les techniques d'imagerie n'atteignent pas le niveau de résolution requis pour l'analyse de la microporosité. Cependant il existe une méthode par l'adsorption d'azote sur matériau poreux qui permet l'analyse quantitative de l'aire de surface spécifique, la microporosité et la distribution de taille des pores à l'échelle nanométrique (micro et mésopores).

La première partie de cette thèse consiste en l'application de la technique d'adsorption de gaz à l'étude de la microporosité des NPs polymériques. Les études ont été entreprises afin d'évaluer les effets des facteurs de formulation comme la charge en médicament sur la microporosité de NPs fabriquées à partir du même polymère, le poly(ethylene glycol)_{1%}-*graft*-poly(D,L lactide) ou (PEG_{1%}-*g*-PLA). Il a été trouvé que bien que la quantité de triéthylamine et la charge initiale en médicament augmentent tous les deux la quantité totale de médicament encapsulé, seul la charge initiale en médicament initiale affecte la microporosité des NPs. De façon surprenante ces différences de microporosité bien que marginales peuvent expliquer adéquatement les différences observées dans les cinétiques de libération de la propafenone chlorhydrate (Prop). Il a été

établi qu'une plus grande microporosité entrave les déplacements du médicament dans les pores, diminuant son coefficient de diffusion effectif et ralentissant sa libération.

À partir de ces résultats nous avons été amenés à penser que les changements dans la structure moléculaire devraient conduire à des organisations différentes des chaînes de polymère durant la formation des NPs et donc créer des différences dans leur microporosité dépendant des espaces entre chaînes et volume libre caractéristiques du type de polymère. Pour tester cette hypothèse, des polymères peggylés avec des structures moléculaires différentes ont été utilisés afin de préparer des NPs. Les études d'adsorption de gaz révèlent des différences dans les isothermes d'adsorption de l'azote, la microporosité et l'aire de surface BET. Ces résultats, ainsi que les analyses de surface par XPS et les propriétés thermiques des NPs montrent que les chaînes de polymères se réorganisent de façon distincte et reproductible dans les NPs en fonction de l'architecture moléculaire du polymère. Cette structure microporeuse interne des NPs détermine au final leurs propriétés de libération de médicament, alors que nous avons confirmé qu'une plus grande microporosité ralentissait la libération.

Dans la deuxième partie de ce travail, nous avons entrepris une évaluation détaillée des propriétés de surface des NPs préparées à partir de polymères ayant des architectures différentes. Ces études démontrent que la structure moléculaire du polymère non seulement change la morphologie interne des NPs mais également altère significativement leurs propriétés de surface. En particulier, l'effet des différences chimiques de surface de ces NPs a été étudié en fonction de leur capacité à prévenir l'adsorption de protéines. Également nous avons montré que les taux d'internalisation des NPs sur une lignée de macrophage sont corrélés avec leurs propriétés de surface. Néanmoins toutes les NPs testées montrent une internalisation principalement par le biais d'un processus d'endocytose dépendant de la clathrine.

En bref, ce travail démontre que les NPs polymériques ont une structure interne bien précise et reproductible déterminée par les propriétés des polymères la composant. La structure moléculaire des polymères affecte non seulement l'intérieur de la matrice mais également la morphologie de surface des NPs, qui conséquemment décide de leur performance globale tant au niveau de la libération de médicament que de leurs propriétés biologiques.

Mots clés: Nanoparticules polymériques, adsorption de gaz, structure microporeuse, adsorption de protéines, internalisation intracellulaire,

Abstract

Biodegradable polymers have been investigated extensively for their ability of releasing a wide variety of drug molecules, proteins and peptides in a controlled way over a period of several weeks or months. Factors affecting the drug release rate include physicochemical properties of both, polymer & drug, formulation factors and the internal structure of matrix. However, the nanometric size of nanoparticles (NPs) limits investigation of their internal microporous structure. Nevertheless, nitrogen adsorption provides a means for quantitative analysis of specific surface area, microporosity and pore size distribution in the nanometer range (micropores and mesopores), where imaging techniques have yet to achieve sufficient resolution in this range. The importance of micropores in release kinetics has not been considered in the past due to the absence of adequate measurement methods. However, small pores in the nanometer size range increase the internal surface-to-volume ratio significantly, which affects polymer hydration, permeability and consequently, degradation of the originally water-insoluble polymer into water-soluble fragments. Hence, it is of great importance to gain a better understanding of the internal microporous structure which may permit a more precise prediction of drug release from NPs.

Objective of the present work was to bridge the existing knowledge gap between microporosity of NPs and their drug release kinetics using nitrogen gas adsorption. The first part of the thesis consists of the application of gas adsorption technique to probe the microporosity of polymeric NPs. Studies were undertaken to evaluate the effect of formulation factors like drug loading levels on the microporosity of NPs fabricated from poly(ethylene glycol)_{1%}-*graft*-poly(D,L lactide) (PEG_{1%}-*g*-PLA). It was found that both, the amount of triethylamine and initial drug loading level increased the total encapsulated drug in the polymeric matrix. However, only initial drug loading levels affected the microporosity of the NPs. Surprisingly, these differences in microporosity, although marginal, could adequately explain the differences in the release kinetics of propafenone hydrochloride (Prop). It was established that higher microporosity can hinder the drug movement through such small pores, decreasing its effective diffusion coefficient and consequently, the drug release rate.

From these results, it was concluded that changes in the molecular structure of the polymer would lead to different chain organization during NP formation. This would create greater differences in their microporosity depending on interchain spacing and free volume, characteristic of polymer type etc. Hence, pegylated polymers of different molecular structure were used for preparation of NPs. Gas adsorption studies revealed differences in their nitrogen adsorption isotherms, microporosity and BET surface areas. These results along with XPS surface analysis and thermal properties of NPs pointed out that polymer chains reorganized distinctively inside the NPs depending on molecular structure of the polymer. This internal microporous structure of the NPs determined their drug release properties. Once again, it was confirmed that higher microporosity slows down the release.

The second part of this thesis undertook detailed evaluation of surface properties of NPs fabricated from different polymer architectures. These studies demonstrated that molecular structure of polymer did not only change the bulk morphology of NPs, but significantly altered their surface properties. Further, effect of different surface chemistry of NPs on their ability to prevent protein adsorption was studied. Also, these NPs showed different cellular uptake in macrophage cell line, which was correlated to their surface properties. All these NPs showed clathrin-dependent endocytosis as the main mechanism of their cellular uptake.

In a nutshell, this thesis demonstrates that polymeric NPs have definite and reproducible internal structure determined by the properties of individual polymer. Molecular structure of polymer affects bulk as well as surface morphology of NPs, which consequently determines their overall performance in terms of drug release and biological properties.

Keywords: Polymeric nanoparticles, Gas adsorption, Microporosity, Protein adsorption, Intracellular uptake

Table of contents

Résumé.....	i
Abstract.....	iv
Table of contents.....	vi
List of tables.....	xi
List of figures.....	xii
List of abbreviations.....	xvi
List of equations.....	xviii
Acknowledgements.....	xxii
Chapter 1. Review of Literature.....	1
1.1 General overview.....	1
1.2 Characterization of NPs.....	3
1.2.1 Size and size distribution.....	4
1.2.2 Surface and bulk morphology.....	4
1.2.2.1 Physical Gas Adsorption: Basic Principles [62].....	5
1.2.2.2 Classification of adsorption isotherms [62-64].....	6
1.2.2.3 Adsorption in micropores.....	7
1.2.2.4 Specific surface area.....	9
1.2.2.5 Nitrogen as a standard adsorptive for surface area measurements [62].....	10
1.2.3 Physical state of drug within NPs.....	10
1.2.4 <i>In vitro</i> drug release kinetics.....	11
1.2.5 Surface charge.....	12
1.2.6 Surface chemistry.....	12
1.3 Optimization of surface chemistry of NPs: Essence for their long-circulating behavior and biological activity.....	13
1.3.1 Approaches used for prolonged circulation.....	14
1.3.2 Physicochemical properties of long-circulating carriers.....	14
1.3.2.1 Solubility and Hydrophilicity:.....	15
1.3.2.2 Molecular weight (M_w) and Polymer layer thickness:.....	15
1.3.2.3 Grafting density and conformation:.....	16
1.3.2.4 Charge and charge density:.....	17

1.3.2.5	Flexibility of the polymer chain:.....	18
1.3.2.6	Presence of side group on the protective polymer:	18
1.4	Biological consequences of long-circulating carriers	19
1.5	Nanoparticle Targeting.....	20
1.5.1	Passive Targeting	20
1.5.2	Active targeting.....	21
1.5.3	Intracellular transport mechanisms	22
1.6	References	23
CHAPTER 2. HYPOTHESES AND OBJECTIVES		
2.1	Hypotheses	34
2.1.1	Hypothesis 1.....	34
2.1.1.1	Justification for studying drug release kinetics.....	34
2.1.1.2	Gas adsorption and microstructure of NPs.....	35
2.1.2	Hypothesis 2.....	36
2.1.2.1	Justification of studying effect of polymer architecture on release kinetics.	36
2.1.3	Hypothesis 3.....	37
2.1.3.1	Justification for studying surface properties	37
2.2	Objectives.....	39
2.3	References	40
PRESENTATION OF MANUSCRIPTS.....		
CHAPTER 3. EFFECT OF POROSITY ON THE RELEASE KINETICS OF PROPAFENONE-LOADED PEG-G-PLA NANOPARTICLES		
3.1	Abstract	46
3.2	Introduction.....	47
3.3	Materials and Methods.....	49
3.3.1.	Materials.....	49
3.3.2.	Synthesis of polymer.....	49
3.3.3.	Preparation of Nanoparticles (NPs)	50
3.3.4.	Characterization of NPs	51
3.3.4.1.	Particle size distribution.....	51
3.3.4.2.	Morphology.....	51
3.3.4.3.	Encapsulation Efficiency (EE).....	51
3.3.4.4.	Determination of Residual PVA	52

3.3.4.5.	Differential Scanning Calorimetry (DSC)	52
3.3.4.6.	Porosity measurements.....	52
3.3.4.7.	In vitro release study	53
3.4	Results and Discussion.....	53
3.4.1.	Characterization of polymer.....	53
3.4.2.	Morphology and particle size measurements.....	54
3.4.3.	Encapsulation efficiency (EE)	55
3.4.4.	Residual PVA.....	56
3.4.5.	Thermal analysis	57
3.4.6.	Surface area, pore size distribution and fractal dimension	58
3.4.7.	<i>In vitro</i> Release	61
3.5	Conclusion	64
3.6	References	65
LINK BETWEEN FIRST AND SECOND ARTICLE		
	References:.....	69
CHAPTER 4. MICROPOROUS STRUCTURE AND DRUG RELEASE KINETICS OF POLYMERIC NANOPARTICLES		
4.1	Abstract	71
4.2	Introduction	72
4.3	Materials and methods	73
4.3.1.	Materials.....	73
4.3.2.	Synthesis of the polymers	73
4.3.3.	Preparation of Nanoparticles (NPs)	75
4.3.4.	Characterization of NPs	75
4.3.4.1	Particle size distribution.....	75
4.3.4.2	Encapsulation efficiency (EE).....	75
4.3.4.3	Differential scanning calorimetry (DSC)	76
4.3.4.4.	Porosity measurements	76
4.3.4.5.	XPS analysis	76
4.3.5	<i>In vitro</i> release study	77
4.4	Results and Discussion.....	77
4.4.1.	Characterization of polymers	77
4.4.2.	Particle size distribution and encapsulation efficiency (EE).....	79

4.4.3.	Thermal properties of NPs	81
4.4.4.	Porosity measurements and XPS analysis of blank NPs.....	82
4.4.5.	Microporosity measurements of Prop-loaded NPs	87
4.4.6.	<i>In vitro</i> drug release	88
4.5	Conclusion	91
4.6	Acknowledgements	92
4.7	Supporting information available.....	92
4.8	References	92
3.1	Supporting information	95
LINK BETWEEN SECOND AND THIRD ARTICLE		
CHAPTER 5. EFFECT OF POLYMER ARCHITECTURE ON SURFACE PROPERTIES, PLASMA PROTEIN ADSORPTION AND CELLULAR INTERACTIONS OF PEGYLATED NANOPARTICLES		
5.1	Abstract	103
5.2	Introduction	104
5.3	Materials and methods	106
5.3.1	Materials.....	106
5.3.2	Synthesis of polymers	106
5.3.3	Preparation of nanoparticles (NPs)	107
5.3.4	Fluorescence labeling of blank NPs.....	108
5.3.5	Characterization of NPs	108
5.3.5.1	Particle size distribution.....	108
5.3.5.2	Zeta potential measurement	108
5.3.5.3	Surface morphology and phage image analysis.....	108
5.3.5.4	XPS analysis	109
5.3.5.5	Plasma protein binding.....	109
5.3.6	Cell culture	109
5.3.6.1	Evaluation of cellular toxicity of blank NPs.....	110
5.3.6.2	Cellular interaction with RAW 264.7	110
5.4	Results and Discussion.....	111
5.4.1	Polymer characterization.....	111
5.4.2	Size and charge of NPs	112
5.4.3	Surafec morphology and phase analysis	113

5.4.4	XPS analysis	114
5.4.5	Plasma protein binding.....	116
5.4.6	Cellular toxicity and uptake studies	118
5.5	Conclusion	121
5.6	Acknowledgements	122
5.7	References	122
CHAPTER 6. GENERAL DISCUSSION		
Introduction.....		127
6.1	Synthesis and characterization of pegylated polymers	127
6.1.1	Chemical structure by ¹ H NMR	127
6.1.2	Thermal properties by DSC	128
6.2	NP preparation and impact of formulation factors on their microporosity.....	129
6.2.1	Physicochemical properties of NPs.....	129
6.2.2	<i>In vitro</i> release kinetics	130
6.3	Role of polymer architecture: Study on Blank NPs	132
6.4	Release kinetics.....	134
6.4.1	Considering conventional factors in the literature	134
6.4.2	Significance of microporosity	135
6.4.3	Role of polymer chain organization.....	136
6.5	Characterization of surface properties and Cellular interaction of NPs.....	137
6.5.1	Surface structure.....	137
6.5.1.1	¹ H NMR of NPs in D ₂ O	137
6.5.1.2	AFM image analysis of NPs	139
6.5.1.3	XPS analysis	139
6.5.2	Plasma protein binding.....	139
6.5.3	Cellular uptake studies	140
6.6	References	141
CHAPTER 7. CONCLUSION.....		145
ANNEX I. Curriculum Vitae.....		148

List of tables

Chapter 3 : Effect of Porosity on the Release Kinetics of Propafenone-Loaded PEG-g-PLA Nanoparticles

Table 3.1.	Summary of different formulations and their characterization	56
Table 3.2.	Porosity measurements for different formulations.....	58

Chapter 4 : Drug Release Kinetics and Microporous Structure of Polymeric Nanoparticles

Table 4.1.	Polymer characterization by ¹ H NMR and Size Exclusion Chromatography and DSC.....	79
Table 4.2.	Characterization of blank NPs	80
Table 4.3.	Characterization of Prop-loaded NPs.....	87

Chapter 5 : Effect of Polymer Architecture on Surface Properties, Plasma Protein Adsorption and Cellular Interactions of Pegylated Nanoparticles

Table 5.1.	Polymer characterization by gel permeation chromatography, ¹ H NMR and DSC.....	111
Table 5.2.	Characterization of NPs	112
Table 5.3.	Relative peak areas from XPS surface analysis	114
Table 5.4.	Relative percentage of monomer from area under the curves from respective C1s peaks	116

List of figures

Chapter 1 : Review of literature

- Figure 1.1. IUPAC classification of adsorption isotherms..... 7
- Figure 1.2. Mushroom and brush regime [Upper: Mushroom (low density.); Lower: Brush (High density), A_L : Area of particle surface; D: Distance between grafting points; L: Length of the polymer segment (N_p); X_p : mole fraction of polymer 17
- Figure 1.3. Physicochemical properties and total protein amounts adsorbed on lattices 1–5 expressed in arbitrary units (cpm). The values are the mean of three experiments; error bars represent the standard deviation [96]...... 18
- Figure 1.4. Pharmacokinetics and distribution to the MPS of different poly(hydroxyalkyl L-glutamine)s incorporated with a grafting density of 7.5% in 150 nm DPPC-cholesterol liposomes. (A) %-injected dose in blood-curves of PEG2000-Distearoyl phosphatidylethanolamine (closed circles), PHEG (poly(hydroxyethyl L-glutamine))4000-DODASuc (gray squares), PHPG (poly(hydroxypropyl L-glutamine))5000-DODASuc (gray diamonds), PHBG poly(hydroxybutyl L-glutamine))5000-DODASuc (gray triangles), and bare liposomes without polymer-lipid conjugate (open circles). (B) Distribution to spleen (open bars), liver (gray bars) and total distribution to the MPS (liver and spleen) (black bars). Results are expressed as the mean percentage of the injected dose of four rats \pm SD. (Taken from Ref [90])..... 19
- Figure 1.5. EPR effect, taken from reference [110] 21
- Figure 1.6. Active targeting..... 21

Chapter 3 : Effect of Porosity on the Release Kinetics of Propafenone-Loaded PEG-g-PLA Nanoparticles

- Figure 3.1. Chemical structure and NMR spectrum of the polymer, PEG-g-PLA 54
- Figure 3.2. Surface morphology of NPs (formulation 10_{1:1}) by AFM. 55

Figure 3.3.	DSC curves of (1) Prop.HCl; (2) base (Prop); (3) Polymer; (4) Physical mixture of Prop.HCl: Polymer; (5) Physical mixture of Prop: Polymer and (6) Drug loaded NPs (10 _{1:2})	57
Figure 3.4.	Pore size distribution for various formulations with (a) or without (b) TEA. All values are mean \pm S. D. for n= 3, Inset in fig b shows the pore size distribution on the same scale as Fig. 3.4 a.....	59
Figure 3.5.	Effect of TEA (0, 1:1, 1:2) on the release profile of NPs at different drug loading levels, a; 10 % and b; 5 %. Error bars indicate mean \pm S. D. for n= 3	61
Figure 3.6.	Effect of initial drug loading level on the release profile of NPs in the presence (a, 1:2 M Prop: TEA) or absence (b) of TEA. Error bars indicate mean \pm S. D. for n= 3	63

Chapter 4 : Drug Release Kinetics and Microporous Structure of Polymeric Nanoparticles

Figure 4.1.	¹ H NMR spectra and chemical structures of multiblock copolymer, PEG _{1%} -g-PLA (m = 1) and PEG _{5%} -g-PLA (m = 5).....	78
Figure 4.2.	DSC thermograms of 4 different polymers heated at the rate of 10°C/min from -50 to 220°C, PLA (a), PEG _{1%} -g-PLA (b), PEG _{5%} -g-PLA (c), and (PLA-PEG-PLA) _n (d).....	80
Figure 4.3.	Second run of DSC thermograms of blank NPs heated at the rate of 10°C/min from -50 to 70°C, PLA (a), PEG _{1%} -g-PLA (b), PEG _{5%} -g-PLA (c), and (PLA-PEG-PLA) _n (d).....	81
Figure 4.4.	High resolution nitrogen adsorption isotherms of blank NPs of PEG _{1%} -g-PLA (\square), PLA (Δ), PEG _{5%} -g-PLA ($*$) and (PLA-PEG-PLA) _n (\circ). Inset shows magnified region between 0-5 cc/g on y-axis to reveal the detailed adsorption behavior of nitrogen in relative pressure range 10 ⁻⁶ to 10 ⁻¹	82
Figure 4.5.	Effect of molecular structure of polymer on microporosity of blank NPs of PEG _{1%} -g-PLA (\square), PLA (Δ), PEG _{5%} -g-PLA ($*$) and (PLA-PEG-PLA) _n (\circ)	84

- Figure 4.6. Schematic representation of arrangement of polymer chains inside NPs and mechanism of drug release; PLA (a), grafted polymers (b) and multiblock copolymer (c).....85
- Figure 4.7. Effect of polymer type on *in vitro* release profile of Prop-loaded NPs; values are represented as mean \pm S. D. of 3 independent experiments. PEG_{1%}-g-PLA (\square), (PLA-PEG-PLA)_n (\times)..... 89

Chapter 5 : Effect of Polymer Architecture on Surface Properties, Plasma Protein Adsorption and Cellular Interactions of Pegylated Nanoparticles

- Figure 5.1. Chemical structures of multiblock copolymer (a) and grafted copolymers (b) where m=1 and 5 for PEG_{1%}-g-PLA and PEG_{5%}-g-PLA..... 111
- Figure 5.2. Tapping mode AFM phase images of NPs, all images are acquired in air. Scan size: 250 \times 250 (nm \times nm); PLA (a), PEG_{1%}-g-PLA (b), PEG_{5%}-g-PLA (c), PLA-PEG-PLA)_n (d)..... 113
- Figure 5.3. Plasma protein adsorption of different NPs by SDS-PAGE gel electrophoresis..... 117
- Figure 5.4. Cytotoxicity of NPs in RAW 264.7 cells by MTT assay. PLA (\blacklozenge); PEG_{1%}-g-PLA (\blacksquare); PEG_{5%}-g-PLA (\blacktriangle); (PLA-PEG-PLA)_n (\times)..... 118
- Figure 5.5. **A.** Effect of NP concentration on cellular uptake by RAW 264.7 cells. Cells were incubated with NPs at concentrations 40, 80, 120, 160 and 200 μ g/mL at 37 $^{\circ}$ C for 3 h. Mean \pm SD, n = 5; PLA (\blacklozenge); PEG_{1%}-g-PLA (\square); PEG_{5%}-g-PLA (\blacktriangle); (PLA-PEG-PLA)_n (\times); **B.** Effect of temperature on cellular uptake of NPS by RAW 264.7 cells. Cells were incubated with NPs at 37 $^{\circ}$ C (open bar) and 4 $^{\circ}$ C (filled bar) at a dose of 20 μ g/mL..... 121
- Figure 5.6. Uptake of fluorescent NPs of different polymers by RAW 264.7 cells at 37 $^{\circ}$ C in the presence of sodium azide (0.1% w/v), hyperosmolar sucrose (0.45 M), Chlorpromazine (10 μ g/mL), and Cytochalasin B (10 μ g/mL) (B), Cells were pretreated with the inhibitors for 1 h followed by NPs (160 μ g/mL) for another 3 h. Mean \pm SD, n \geq 4; *: values significantly different at P > 0.01. 122

Chapter 6 : General Discussion

- Figure 6.1. Microporosity determines the release; Formulations (5_{1:2}, 10₀) having same real loading (% w/w), but different microporosity resulted in different release kinetics; higher the microporosity (100), slower the release is..... 132
- Figure 6.2. ¹H NMR of blank NPs of PLA, PEG_{1%}-g-PLA, PEG_{5%}-g-PLA, and (PLA-PEG-PLA)_n..... 138

List of abbreviations

ADR	Adriamycin
AFM	Atomic force microscope
BET	Brunauer-Emmette-Teller
DCM	Dichloromethane
DLS	Dynamic light scattering
DSC	Differential scanning calorimetry
EE	Encapsulation efficiency
GPC	Gel permeation chromatography
HK method	Horvath-Kawazoe method
M_n	Number average molecular weight
MPS	Mononuclear phagocytic system
M_w	Weight average molecular weight
NK	Neimark-Kiselev
N_p	Degree of polymerization
NPs	Nanoparticles
O/W	oil in water
PCL	Poly(ϵ -caprolactone)
PCS	Photon correlation spectroscopy
PE	Phosphatidylethanolamine
PEG	Polyethylene glycol
PEG-g-PLA	Poly(ethylene glycol)- <i>graft</i> -poly(D,L lactide)
PEG _{1%} -g-PLA	Poly(ethylene glycol) _{1%} - <i>graft</i> -poly(D,L lactide)
PEG _{5%} -g-PLA	Poly(ethylene glycol) _{5%} - <i>graft</i> -poly(D,L lactide)
PLA	Poly(lactide)
PLGA	Poly(lactide-co-glycolide)
PLLA	Poly(L-lactide)
(PLA-PEG-PLA) _n	(poly(D,L lactide)- <i>block</i> -poly(ethylene glycol)- <i>block</i> -poly(D,L lactide)) _n
Prop	Propafenone hydrochloride
PSD	Pore size distribution
PVA	Polyvinyl alcohol
SDP	Size distribution processor

SEC	Size exclusion chromatography
SEM	Scanning electron microscope
TEA	Triethylamine
TEM	Transmission electron microscopy
T_g	Glass transition temperature
TM-AFM	Tapping mode atomic force microscopy

List of equations

$$\ln \frac{P}{P_0} = \frac{N_A}{RT} \times \frac{N_s A_s + N_a A_a}{\sigma^4 (l-2d_0)} \times \frac{\sigma^4}{3(l-d_0)^3} - \frac{\sigma^{10}}{9(l-d_0)^9} - \frac{\sigma^4}{3(l-d_0)^3} + \frac{\sigma^{10}}{9(d_0)^3} \quad (1)$$

$$d_0 = \frac{d_a + d_s}{2} \quad (2)$$

$$\sigma = \left\{ \frac{2}{5} \right\}^{1/6} \cdot d_0 \quad (3)$$

$$A_s = \frac{6m_e c^2 \alpha_s \alpha_a}{\frac{\alpha_s}{\chi_s} + \frac{\alpha_a}{\chi_a}} \quad (4)$$

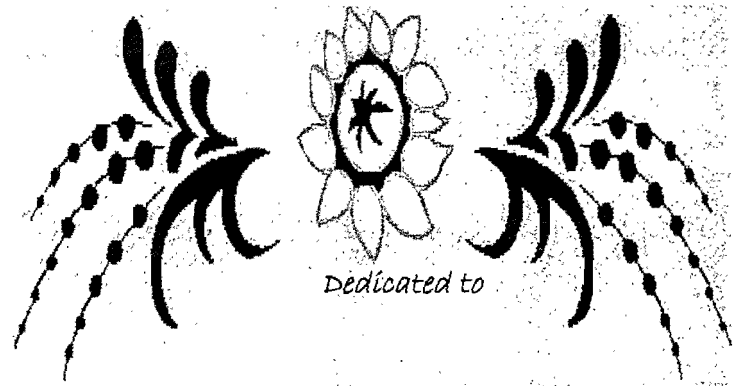
$$A_a = \frac{3}{2} m_e c^2 \alpha_a \chi_a \quad (5)$$

$$\frac{1}{W [P/P_0 - 1]} = \frac{1}{W_m C} + \frac{C-1}{W_m C} \frac{P}{P_0} \quad (6)$$

$$Q(t) = D_s \times \varepsilon/\tau \times C_a \times (2C_0 - \varepsilon C_a)t \quad (7)$$

$$Q(t) = \sqrt{D_{app} C_a \times (2C_0 - \varepsilon C_a)t} \quad (8)$$

$$Q(t) = k \sqrt{t} \quad (9)$$

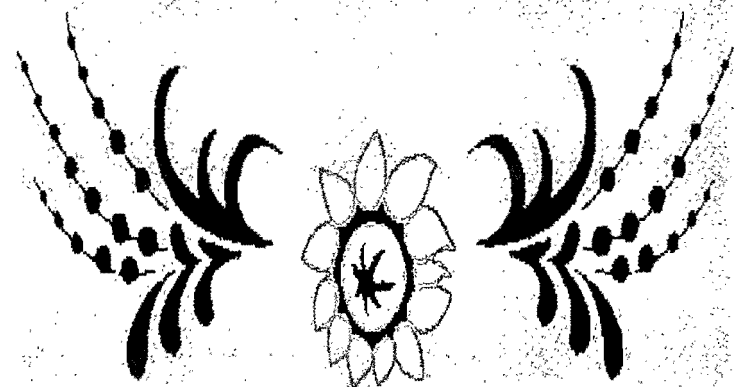


Dedicated to

*My cute little daughter, Vinisha for her love
and affection,*

*My wonderful husband, Vinayak for the
strength, confidence and emotional support
he gave me*

*And my parents for their blessings, support
and values of life they taught me*



"My Inspiration"

*I was there standing on the aisle
Looking beyond the horizon
The horizon where the Sun and the Moon meet
The sky and the ocean greet
Suddenly I felt weak,
I saw a cloud that was dark, floating on my moon
It was hazy, I tried to look beyond, I couldn't.
Foes disabled me, Friends asked me to be brave
I thought,
Do I have courage account in the bank of bravery?
Or am I too lazy to draw a cheque?
I was still on the aisle,
The breeze whipsered,
Look at the cloud once again dear,
It has a silver lining,
It said, the night is darker just before dawn
The dawn is breaking
I am looking at the sun
I hear the sun whispering to me
The only thing that makes you strong
Is seeing somebody like you
Achieving something great.
Then you know, how much is possible
& you reach out further
Than you ever thought you could.*

You reach out for the Stars & Sun;

Look at the sky

It says, don't look back.

I give you my clouds,

The clouds give you the wings,

All you have todo is

To Fly ! Fly ! Fly !.....

.....Author unknown

I will love the light for it shows me the way

Yet, I will endure the darkness for it shows me the stars

.....Author unknown

It is the hour of 'Trial'

That makes men Great

Not the hour of 'Triumph'

.....Author unknown

Acknowledgements

It gives me great pleasure to present my Ph. D. thesis entitled “Polymeric Nanoparticles: From Microporosity and Drug Release Kinetics to Cellular Interactions”.

*The respect and gratitude for my revered teacher and Director of research **Dr. Patrice Hildgen, Professor, Faculty of Pharmacy, University of Montreal** cannot be expressed in words. The complete autonomy given by him to plan the experiments along with his timely guidance and criticism in difficult times has played a big role in shaping my approach towards the research. It is indeed my good fortune to have been able to work under the guidance of the teacher of his caliber. Also, I really value his deep involvement and unstinting fatherly support throughout the course of my doctoral studies without which it would have been extremely difficult to endure the ups and downs in my research work along with my family responsibilities.*

*I sincerely thank all the co-authors of my articles, **Matthias Thommes, Suzie Poulin and Veronique Nadeau**. Words fail to express my deep sense of gratitude towards **Dr. Matthias Thommes, Director, Quantachrome Instruments, Florida, USA** for his keen interest, active guidance and precious time in helping me to interpret the porosimetry results. His priceless suggestions have been an extremely important factor in diffusing our microporosity results to the scientific community. I wholeheartedly acknowledge **Suzie Poulin, Research Associate, Ecole polytechnique, Montreal** for her unbounded efforts and patience in interpretation of XPS data. Thank you **Veronique** for helping me in the synthesis of polymers.*

*My thanks are due to **Natural Science and Engineering Research Council (NSERC) of Canada** for the financial support through the award of Postgraduate Scholarship for my Ph. D.*

*I am thankful to my jury members, **Dr. Fahima Nekka, Assistant Professor, Faculty of Pharmacy, University of Montreal; Dr. Suzanne Giasson, Assistant Professor, Faculty of Pharmacy, University of Montreal; and Dr. Abdel Omri, Associate Professor, Department of Chemistry and Biochemistry, Laurentian University** for accepting to evaluate my thesis.*

*I express my deep sense of gratitude to **Dr. Jean-Christophe Leroux, Professor, Faculty of Pharmacy, university of Montreal** for his valuable suggestions during my predoctoral examination and seminars. I also thank him for his wholehearted support including timely recommendations and utilization of facilities in his laboratory like nanosizer, zetasizer and macrophage cell line.*

*I am grateful to **Dr. Sophie-Dorothée Clas, R & D department, Merck-Frosst, Canada** for granting me permission to perform differential scanning calorimetric studies at Merck-Frosst. I am also thankful to **Karine Khougaz and Rafik Naccache, Merck-Frosst, Canada** for their help in this work.*

*My heartfelt thanks are due to **Julie Boivin and Sylvain Essiembre, Research agents, Department of Chemistry, University of Montreal** for their willingness to help me in the interpretation of DSC studies.*

*I am ever grateful to **Dr. Christian Pellerin, Professeur Adjoint, Department of Chemistry, University of Montreal** for his valuable suggestions in designing DSC experiments on nanoparticles and analysis of data.*

*I sincerely appreciate the valuable efforts, timely help and co-operation of **Patricia Moraille, Research agent, Department of Chemistry, University of Montreal** during AFM studies. I was fortunate to have a friend as nice as her during these studies.*

*The help extended by **Véronique Desjardin, Department of Chemistry, University of Montreal** during NMR studies is also appreciated. My thanks are due to **Petra Pohankova, technician, Faculty for Pharmacy, University of Montreal** for her help during my studies.*

*I find myself lucky to have a colleague and friend like **Jean-Michel**. I will never forget his ever willingness to help, overwhelming support and valuable suggestions given to me during the entire course of my Ph. D. I also thank the kind co-operation given to me by my colleagues **Névine, Véronique, Nicolas, Taha, Renu and Hamza** during my work.*

*It is my pleasure to thank **Pierre Simard** who extended helping hand to teach me cell culture techniques. My sincere thanks are also due to **Marie-Andrée** for all the minute*

details of Gel electrophoresis. I also appreciate the help provided by **Marie-Christine** during my Ph. D.

I take this opportunity to thank Prashant Satturwar for all his help and critical suggestions during this work. My heartfelt thanks are due to my close friend, Mohan for being always there in good and bad times lending his constant support and help.

Thank you very much **Dorothee and Sandra** for your support and encouragement!

How can I forget my close friends, **Hetal, Nisha, Sunila, Rupesh, Sonali, Madhuri, Seema and other marathi community** who were always there like my own family to support me whenever I needed a helping hand?

I express my deepest sense of gratitude towards **my parents, my brothers; Vinod and Sunil; and my sister Swati** for their boundless love, affection and continuous encouragement. I always missed them during these years, but at the same time, I always found them besides me and encouraging me to fight the tough moments in my life. The position achieved by me today is solely because of their blessings and constant support and the values of life they have taught me.

I wholeheartedly express my gratitude towards my **in-laws, Aai-Aba, Appa, Swati vahini, Jayutai and Vivek bhau** for their unstinting support, love and care. I consider myself lucky to have in-laws like them.

Last but not the least, thank you **Vinisha, my little adorable daughter**, whose birth and growth progressed hand-in-hand with my Ph. D.! Her little gestures and big smiles have great power to revive me and it really made me forget all the bad and tough times during the course of this work!

And now, the most important person in my life, **my inspiration, my beloved husband, Vinayak**..... How do I thank you? I find all the words inadequate for his thoughtfulness, constant moral support, helping hand at home, valuable suggestions and brainstorming discussions.....He is everything to me, a very loving and caring husband, an excellent mentor, an excellent critic, and above all, a wonderful & perfect friend! I will never find enough words to express my feelings towards him, but suffice to say

that this great moment of triumph would not have arrived without his support and inspiration.

*Finally, I am thankful to **God** for giving me lot of patience and perseverance because of which this thesis has become a reality!*

Chapter 1.
Review of Literature

1.1 General overview

According to the report by the Royal Society of London in July 2004, nanotechnologies are the design, characterization, production and application of structures, devices and systems by controlling shape and size at nanometric scale [1]. Nanotechnologies are not new and have been studied for many decades. However, only in recent years, scientists have gained an in depth understanding of nanostructured substances by using sophisticated tools such as the atomic force microscope. It is reported from different sources that the global market of nanotechnology will expand very fast. This year, it should reach \$1 trillion [2]. Its applications in pharmacology are included in this action, and the National Institutes of Health estimated that more than 50% of all biomedical advances will be in the nanotechnological sector by the year 2010 [2].

Nobel laureate and immunologist, Paul Ehrlich, proposed the concept of the so-called “magic bullets” for the drugs that might be selectively directed to their site of action [3]. This dream is fast turning into reality, thanks to the recent milestones achieved in the field of ‘polymer therapeutics’ viz. polymeric drugs, polymer drug-conjugates and polymeric nanoparticles (NPs). This breakthrough was achieved by multidisciplinary approach encompassing physics, chemistry, cellular & molecular biology and biotechnology.

Various steps have been recognized in the development of successful drug delivery device; the first and foremost of which is the availability of well-characterized, biodegradable, biocompatible polymers with potential of controlled release and drug targeting to specific tissue/cells. Biodegradable polymers have had a remarkable impact in the field of controlled drug delivery. Over past two decades, Poly (L-lactide) (PLLA) and other copolymers based on D-lactide or glycolic acid or poly(ϵ -caprolactone) (PCL) or polyethylene glycol (PEG) have been extensively studied as controlled drug delivery carriers. Such carriers offer various advantages such as controlled drug release rate, improved therapeutic efficacy, prolonged biological activity and decreased administration frequency [4]. Block and graft copolymers of polylactide (PLA) and PEG have opened new avenues in the field of targeted drug delivery by prolonging the circulation time of the polymeric colloidal drug carriers *in vivo*. However, with in-depth understanding of

pathophysiology and cellular mechanisms of the disease, targeted or cell specific drug delivery is becoming the focus of the current research. Presence of specific ligands on the surface of colloidal carriers is necessary to target specific cell type in the body (as in case of tumour cells). This can reduce systemic side effects of the drug by improving receptor-mediated uptake by the targeted cells. For instance, targeted doxorubicin delivery could be achieved by folate conjugated mixed micelles of PLGA-*b*-PEG-folate polymer [5]. Thus, targeted drug delivery has generated a great need for biomaterials with bioadhesive and/or specific recognition properties. The ability to impart bioadhesivity, cell specificity or other specific characteristics to the existing biocompatible polymers represents an important synthetic challenge. Indeed, availability of functional pendant groups is highly desirable for fine-tuning of above mentioned properties. Various efforts are directed towards achieving this goal [6, 7]. However, chemistry involved in the synthesis of functional monomers is complex and/or tedious. For example, Bizzarri et al [6] have synthesized functionalized malolactonate polymers and copolymers, where the synthesis of monomers itself was long with low yields (12-45 %) and polymerization reactions required over 4-30 days. Similarly, Ouchi et al [8] have reported the synthesis of PLA-grafted polysaccharides; however, their method involved protection and deprotection. Thus, there are very few reports on the efficient and easy synthesis of functionalized polyesters. Amongst them, Finne et al [9] have reported very efficient synthesis method for functionalized PCL and PLLA with controlled molecular weight and low polydispersity.

The next goal is formulation of drug delivery vehicle like NPs, liposomes, micelles etc. providing protection to the encapsulated therapeutic agent and optimizing its formulation factors to obtain desired release kinetics. The recent advances in nanotechnologies, especially nanoparticles (NPs) make them very promising in the drug delivery and diagnostics. NPs were first developed around 1970 and are defined as solid colloidal particles, less than 1 μm in size [10]. They can be made from inorganic and polymeric materials, however, polymeric NPs are more desirable because they can be chemically designed to be degradable and biocompatible, the first and foremost requirement of any system for biological application. Despite of their own disadvantages such as low drug-loading capacity and wide size distribution [11], NPs offer numerous advantages over conventional dosage forms, including the ability to protect drugs from enzymatic degradation, target the drug to specific tissues, cells & cell compartments and

reduce the side-effects of chemotherapy. Hence, over past few decades, there has been considerable interest in developing biodegradable NPs as effective drug delivery devices [4, 12-16].

Various polymers have been investigated for preparation of NPs including polylactide (PLA) [17-20]; poly(lactide-co-glycolide) (PLGA)[11, 16, 21-27]; poly(ϵ -caprolactone) (PCL) [28, 29] and pegylated polymers [29-40]. NPs have also been prepared using polyalkylcyanoacrylate polymers [41-45]. The drug of interest is dissolved, entrapped, adsorbed or attached to the nanoparticle matrix. Depending on the method of preparation, nanospheres or nanocapsules can be obtained with different properties and release characteristics. Nanocapsules are vesicular systems in which the drug is confined to a cavity surrounded by a unique polymeric membrane, whereas nanospheres are matrix systems in which the drug is physically and uniformly dispersed [33, 46-49]. A drug can be loaded into NPs by oil-in-water emulsion method if the drug is water insoluble [25, 50] or water-in-oil-in-water double emulsion [11, 19, 30, 50, 51] if the drug is water soluble. Other methods reported for preparation of NPs include nanoprecipitation [17, 52] and electrospraying [20]. Drug loading efficiency of NPs depends on the properties of the drug and polymer as well as formulation parameters.

1.2 Characterization of NPs

The therapeutic success of any smart drug delivery system requires it to i) be non-toxic, non-immunogenic and stable in the biological fluids, especially during circulation ii) protect the encapsulated moiety from premature degradation, iii) overcome biological barriers that it will encounter once administered *in vivo*, iv) be recognized efficiently and selectively by the target cells and tissues, v) be able to penetrate the target cell membranes and gain access to the intracellular structure and of course, vi) release the encapsulated therapeutic moiety in a controlled and/or sustained manner depending on the need of the application. In short, innovative and successful developments in these drug delivery systems will require a multidisciplinary approach encompassing engineering, physical chemistry and biological sciences. Fine-tuning of various physicochemical properties is equally necessary to obtain biologically successful therapeutic system. Behavior of NPs within the biological microenvironment, stability, extracellular and cellular distribution

varies with their chemical makeup, morphology, and size. The following section gives the brief summary of these properties.

1.2.1 Size and size distribution

Most widely studied parameter in case of particulate carriers is the size. The size and size distribution are important parameters in determining their release kinetics as well as the interaction of NPs with the cells and penetration through biological barriers such as gastrointestinal barrier for oral chemotherapy and blood brain barrier for the treatment of brain cancers or Alzheimer's disease. It has been confirmed with repetitive studies that generally larger particles are rapidly cleared by mononuclear phagocytic system (MPS) than smaller particles [13, 53, 54]. Complement activation is also suggested to be dependent on the size [53, 54]. Even in case of long-circulating colloidal particles, optimum size is proposed to be 150-200 nm [14, 55, 56].

1.2.2 Surface and bulk morphology

The surface and bulk morphology are important in determining the drug release kinetics from NPs. NPs are too small to be visualized under the light microscope. As a result of the rapid progress in high-resolution microscopies such as scanning electron microscopy (SEM), atomic force microscopy (AFM), NPs can be visualized with a resolution of few nanometers. AFM provides a higher resolution than SEM. Both contact and non-contact modes can be employed. Tapping mode AFM (TM-AFM) is more preferred than the contact-mode and the non-contact mode because of its ability to probe soft samples such as biological and polymeric materials under ambient conditions [57, 58]. In tapping mode, the cantilever oscillates close to its bending mode resonance frequency so that tip makes contact with the sample only for a short duration in each oscillation cycle. As the tip approaches the sample, the tip-sample interactions alter the amplitude, resonance frequency, and the phase angle of oscillating cantilever. During scanning, the amplitude at the operating frequency is maintained at the constant level, called the set-point amplitude, by adjusting the relative position of the tip with respect to the sample. This operating method results in lower surface forces, particularly lateral forces, causing less surface

damage [57]. One recent approach in TM-AFM is the use of the changes in the phase angle of the cantilever probe to produce phase image. This image often provides more contrast than the topographic image and has been shown to be sensitive to material surface properties such as stiffness, viscoelasticity and chemical composition [57-60].

It is possible to observe the bulk morphology of NPs by cross-section; however, their small size makes this difficult. This may be the reason of lack of such investigations in the literature, except that reported by Rizkalla et al [61]. Using this technique, authors could successfully demonstrate co-existence nanocapsules having large central cavity along with nanospheres with solid core.

Another possible technique to study the internal morphology of NPs is physical gas adsorption. The next section will give brief synopsis of basic principles of gas adsorption in general and summary of methods used for microporosity analysis in specific.

1.2.2.1 Physical Gas Adsorption: Basic Principles [62]

Gas adsorption is one of the many experimental techniques available for the surface and pore size characterization of porous materials. Other techniques include small angle X-ray and neutron scattering, mercury porosimetry, electron microscopy, thermoporometry and NMR-methods. Each method has limited length scale applicability for pore size analysis. Among these methods, gas adsorption is the most popular method because it allows assessment of wide range of pore sizes (from 3.5 Å up to > 1000 Å), including the complete range of micropores (0 to 20 Å), mesopores (20 to 500 Å) and even macropores (500 to 5000 Å). In addition, gas adsorption techniques are convenient to use and are not that cost intensive as compared to some of the other methods. Adsorption can be divided into chemical and physical adsorption, depending on the strength of the interaction. Physical adsorption is a general phenomenon and occurs whenever adsorbable gas is in contact with the surface of solid adsorbent. Physisorption exhibits characteristics which make it most suitable for surface area measurements as indicated

1. Physisorption is accompanied by low heats of adsorption with no disruptive surface structural changes during the measurement.

2. Pores can be filled completely by the adsorptive gas for pore volume measurements. Such pore condensation phenomena can be used to calculate pore size and size distribution.
3. Physisorption is completely reversible, enabling both the adsorption and desorption to be studied.
4. Physically adsorbed molecules are not restricted to specific sites but, can cover the entire surface, enabling calculation of surface areas rather than number of sites.

1.2.2.2 Classification of adsorption isotherms [62-64]

As per IUPAC classification [63], adsorption isotherms are divided into 6 types as shown below.

The reversible type I isotherm is concave to P/P_0 axis and amount approaches a limiting value as $P/P_0 \rightarrow 1$. This type of isotherm is generally encountered in case of adsorption on microporous materials. Micropore filling and therefore, high uptakes are observed at relatively low pressures. The strong increase in the adsorbed amount close to the saturation pressure results from the pore condensation into large meso- and macropores or interparticulate space.

Type II isotherms are typically obtained in case of macroporous or non-porous adsorbent, where monolayer-multilayer adsorption can occur. The inflection point (B) indicates the stage at which monolayer is complete.

The reversible type III adsorption isotherm is convex to the P/P_0 axis and is very uncommon, but an example includes nitrogen adsorption on polyethylene.

Type IV isotherms are typical of mesoporous materials and exhibit characteristic hysteresis loop associated with the pore condensation.

Type V isotherms also show pore condensation and hysteresis phenomenon, however, initial part of this isotherm is related to the type III isotherm.

Type VI isotherm is a special case showing multilayer adsorption on a uniform, non-porous surface.

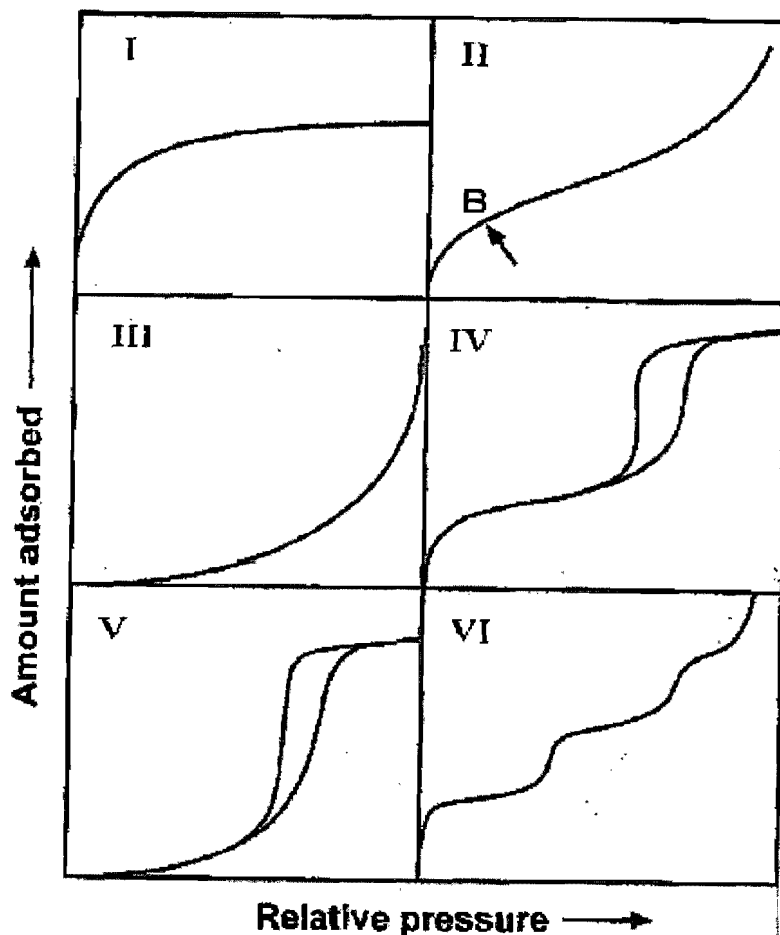


Figure 1.1. IUPAC classification of adsorption isotherms

1.2.2.3 Adsorption in micropores

As defined earlier, pores are classified as macropores (pore widths greater than 500 Å), mesopores (pore widths from 20-500 Å) and micropores (pore widths less than 20 Å). For NPs of size 200 nm, micropores will be more important. The mechanism of pore filling is different in meso- and micropores. Mesopores fill via pore condensation, representing a first order gas-liquid phase transition. In contrast, the filling of micropores represents a continuous process, in most cases. The micropores are further subdivided into those smaller than 7 Å (ultramicropores) and those in the range of 7-20 Å (supermicropores). The filling of ultramicropores occurs at very low relative pressures and is entirely governed by the

enhanced gas-solid interactions. The relative pressure where micropore filling occurs is dependent on a number of factors such as the size and nature of adsorptive gas molecules, the pore shape and the effective pore width. The pore filling capacity depends on the pore accessibility to the probe molecules which in turn, is determined by the size of the probe molecule. In an ideal case, pure microporous materials exhibit type I isotherm as IUPAC classification. Various methods and theories have been developed for micropore characterization, which include Polyani, Dubinin including most recent approaches by Horvath-Kawazoe [65, 66] known as HK method. It should be noted that this method cannot be applied to mesopore size analysis. The following equation is used for micropore analysis using HK method:

$$\ln \left\{ \frac{P}{P_0} \right\} = \frac{N_A}{RT} \times \frac{N_s A_s + N_a A_a}{\sigma^4 (l-2d_0)} \times \frac{\sigma^4}{3(l-d_0)^3} - \frac{\sigma^{10}}{9(l-d_0)^9} - \frac{\sigma^4}{3(l-d_0)^3} + \frac{\sigma^{10}}{9(d_0)^3} \quad (1)$$

Where,

$$d_0 = \frac{d_a + d_s}{2} \quad (2)$$

$$\sigma = \left\{ \frac{2}{5} \right\}^{1/6} \cdot d_0 \quad (3)$$

$$A_s = \frac{6m_e c^2 \alpha_s \alpha_a}{\frac{\alpha_s}{\chi_s} + \frac{\alpha_a}{\chi_a}} \quad (4)$$

$$A_a = \frac{3}{2} m_e c^2 \alpha_a \chi_a \quad (5)$$

A_a = Kirkwood-Mueller constant of adsorbate

A_s = Kirkwood-Mueller constant of adsorbent

d_0 = distance between adsorptive and adsorbent molecules

d_a = diameter of an adsorbate molecule

d_s = diameter of an adsorbent molecule

N_a = number of atoms per unit area (m^2) of adsorbent

N_A = number of adsorptive molecules per unit area (m^2) of adsorbent

m_e = mass of an electron

c = speed of light

α_a = polarizability of adsorbate

α_s = polarizability of adsorbent

σ = distance between two molecules at zero interaction energy

χ_a = magnetic susceptibility of adsorbate

χ_s = magnetic susceptibility of adsorbent

l = the separation between nuclei of two layers

According to this equation, the filling of micropores of a given size and shape takes place at a characteristic relative pressure.

1.2.2.4 Specific surface area

Gas adsorption technique also serves in the analysis of specific surface area of the sample. Specific surface area depends on size, shape and porosity. The BET-nitrogen adsorption method continues to be a universally employed method for determining the surface area of adsorbents, catalysts and other materials [67]. It is based on a simple model of monolayer-multilayer adsorption and given by the following equation:

$$\frac{1}{W [P/P_0 - 1]} = \frac{1}{W_m C} + \left\{ \frac{C-1}{W_m C} \right\} \frac{P}{P_0} \dots\dots\dots (6)$$

Where,

W = weight of the adsorbed molecules

W_m = weight of the adsorbed molecules at monolayer coverage

C = BET constant

P_0 = saturation pressure

A plot of $1/W [P/P_0 - 1]$ versus P/P_0 gives a straight line in the range of $0.05 \leq P/P_0 \leq 0.35$.

1.2.2.5 Nitrogen as a standard adsorptive for surface area measurements [62]

The unique properties and the availability of liquid nitrogen have led to the universal acceptance of nitrogen as the standard BET adsorptive. The fact that nitrogen has a permanent quadrupole moment is important, because it is responsible for the formation of a well-defined monolayer on most of the surfaces. However, quadrupole moment of nitrogen affects its adsorption on highly polar surfaces due to specific interactions between these polar groups and its quadrupole moment. Thus, nitrogen is not completely inert and this may result in overestimation of BET surface area in case of polar surfaces.

In contrast to nitrogen, argon has no quadrupole moment. Argon is much more sensitive to the details of the surface structure if used at liquid nitrogen temperature (77 K).

For accurate measurement of surface areas as low as $0.5 - 1 \text{ m}^2$, number of molecules trapped in the void volume of the sample cell needs to be reduced. This can be achieved by using krypton adsorption at liquid nitrogen temperature for the surface area analysis. Krypton has a much smaller saturation pressure (1.63 Torr i.e. 217.25 Pa) compared to nitrogen (270 Torr) at 77.35 K and hence, the amount of krypton remaining in the void volume will be much less as compared to that of nitrogen. This increases the sensitivity of the manometric adsorption measurements significantly thereby, allowing accurate surface area measurements for materials with small specific surface areas ($< 0.05 \text{ m}^2/\text{g}$), or if only a very small amount of sample is available.

1.2.3 Physical state of drug within NPs

It is important to know whether the drug is present in crystalline or amorphous form within the matrix. This provides certain information about the rate of drug release. The first step in the release requires dissolution of drug in the release medium followed by its diffusion. Drug dispersed in the matrix in crystalline form will dissolve slowly than its amorphous or molecularly dispersed form affecting the release kinetics. Differential scanning calorimetry (DSC) can be used to gain information about physical state of the drug as well as polymer-drug interaction. For instance, Mu et al [68] have detected no melting endotherm of paclitaxel in PLGA nanospheres, attributing it to the molecular dispersion of paclitaxel in the polymeric matrix. On the other hand, Okada et al [69] have

shown an increase in the glass transition temperature (T_g) of leuprorelin-loaded PLA microspheres due to ionic interaction between the drug and the polymer.

1.2.4 *In vitro* drug release kinetics

In vitro release studies are important in the characterization of any drug delivery system. Although *in vivo* release could be different, the *in vitro* release experiments provide some guidance for prediction of possible effects of the drug delivery system. It also gives an insight to the possible burst effect, which should be avoided to prevent toxic concentration in the body. It is well established that drug release from polymeric matrices is governed by both diffusion and degradation depending on the polymer type [70]. This release phenomenon is a complex interplay of various factors such as properties of the drug and polymer, their compatibility with each other, type of emulsifier used, drug loading level, physical state of the drug inside the matrix and various other formulation parameters.

The Higuchi square root model has been successfully applied to model the kinetics of drug release from matrix system. Equation 9 was derived from Fick's first law of diffusion and applied to porous hydrophobic polymeric drug delivery systems in homogenous matrices [71].

$$Q(t) = \sqrt{D_s \times \varepsilon/\tau \times C_a \times (2C_0 - \varepsilon C_a)t} \dots\dots\dots (7)$$

$$= \sqrt{D_{app} C_a \times (2C_0 - \varepsilon C_a)t} \dots\dots\dots (8)$$

$$= k \sqrt{t} \dots\dots\dots (9)$$

Where,

$Q(t)$:Cumulative amount of drug released in time t per unit surface area

D_s : Drug diffusion coefficient in the release medium

C_0 : Total amount of drug in the matrix

C_a : Solubility of drug in the release medium

ε : Porosity of the matrix

τ : Tortuosity of the matrix

$D_{app} = D_s \epsilon / \tau$: Apparent observed diffusion coefficient

k : Dissolution rate constant

Thus, drug release from such a system will depend on the initial concentration of the drug in the matrix, porosity, tortuosity, properties of the polymer system forming matrix and the solubility of the drug. Drug release from hydrophobic polymeric drug delivery system will occur when the drug comes into contact with the release media, subsequently dissolves and diffuses through the media filled pores. Thus, geometry and structure of pores is important in this process.

1.2.5 Surface charge

Surface charge is important in determining the *in vivo* stability as well as cellular interaction capability of NPs. Zeta potential measurements can give idea of surface charge of particles. Generally, surface charge should be near neutral to avoid non-specific cell sticking or uptake of NPs. This is discussed along with the properties of long-circulating polymers.

1.2.6 Surface chemistry

Once the release properties are tailor-made for particular application, the next milestone to be achieved in the development of drug delivery device is suitability of the surface properties of such polymeric colloidal carrier in terms of its *in vivo* stability, compatibility and cellular interaction capabilities. Physicochemical surface characteristics also give clear evidence of the effect of coatings and residual emulsifiers on the NP surface. The amount of emulsifier on the surface has significant effect on various physicochemical and biological properties of the NPs. Polyvinyl alcohol (PVA) is the most commonly used emulsifier in the formulation of polymeric NPs. It has been proven that a fraction of PVA remains associated with the NPs despite repeated washing and has been proposed that this is due to formation of an interconnected network with the polymer through hydrophobic interactions at the interface. Sahoo et al [23] have systematically shown that this residual PVA, in turn, affected different pharmaceutical properties of NPs such as particle size, zeta potential, polydispersity index, surface hydrophobicity, protein loading and also slightly influenced *in vitro* release of the encapsulated protein. Importantly, NPs with higher

amount of residual PVA had relatively lower cellular uptake despite their smaller particle size. It was proposed that lower intracellular uptake of NPs with higher amount of residual PVA could be related to higher hydrophilicity of NP surface.

Various efforts have been directed to create particles with precise surface chemistry, especially for their long-circulating properties. Their summary and properties required for long-circulating polymers/carriers will be described in the next section.

1.3 Optimization of surface chemistry of NPs: Essence for their long-circulating behavior and biological activity

Amongst various physicochemical properties, surface properties of any system are thought to play a crucial role in interactions with the cells and their intracellular transport machinery, and can significantly affect the efficacy of the encapsulated drugs [72]. Hence, it is critical in targeted gene and drug delivery to carefully design and control the surface properties of such systems. A prerequisite to selective targeting is particle stability *in vivo* and the minimization of nonspecific uptake. This can be done by designing surfaces with no or little protein adsorption. In particular, the adsorption of biological proteins onto biomaterials plays an important role in determining their fate. Hence, elimination of protein adsorption onto biomaterials is one of the key elements in preventing thrombosis, platelet activation and immunological responses [73]. Similarly, this phenomenon of adsorption of proteins and opsonins on polymeric drug delivery systems leads to their recognition and rapid elimination from systemic circulation by Mononuclear Phagocytic System (MPS). To avoid this, the concept of long-circulating polymers has been emerged [12, 30, 74]. In the past two decades, we have witnessed a surge in the development of long circulating vehicles. Among the various polymers studied, poly (ethylene glycol) (PEG) has been the most extensively investigated polymer. PEG is an uncharged hydrophilic and non-immunogenic polymer that can be physically adsorbed onto or preferably, covalently attached to the surface of colloidal systems [75, 76]. Various pioneering studies and

especially, the entry of pegylated or so-called “sterically stabilized” liposomal doxorubicin (DoxilTM, CaelyxTM) into the market signify the importance of the stealth technology.

1.3.1 Approaches used for prolonged circulation

Since the past two decades, various approaches have been used for imparting the stealth behavior to the polymeric carriers, which include:

- Adsorption of hydrophilic polymers containing hydrophobic substituents onto the surface via hydrophobic interactions, e. g. surfactants such as poloxamers, poloxamines [12, 74].
- Covalent bonding of hydrophilic polymers onto the surface e.g. surface-grafted polymers or use of PEGylated copolymers with some other biodegradable polymer such as PLA, PLGA, PCL [16, 30, 31, 33, 34, 39, 47, 77-83].

It is proposed that in both these cases, the hydrophilic parts protrude out in aqueous milieu forming “molecular cloud” on the surface of the carrier, thus protecting the carrier from recognition by MPS [13, 46, 76]. However, in the first approach, possibility of rapid desorption of the adsorbed coat may deceive the true purpose, as observed in case of NPs [74]. Covalently linking PEG to the surface of the polymer has some disadvantages as well. It is sometimes difficult to ensure that covalently bound PEG comes out on the surface and does not penetrate in the bulk of the material. This will affect PEG surface coverage and conformation. At the same time, presence of covalently bound PEG chains throughout the particle may be advantageous for degradable particles, ensuring availability of surface exposed PEG during the entire degradation and erosion process. Hence, copolymers of PEG with other polymers were used; nevertheless, this does not assure presence of all PEG chains on the surface of particles prepared from these polymers.

1.3.2 Physicochemical properties of long-circulating carriers

Several theories have been proposed to explain the apparent protein binding and long-circulating properties of pegylated carriers. Some authors correlated long-circulating

behavior of pegylated carriers to the results of overloading the clearance system in the body thereby giving false stealthy appearance to particles [13]. Nonetheless, most widely accepted theory is the one based on ability of PEG to impart protein resistant properties to the particles [84, 85]. This theory makes the argument that the hydrophilic and flexible nature of surface PEG chains allows them to have more extended conformation when free in solution. Therefore, when opsonins or other proteins are attracted towards the particle surface by van der Waals and other electrostatic forces, they encounter the extended PEG cloud and begin to compress them, which forces the PEG chains into more condensed and hence, high energy conformation. This creates an opposing repulsive force which, if great enough can completely balance or overpower the attractive forces between the protein and the particle surface. High (optimal) surface density and long chain length (degree of polymerization) was suggested to be desirable for protein resistance [84, 85]. The most important physicochemical properties required for long-circulating polymers and polymeric carriers are summarized below with the relevant experimental evidence wherever possible.

1.3.2.1 Solubility and Hydrophilicity:

In general, the surface grafted polymer should be soluble and hydrophilic. Along with this, it was also proposed by Jeon et al [84, 85] that the composition of terminally attached polymer chain affects the refractive index and static dielectric constant of the polymer layer. Lower the refractive index, lower are the van der Waals interactions and thus, greater would be the steric barrier for approaching protein. According to Jeon et al, PEG of relatively low molecular weight has the lowest refractive index as compared to any common water-soluble synthetic polymers and that may be one of the reasons of its excellent protein resistant property. Lot of studies carried out on the surface hydrophobicity and protein adsorption clearly indicate that decreasing hydrophobicity of the particle surface leads to decreased protein adsorption [86-88].

1.3.2.2 Molecular weight (M_w) and Polymer layer thickness:

It has been demonstrated in various studies [89, 90] that increasing PEG M_w from 6-20 kDa increased PEG layer thickness and chain flexibility and subsequently enhanced circulation half-life. On the other hand, it is important to note that there is a maxima after which, increasing molecular weight or polymer layer thickness may not have any effect

[89, 90]. This can be illustrated by the following example. When protective effect of phosphatidylethanolamine (PE) having 1 or 2 attached PEG molecules was compared in liposomes, at a concentration of 3 mole %, the circulation half-life of these liposomes was found to be 140 vs 80 min, respectively. However, when used in the concentration of 7 mole %, both of these liposomes showed the same half-life of about 230 min [91], showing that maximum surface density had reached. Also, it should be stressed that components of any molecular brush cannot be completely inert. Very long polymer chains and dense brushes are more capable of forming co-operative weak association due to presence of a greater number of groups forming weak bonds. In fact, there are reports that excessively long PEG chain (> 5 kDa) was inferior as long-circulating polymer [91].

1.3.2.3 Grafting density and conformation:

Grafting density may be defined as the moles of grafted polymer per unit area of the surface. Increased grafting density means better steric protection as confirmed by Michel et al [82]. They showed that increasing PEG grafting density resulted in less protein adsorption of small as well as large proteins.

Grafting density and conformation are inter-related. For instance, at low grafting density, PEG chains will have larger range of motion and will take on a “mushroom” conformation, where they will be located near the surface of the particle. On the other hand, at higher grafting density, the motion of PEG chains is highly restricted and they will exhibit “brush” configuration. The term ‘mushroom’ relates to the semi-spherical volume occupied by a single flexible elongated molecule whereas ‘brushes’ are long-chain polymer molecules attached onto the one end of surface with the density of attachment high enough so that the chains are obliged to stretch away from the interface (Fig. 1.2) [92].

Very low surface grafting density will also lead to gaps or unprotected surfaces where proteins can easily bind to the particle surface. On the other hand, although a high grafting density ensures a complete surface coverage, it decreases PEG chain mobility and its steric hindrance properties. Therefore, the optimal surface coverage is located between “brush” and “mushroom” configurations where the surface density should be high enough to cover the whole surface without compromising the chain flexibility [53].

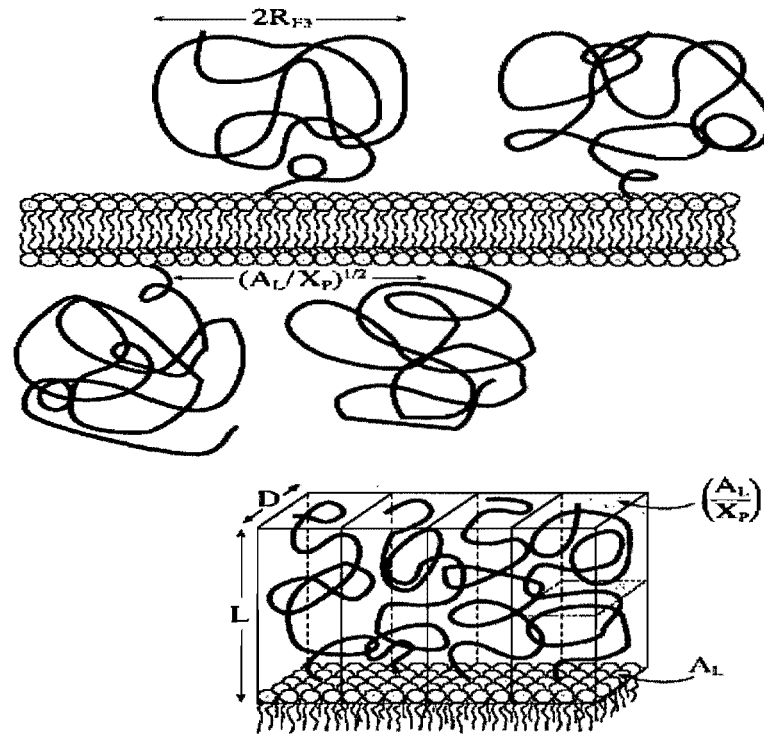


Figure 1.2. Mushroom and brush regime [Upper: Mushroom (low density.); Lower: Brush (High density), A_L : Area of particle surface; D : Distance between grafting points; L : Length of the polymer segment (N_p); X_p : mole fraction of polymer

1.3.2.4 Charge and charge density:

Charge on the surface of biomaterial is a very important factor, playing role in its interaction with any living cell/tissue as proposed by Dan [93]. It is well-established that positively and negatively charged particles are cleared from the body faster than those with near-neutral charge [15, 38, 94, 95]. Positively charged particles cause non-specific cell sticking to the negatively charged cell surfaces whereas, negatively charged NPs are efficiently taken up by scavenger endothelial cells or Kupffer cells in the liver [15, 95]. Thus, near-neutral and hydrophilic NPs are needed to avoid undesirable protein and cellular interactions. Similarly, Gessner *et al.* [96], have synthesized a range of model latex particles having constant particle parameters except charge density and confirmed that increasing surface charge density led to increased protein adsorption (Fig. 1.3).

Table 1
Physicochemical characterization data of model nanoparticles (latex 1–5)

Latex	1	2	3	4	5
Surface charge density ($\mu\text{C}/\text{cm}^2$)	-3.7	-5.2	-6.0	-6.7	-8.2
Particle size (nm) (SD 0.01)	54	61	64	57	60
Hydrophobicity: slope from Rose Bengal partitioning experiment (mL/m^2)	7	7	8	8	10

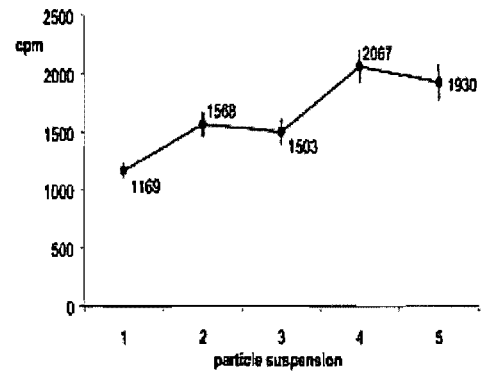


Figure 1.3. Physicochemical properties and total protein amounts adsorbed on lattices 1–5 expressed in arbitrary units (cpm). The values are the mean of three experiments; error bars represent the standard deviation [96].

1.3.2.5 Flexibility of the polymer chain:

This is another important factor for PEG being so popular as a protective polymer. In general, more flexible the molecule, the larger the total number of its conformations and higher the rate of transition from one conformation to other leading to formation of “high probability cloud” occupying lot of place and squeezing the water out of them. Due to water exclusion effect, it apparently hinders the permeability of the approaching proteins [76]. In case of rigid polymer, unit motion is hindered and even its high solubility and hydrophilicity may not provide sufficient protection [97]. This was established as a reason why small quantities of PEG could show protection to liposomes however, rigid dextran failed to do so [98].

1.3.2.6 Presence of side group on the protective polymer:

Metselaar *et al.* [90] have studied novel family of polymers, namely, lipid conjugated poly(hydroxyalkyl L-asparagine/L-glutamine) and studied effect of various variables like type of lipid anchor, grafting density, lipid dose as well as side group present in the poly (L-Amino acid) which was used as protective polymer instead of PEG. It was observed that substitution of longer hydroxyalkyl groups in place of polyhydroxyethyl, (viz., polyhydroxy -propyl or -butyl) in their glutamine chain reduced the circulation half-life (Fig. 1.4). This was attributed to reduced chain flexibility, thus, compromising the size of conformational cloud.

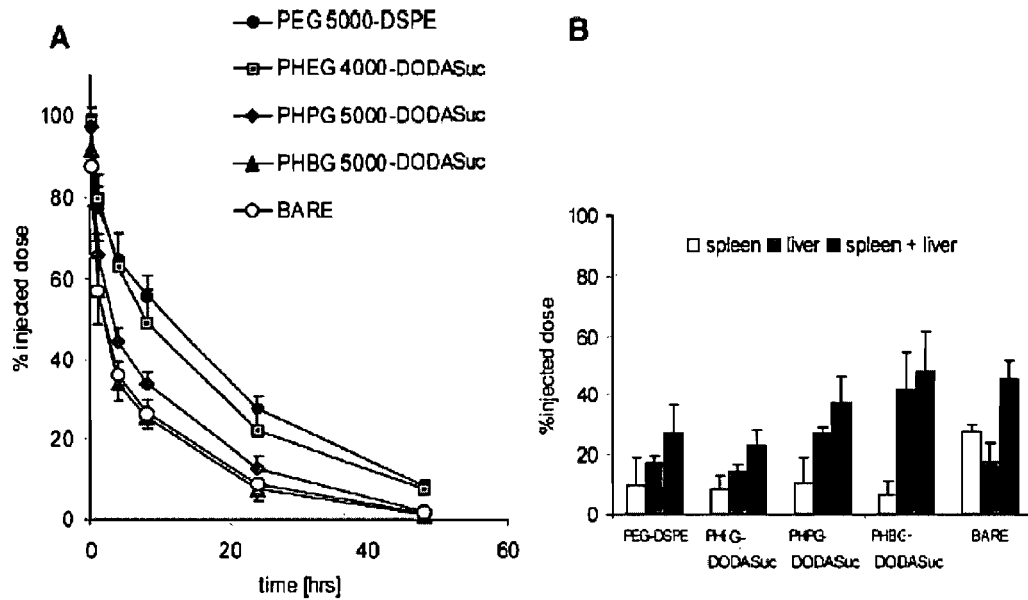


Figure 1.4. Pharmacokinetics and distribution to the MPS of different poly(hydroxyalkyl L-glutamine)s incorporated with a grafting density of 7.5% in 150 nm DPPC-cholesterol liposomes. (A) %-injected dose in blood-curves of PEG2000-Distearoyl phosphatidylethanolamine (closed circles), PHEG (poly(hydroxyethyl L-glutamine))4000-DODASuc (gray squares), PHPG (poly(hydroxypropyl L-glutamine))5000-DODASuc (gray diamonds), PHBG poly(hydroxybutyl L-glutamine))5000-DODASuc (gray triangles), and bare liposomes without polymer-lipid conjugate (open circles). (B) Distribution to spleen (open bars), liver (gray bars) and total distribution to the MPS (liver and spleen) (black bars). Results are expressed as the mean percentage of the injected dose of four rats \pm SD. (Taken from Ref [90])

1.4 Biological consequences of long-circulating carriers

The most important biological consequence of long-circulating polymers is their effect on pharmacokinetics of the macromolecules/particulate carrier systems. Indeed, there is accumulating body of evidence for various liposomal [99], nanoparticulate [14] and micellar systems [100]. As discussed throughout this section, this is assumed to be due suppression of surface opsonization by serum or plasma proteins and in turn, decreased uptake by MPS [12].

The altered pharmacokinetic parameters show delayed drug absorption, restricted drug biodistribution, delayed drug clearance and retarded drug metabolism. These effects are due to hindered interstitial drug penetration and restricted drug accessibility to the

biological milieu due to encapsulation in the polymeric carrier [53]. While unprotected, conventional carriers show non-linear saturable pharmacokinetics, long circulating carriers show dose-independent, non-saturable, and log-linear pharmacokinetics [55, 101]. This is explained by significant decrease in the first phase of particulate clearance into a high affinity and relatively low capacity system, such as MPS.

1.5 Nanoparticle Targeting

NPs can be targeted to specific tissues especially tumor cells through a physical sieving mechanism based on their size (passive targeting) or through specific molecular binding interactions (active targeting).

1.5.1 Passive Targeting

Passive targeting of NPs takes advantage of their inherent size and unique properties of the tumor vasculature. In contrast to normal endothelium, tumor vessels are lined by a simple layer of endothelium with few pericytes and smooth muscle cells. Tumor blood vessels are distinct from normal vessels, in that the tumor endothelial cells have wide fenestrations, ranging from 200 nm to 1.2 μm (Fig. 1.5) [102-105]. This increased permeability of tumor vascular tissue combined with impaired lymphatic drainage from tumor interstitium is known as Enhanced Permeability and Retention (EPR) effect. This has been exploited to improve drug delivery to tumors and other sites including inflammation and infarcts possessing similar pathological characteristics. Thus, due to the presence of leaky vasculature and compromised lymphatic drainage, small colloidal particles (100-200 nm) can extravasate in the pathological sites such as tumor, infection, inflammation. In addition, long-circulating character of these particles makes them circulate for longer time, thus, enhancing their capture by tumor cells. This leads to increased local drug concentration improving the therapeutic efficacy, and at the same time, reducing non-specific accumulation of the drug in the healthy tissues, decreasing their toxicity [33, 103-109]. A significant drawback of using the EPR effect is that it works only in solid tumors. However, the therapy for spreading tumors and metastases presents the great challenge for the chemotherapy as these tumors do not develop EPR effect and therefore, their therapy requires active targeting strategies.

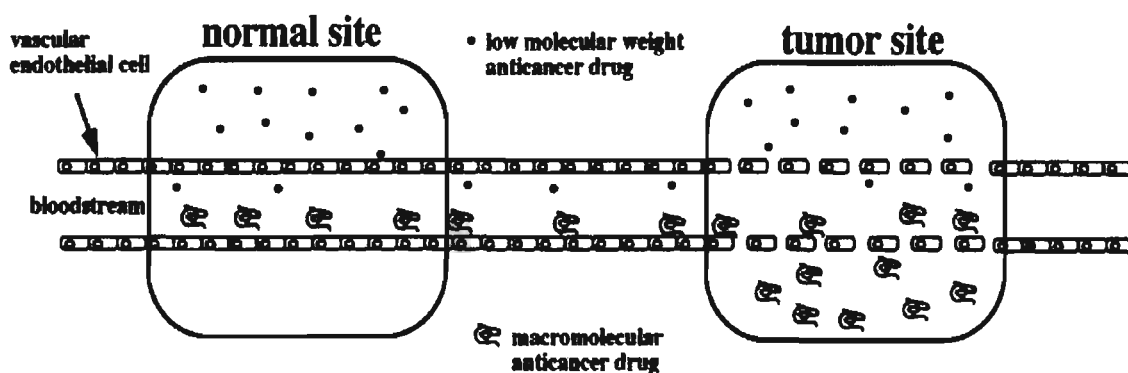


Figure 1.5. EPR effect, taken from reference [110]

1.5.2 Active targeting

Active targeting is achieved by conjugating the carrier system to some ligands unique to the cells/tissues to be targeted (Fig. 1.6). An ideal targeting ligand should be abundant, with a high affinity and specificity for binding to the cell surface receptors and should be compatible to chemical modification by conjugation. The tumor endothelium provides many targets for cancer therapy including tumor growth factor- α , matrix metalloproteinases, integrins etc. (reviewed in [2, 111, 112]). Other targeting moieties used so far include RGD-peptide [113, 114], folic acid [37], and monoclonal antibodies.

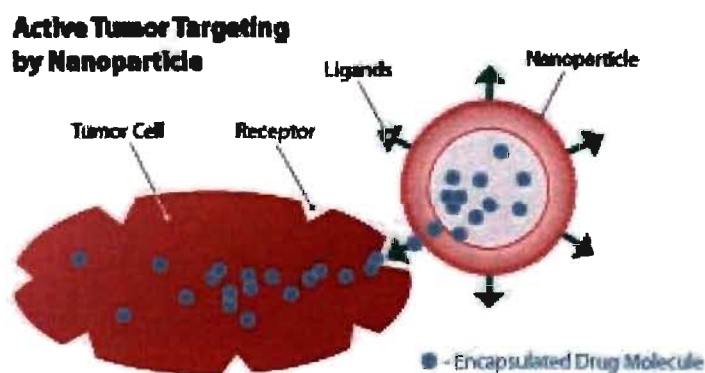


Figure 1.6. Active targeting

1.5.3 Intracellular transport mechanisms

Once the colloidal carrier remains in circulation by escaping opsonization and components of MPS, it should reach the target cell populations to exhibit its activity. Intracellular organelles, such as mitochondria, nucleus etc. form the site of actions of many therapeutic agents [72]. The cytoplasm itself is the target for certain drugs like glucocorticoids, the receptors of which are cytoplasmic. Hence, the efficient intracellular delivery of NPs is crucial in enhancing the efficacy of encapsulated therapeutic agent. To develop such a system, it is indispensable to learn intracellular transport mechanisms.

Most colloidal drug delivery devices gain entry inside the cell through the process of endocytosis. Endocytosis is divided into phagocytosis and pinocytosis. Phagocytosis is the ingestion of relatively large particulates by specialized cell types (i. e. macrophages, neutrophils and dendritic cells) that adhere to the particle and generate membrane extensions around the particle. Eventually, these membrane extensions fuse together to enclose the particle within an membrane bound compartment called 'Phagosome'. Internal fusion of phagosome with lysosome generates 'phagolysosome' where particle is degraded by action of various enzymes like proteases and nucleases.

In contrast to phagocytosis, essentially all the cells undertake pinocytosis which refers to the internalization or invagination of plasma membrane domains. With invagination and internal budding of such domains any bound molecules and associated extracellular fluid are also taken into the cell. Pinocytosis begins at specialized plasma membrane domains including clathrin- coated pits, caveolae and non-coated lipid rafts. The invaginated plasma membrane gives rise to the membrane-enclosed vesicles within the cytoplasm termed 'endosomes'.

Cells will endocytose materials from their extracellular environment through one of the following processes:

Receptor-mediated endocytosis: Here, particle will bind to its cognate receptor and the receptor-ligand pair is internalized through plasma membrane invaginations to form endosomes. Broadly, receptor-mediated endocytosis can be constitutive (class I) or ligand-stimulated (Class II). Constitutive endocytosis results from continual plasma membrane turnover. This type of internalization occurs for receptors for transferring and low density

lipoprotein. In ligand-stimulated endocytosis, ligand binding to its receptor triggers the internalization. Examples include inulin and epidermal growth factor binding to their receptors.

Adsorptive endocytosis: The material to be endocytosed binds to the cell surface not through specific receptor-ligand pairing but through non-specific mechanisms like electrostatic interactions. Saturation of non-specific membrane binding sites is less likely than with receptor-mediated process.

Fluid-phase endocytosis: The material to be endocytosed is simply present within the extracellular fluid bathing the cell surface and as the plasma membrane invaginates to form endocytic vesicle, some of the extracellular fluid is captured within the lumen of the budding vesicle. The examples include horseradish peroxidase or dextrans which are referred to as fluid-phase markers. This is associated with the slowest rates of internalization.

1.6 References

1. The Royal Society L. Nanomedicine and Nanotechnology: Opportunities and Uncertainties, <http://www.nanotech.org.uk/>
2. Couvreur P, Vauthier C. Nanotechnology: Intelligent design to treat complex disease. *Pharm Res* 2006;23:1417-1450.
3. Winau F, Westphal O, Winau R. Paul Ehrlich - in search of the magic bullet. *Microbes and Infection* 2004;6:786-789.
4. Soppimath KS, Aminabhavi TM, Kulkarni AR, Rudzinski WE. Biodegradable polymeric nanoparticles as drug delivery devices. *J Control Release* 2001;70:1-20.
5. Yoo HS, Park TG. Folate receptor targeted biodegradable polymeric doxorubicin micelles. *J Control Release* 2004;96:273-283.
6. Bizzarri R, Chiellini F, Solaro R, Chiellini E, Cammas-Marion S, Guerin P. Synthesis and characterization of new malolactonate polymers and copolymers for biomedical applications. *Macromolecules* 2002;35:1215-1223.
7. Tian D, Dubois P, Grandfils C, Jerome R. Ring-opening polymerization of 1,4,8-trioxaspiro[4.6]-9-undecanone: A new route to aliphatic polyesters bearing functional pendent groups. *Macromolecules* 1997;30:406-409.
8. Ouchi T, Ohya Y. Design of lactide copolymers as biomaterials. *J Polym Sci A Polymer Chem* 2004;42:453-462.
9. Finne A, Albertsson AC. New functionalized polyesters to achieve controlled architectures. *J Polymer Sci A: Polym Chem* 2004;42:444-452.
10. Kumar M, Kumar N, Domb AJ, Arora M. Pharmaceutical polymeric controlled drug delivery systems. *Filled Elastomers Drug Delivery Systems*; 2002. p. 45-117.
11. Lamprecht A, Ubrich N, Hombreiro Perez M, Lehr C, Hoffman M, Maincent P. Biodegradable monodispersed nanoparticles prepared by pressure homogenization-emulsification. *Int J Pharm* 1999;184:97-105.
12. Moghimi SM, Hunter AC, Murray JC. Long-circulating and target-specific nanoparticles: theory to practice. *Pharmacol Rev* 2001;53:283-318.
13. Moghimi SM, Szebeni J. Stealth liposomes and long circulating nanoparticles: critical issues in pharmacokinetics, opsonization and protein-binding properties. *Prog Lipid Res* 2003;42:463-478.

14. Brigger I, Dubernet C, Couvreur P. Nanoparticles in cancer therapy and diagnosis. *Adv Drug Deliv Rev* 2002;54:631-651.
15. Sunderland CJ, Steiert M, Talmadge JE, Derfus AM, Barry SE. Targeted nanoparticles for detecting and treating cancer. *Drug Dev Res* 2006;67:70-93.
16. Panyam J, Labhasetwar V. Biodegradable nanoparticles for drug and gene delivery to cells and tissue. *Adv Drug Deliv Rev* 2003;55:329-347.
17. Chorny M, Fishbein I, Danenberg HD, Golomb G. Lipophilic drug loaded nanospheres prepared by nanoprecipitation: effect of formulation variables on size, drug recovery and release kinetics. *J Control Release* 2002;83:389-400.
18. Gorner T, Gref R, Michenot D, Sommer F, Tran MN, Dellacherie E. Lidocaine-loaded biodegradable nanospheres. I. Optimization Of the drug incorporation into the polymer matrix. *J Control Release* 1999;57:259-268.
19. Zambaux MF, Bonneaux F, Gref R, Maincent P, Dellacherie E, Alonso MJ, et al. Influence of experimental parameters on the characteristics of poly(lactic acid) nanoparticles prepared by a double emulsion method. *J Control Release* 1998;50:31-40.
20. Xu YX, Hanna MA. Electrospray encapsulation of water-soluble protein with polylactide - Effects of formulations on morphology, encapsulation efficiency and release profile of particles. *Int J Pharm* 2006;320:30-36.
21. Luck M, Pistel KF, Li YX, Blunk T, Muller RH, Kissel T. Plasma protein adsorption on biodegradable microspheres consisting of poly(D,L-lactide-co-glycolide), poly(L-lactide) or ABA triblock copolymers containing poly(oxyethylene). Influence of production method and polymer composition. *J Control Release* 1998;55:107-120.
22. Yoo HS, Oh JE, Lee KH, Park TG. Biodegradable nanoparticles containing doxorubicin-PLGA conjugate for sustained release. *Pharm Res* 1999;16:1114-1118.
23. Sahoo SK, Panyam J, Prabha S, Labhasetwar V. Residual polyvinyl alcohol associated with poly (D,L-lactide-co-glycolide) nanoparticles affects their physical properties and cellular uptake. *J Control Release* 2002;82:105-114.
24. Panyam J, Sahoo SK, Prabha S, Bargar T, Labhasetwar V. Fluorescence and electron microscopy probes for cellular and tissue uptake of poly(D,L-lactide-co-glycolide) nanoparticles. *Int J Pharm* 2003;262:1-11.

25. Mu L, Feng SS. PLGA/TPGS nanoparticles for controlled release of paclitaxel: effects of the emulsifier and drug loading ratio. *Pharm Res* 2003;20:1864-1872.
26. Mu L, Feng SS. A novel controlled release formulation for the anticancer drug paclitaxel (Taxol): PLGA nanoparticles containing vitamin E TPGS. *J Control Release* 2003;86:33-48.
27. Mo Y, Lim LY. Mechanistic study of the uptake of wheat germ agglutinin-conjugated PLGA nanoparticles by A549 cells. *J Pharm Sci* 2004;93:20-28.
28. Molpeceres J, Aberturas MR, Guzman M. Biodegradable nanoparticles as a delivery system for cyclosporine: preparation and characterization. *J Microencapsul* 2000;17:599-614.
29. Gref R, Luck M, Quellec P, Marchand M, Dellacherie E, Harnisch S, et al. 'Stealth' corona-core nanoparticles surface modified by polyethylene glycol (PEG): influences of the corona (PEG chain length and surface density) and of the core composition on phagocytic uptake and plasma protein adsorption. *Colloids Surf B Biointerfaces* 2000;18:301-313.
30. Li Y, Pei Y, Zhang X, Gu Z, Zhou Z, Yuan W, et al. PEGylated PLGA nanoparticles as protein carriers: synthesis, preparation and biodistribution in rats. *J Control Release* 2001;71:203-211.
31. Calvo P, Gouritin B, Chacun H, Desmaele D, D'Angelo J, Noel JP, et al. Long-circulating PEGylated polycyanoacrylate nanoparticles as new drug carrier for brain delivery. *Pharm Res* 2001;18:1157-1166.
32. Gbadamosi JK, Hunter AC, Moghimi SM. PEGylation of microspheres generates a heterogeneous population of particles with differential surface characteristics and biological performance. *FEBS Lett* 2002;532:338-344.
33. Ameller T, Marsaud V, Legrand P, Gref R, Barratt G, Renoir JM. Polyester-poly(ethylene glycol) nanoparticles loaded with the pure antiestrogen RU 58668: physicochemical and opsonization properties. *Pharm Res* 2003;20:1063-1070.
34. Matsumoto J, Nakada Y, Sakurai K, Nakamura T, Takahashi Y. Preparation of nanoparticles consisted of poly(L-lactide)-poly(ethylene glycol)-poly(L-lactide) and their evaluation in vitro. *Int J Pharm* 1999;185:93-101.
35. Dong YC, Feng SS. Methoxy poly(ethylene glycol)-poly(lactide) (MPEG-PLA) nanoparticles for controlled delivery of anticancer drugs. *Biomaterials* 2004;25:2843-2849.

36. Sant S, Nadeau V, Hildgen P. Effect of porosity on the release kinetics of propafenone-loaded PEG-g-PLA nanoparticles. *J Control Release* 2005;107:203-214.
37. Zhang Y, Zhang J. Surface modification of monodisperse magnetite nanoparticles for improved intracellular uptake to breast cancer cells. *J Colloid Interface Sci* 2005;283:352-357.
38. Fang C, Shi B, Pei YY, Hong MH, Wu J, Chen HZ. In vivo tumor targeting of tumor necrosis factor-alpha-loaded stealth nanoparticles: Effect of MePEG molecular weight and particle size. *Eur J Pharm Sci* 2006;27:27-36.
39. Peracchia MT, Vauthier C, Puisieux F, Couvreur P. Development of sterically stabilized poly(isobutyl 2-cyanoacrylate) nanoparticles by chemical coupling of poly(ethylene glycol). *J Biomed Mater Res* 1997;34:317-326.
40. Zhang QZ, Zha LS, Zhang Y, Jiang WM, Lu W, Shi ZQ, et al. The brain targeting efficiency following nasally applied MPEG-PLA nanoparticles in rats. *J Drug Target* 2006;14:281-290.
41. Couvreur P, Kante B, Grislain L, Roland M, Speiser P. Toxicity of polyalkylcyanoacrylate nanoparticles II: Doxorubicin-loaded nanoparticles. *J Pharm Sci* 1982;71:790-792.
42. Gibaud S, Andreux JP, Weingarten C, Renard M, Couvreur P. Increased bone marrow toxicity of doxorubicin bound to nanoparticles. *Eur J Cancer* 1994;30A:820-826.
43. Nemati F, Dubernet C, Fessi H, Colin de Verdiere A, Poupon MF, Puisieux F, et al. Reversion of multidrug resistance using nanoparticles in vitro: influence of the nature of the polymer. *Int J Pharm* 1996;138:237-246.
44. Soma CE, Dubernet C, Bentolila D, Benita S, Couvreur P. Reversion of multidrug resistance by co-encapsulation of doxorubicin and cyclosporin A in polyalkylcyanoacrylate nanoparticles. *Biomaterials* 2000;21:1-7.
45. Colin de Verdiere A, Dubernet C, Nemati F, Poupon MF, Puisieux F, Couvreur P. Uptake of doxorubicin from loaded nanoparticles in multidrug-resistant leukemic murine cells. *Cancer Chemother Pharmacol* 1994;33:504-508.
46. Mosqueira VC, Legrand P, Gulik A, Bourdon O, Gref R, Labarre D, et al. Relationship between complement activation, cellular uptake and surface

- physicochemical aspects of novel PEG-modified nanocapsules. *Biomaterials* 2001;22:2967-2979.
47. Mosqueira VC, Legrand P, Morgat JL, Vert M, Mysiakine E, Gref R, et al. Biodistribution of long-circulating PEG-grafted nanocapsules in mice: effects of PEG chain length and density. *Pharm Res* 2001;18:1411-1419.
 48. Raffin Pohlmann A, Weiss V, Mertins O, Pesce da Silveira N, Staniscuaski Guterres S. Spray-dried indomethacin-loaded polyester nanocapsules and nanospheres: development, stability evaluation and nanostructure models. *Eur J Pharm Sci* 2002;16:305-312.
 49. Vonarbourg A, Passirani C, Saulnier P, Simard P, Leroux JC, Benoit JP. Evaluation of pegylated lipid nanocapsules versus complement system activation and macrophage uptake. *J Biomed Mater Res A* 2006;78A:620-628.
 50. Rosca ID, Watari F, Uo M. Microparticle formation and its mechanism in single and double emulsion solvent evaporation. *J Control Release* 2004;99:271-280.
 51. Bilati U. Poly(D,L-lactide-co-glycolide) protein-loaded nanoparticles prepared by the double emulsion method-processing and formulation issues for enhanced entrapment efficiency. *J Microencapsul* 2005;22:205-214.
 52. Ren J, Hong HY, Song JX, Ren TB. Particle size and distribution of biodegradable poly-D,L-lactide-co-poly(ethylene glycol) block polymer nanoparticles prepared by nanoprecipitation. *J Appl Polym Sci* 2005;98:1884-1890.
 53. Owens DE, Peppas NA. Opsonization, biodistribution, and pharmacokinetics of polymeric nanoparticles. *Int J Pharm* 2006;307:93-102.
 54. Passirani C, Benoit JP. Complement activation by injectable colloidal drug carriers. In: Mahato R, editor. *Biomaterials for delivery and targeting of proteins and nucleic acids*. Boca Raton: CRC Press; 2005. p. 187-230.
 55. Lian T, Ho RJ. Trends and developments in liposome drug delivery systems. *J Pharm Sci* 2001;90:667-680.
 56. Awasthi VD, Garcia D, Goins BA, Phillips WT. Circulation and biodistribution profiles of long-circulating PEG-liposomes of various sizes in rabbits. *Int J Pharm* 2003;253:121-132.
 57. Raghavan D, Gu X, Nguyen T, VanLandingham M, Karim A. Mapping Polymer Heterogeneity Using Atomic Force Microscopy Phase Imaging and Nanoscale Indentation. *Macromolecules* 2000;33:2573-2583.

58. Kopp-Marsaudon S, Leclere P, Dubourg F, Lazzaroni R, Aime JP. Quantitative Measurement of the Mechanical Contribution to Tapping-Mode Atomic Force Microscopy Images of Soft Materials. *Langmuir* 2000;16:8432-8437.
59. Magonov SN, Elings V, Whangbo MH. Phase imaging and stiffness in tapping-mode atomic force microscopy. *Surf Sci* 1997;375:L385-L391.
60. Paredes JI, Gracia M, Martinez-Alonso A, Tascon JMD. Nanoscale investigation of the structural and chemical changes induced by oxidation on carbon black surfaces: A scanning probe microscopy approach. *J Colloid Interface Sci* 2005;288:190-199.
61. Rizkalla N, Range C, Lacasse FX, Hildgen P. Effect of various formulation parameters on the properties of polymeric nanoparticles prepared by multiple emulsion method. *J Microencapsul* 2006;23:39-57.
62. Lowell S, Shields JE, Thomas MA, Thommes M, editors. *Characterization of Porous Solids and Powders: Surface Area, Pore Size and Density*. Dordrecht: Kluwer Academic Publishers; 2004.
63. Sing KSW, Everett DH, Haul RAW, Moscou L, Pierotti RA, Rouquerol J, et al. Reporting Physisorption Data for Gas Solid Systems with Special Reference to the Determination of Surface-Area and Porosity (Recommendations 1984). *Pure Appl Chem* 1985;57:603-619.
64. Sing KSW. Adsorption methods for the characterization of porous materials. *Adv Colloid Interface Sci* 1998;77:3-11.
65. Horvath G; Kawazoe K. Method for the calculation of effective pore size distribution in molecular sieve carbon. *J Chem Eng Japan* 1983;16:470-475.
66. Dombrowski RJ, Lastoskie CM, Hyduke DR. The Horvath-Kawazoe method revisited. *Colloid Surf A Physicochem Eng Asp* 2001;187:23-39.
67. Sing KSW. Characterization of porous materials: past, present and future. *Colloid Surf A Physicochem Eng Asp* 2004;241:3-7.
68. Mu L, Feng SS. Vitamin E TPGS used as emulsifier in the solvent evaporation/extraction technique for fabrication of polymeric nanospheres for controlled release of paclitaxel (Taxol). *J Control Release* 2002;80:129-144.
69. Okada H, Doken Y, Ogawa Y, Toguchi H. Preparation of three-month depot injectable microspheres of leuprorelin acetate using biodegradable polymers. *Pharm Res* 1994;11:1143-1147.

70. Sung KC. Controlled release of nalbuphine prodrugs from biodegradable polymeric matrices: influence of prodrug hydrophilicity and polymer composition. *Int J Pharm* 1998;172:17-25.
71. Crowley MM, Schroeder B, Fredersdorf A, Obara S, Talarico M, Kucera S, et al. Physicochemical properties and mechanism of drug release from ethyl cellulose matrix tablets prepared by direct compression and hot-melt extrusion. *Int J Pharm* 2004;269:509-522.
72. Labhasetwar V. Nanotechnology for drug and gene therapy: the importance of understanding molecular mechanisms of delivery. *Cur Opin Biotechnol* 2005;16:674.
73. Horbett TA, Cooper KW, Lew KR, Ratner BD. Rapid postadsorptive changes in fibrinogen adsorbed from plasma to segmented polyurethanes. *J Biomater Sci Polym Ed* 1998;9:1071-1087.
74. Moghimi SM, Hunter AC. Capture of stealth nanoparticles by the body's defences. *Crit Rev Ther Drug Carrier Syst* 2001;18:527-550.
75. Gref R, Domb A, Quellec P, Blunk T, Muller RH, Verbavatz JM, et al. The controlled intravenous delivery of drugs using PEG-coated sterically stabilized nanospheres. *Adv Drug Deliv Rev* 1995;16:215-233.
76. Woodle MC. Controlling liposome blood clearance by surface-grafted polymers. *Adv Drug Deliv Rev* 1998;32:139-152.
77. Ruan G, Feng SS. Preparation and characterization of poly(lactic acid)-poly(ethylene glycol)-poly(lactic acid) (PLA-PEG-PLA) microspheres for controlled release of paclitaxel. *Biomaterials* 2003;24:5037-5044.
78. Quellec P, Gref R, Dellacherie E, Sommer F, Tran MD, Alonso MJ. Protein encapsulation within poly(ethylene glycol)-coated nanospheres. II. Controlled release properties. *J Biomed Mater Res* 1999;47:388-395.
79. Yamamoto Y, Nagasaki Y, Kato Y, Sugiyama Y, Kataoka K. Long-circulating poly(ethylene glycol)-poly(D,L-lactide) block copolymer micelles with modulated surface charge. *J Control Release* 2001;77:27-38.
80. Quesnel R, Hildgen P. Synthesis of PLA-b-PEG multiblock copolymers for stealth drug carrier preparation. *Molecules* 2005;10:98-104.

81. Nagahama K, Ohya Y, Ouchi T. Suppression of cell and platelet adhesion to star-shaped 8-armed poly(ethylene glycol)-poly(L-lactide) block copolymer films. *Macromol Biosci* 2006;6:412-419.
82. Michel R, Pasche S, Textor M, Castner DG. Influence of PEG Architecture on Protein Adsorption and Conformation. *Langmuir* 2005;21:12327-12332.
83. Rieger J, Passirani C, Benoit JP, Van Butsele K, Jerome R, Jerome C. Synthesis of amphiphilic copolymers of poly(ethylene oxide) and poly(epsilon-caprolactone) with different architectures, and their role in the preparation of stealthy nanoparticles. *Adv Functional Mater* 2006;16:1506-1514.
84. Jeon SI, Lee JH, Andrade JD, De Gennes PG. Protein-surface interactions in the presence of polyethylene oxide I. Simplified theory. *J Colloid Interface Sci* 1991;142:149-158.
85. Jeon SI, Andrade JD. Protein surface interactions in the presence of polyethylene oxide II. Effect of protein size. *J Colloid Interface Sci* 1991;142:159-166.
86. Gessner A, Waicz R, Lieske A, Paulke B, Mader K, Muller RH. Nanoparticles with decreasing surface hydrophobicities: influence on plasma protein adsorption. *Int J Pharm* 2000;196:245-249.
87. Kim J, Somorjai GA. Molecular packing of lysozyme, fibrinogen, and bovine serum albumin on hydrophilic and hydrophobic surfaces studied by infrared-visible sum frequency generation and fluorescence microscopy. *J Am Chem Soc* 2003;125:3150-3158.
88. Muller RH, Ruhl D, Luck M, Paulke BR. Influence of fluorescent labelling of polystyrene particles on phagocytic uptake, surface hydrophobicity, and plasma protein adsorption. *Pharm Res* 1997;14:18-24.
89. Takeuchi H, Kojima H, Yamamoto H, Kawashima Y. Evaluation of circulation profiles of liposomes coated with hydrophilic polymers having different molecular weights in rats. *J Control Release* 2001;75:83-91.
90. Metselaar JM, Bruin P, de Boer LW, de Vringer T, Snel C, Oussoren C, et al. A novel family of L-amino acid-based biodegradable polymer-lipid conjugates for the development of long-circulating liposomes with effective drug-targeting capacity. *Bioconjug Chem* 2003;14:1156-1164.
91. Torchilin VP, Trubetskoy VS. Which polymers can make nanoparticulate drug carriers long-circulating? *Adv Drug Deliv rev* 1995;16:141-155.

92. Milner ST. Polymer brushes. *Science* 1991;251:905-914.
93. Dan N. Effect of liposome charge and PEG polymer layer thickness on cell-liposome electrostatic interactions. *Biochim Biophys Acta* 2002;1564:343-348.
94. Roser M, Fischer D, Kissel T. Surface-modified biodegradable albumin nano- and microspheres. II: effect of surface charges on in vitro phagocytosis and biodistribution in rats. *Eur J Pharm Biopharm* 1998;46:255-263.
95. Popielarski SR, Pun SH, Davis ME. A nanoparticle-based model delivery system to guide the rational design of gene delivery to the liver. 1. Synthesis and characterization. *Bioconjug Chem* 2005;16:1063-1070.
96. Gessner A, Lieske A, Paulke B, Muller R. Influence of surface charge density on protein adsorption on polymeric nanoparticles: analysis by two-dimensional electrophoresis. *Eur J Pharm Biopharm* 2002;54:165-170.
97. Torchilin VP, Omelyanenko VG, Papisov MI, Bogdanov AA, Jr., Trubetskoy VS, Herron JN, et al. Poly(ethylene glycol) on the liposome surface: on the mechanism of polymer-coated liposome longevity. *Biochim Biophys Acta* 1994;1195:11-20.
98. Papisov MI. Theoretical considerations of RES-avoiding liposomes: Molecular mechanics and chemistry of liposome interactions. *Adv Drug Deliv Rev* 1998;32:119-138.
99. Torchilin VP. Polymer-coated long-circulating microparticulate pharmaceuticals. *J Microencapsul* 1998;15:1-19.
100. Kwon GS. Polymeric micelles for delivery of poorly water-soluble compounds. *Crit Rev Ther Drug Carrier Syst* 2003;20:357-403.
101. Peracchia MT. Stealth nanoparticles for intravenous administration. *S T P Pharma Sci* 2003;13:155-161.
102. Minko T. Mechanisms of Cellular Drug Resistance and Strategies to Overcome it. In: Mahato R, editor. *Biomaterials for Delivery and Targeting of Proteins and Nucleic Acids*. Boca Raton: CRC Press; 2005. p. 461-492.
103. Cuenca AG, Jiang HB, Hochwald SN, Delano M, Cance WG, Grobmyer SR. Emerging implications of nanotechnology on cancer diagnostics and therapeutics. *Cancer* 2006;107:459-466.
104. Maeda H, Greish K, Fang J. The EPR effect and polymeric drugs: A paradigm shift for cancer chemotherapy in the 21st century. *Polymer Therapeutics I: Polymers as Drugs, Conjug Gene Deliv Syst*; 2006. p. 103-121.

105. Sahoo SK, Labhasetwar V. Nanotech approaches to delivery and imaging drug. *Drug Discovery Today* 2003;8:1112-1120.
106. Soma CE, Dubernet C, Barratt G, Nemati F, Appel M, Benita S, et al. Ability of doxorubicin-loaded nanoparticles to overcome multidrug resistance of tumor cells after their capture by macrophages. *Pharm Res* 1999;16:1710-1716.
107. Astier A, Doat B, Ferrer MJ, Benoit G, Fleury J, Rolland A, et al. Enhancement of adriamycin antitumor activity by its binding with an intracellular sustained-release form, polymethacrylate nanospheres, in U-937 cells. *Cancer Res* 1988;48:1835-1841.
108. Jie P, Venkatraman SS, Min F, Freddy BYC, Huat GL. Micelle-like nanoparticles of star-branched PEO-PLA copolymers as chemotherapeutic carrier. *J Control Release* 2005;110:20-33.
109. Yang YY, Wang Y, Powell R, Chan P. Polymeric core-shell nanoparticles for therapeutics. *Clin Exper Pharmacol Physiol* 2006;33:557-562.
110. Masayuki Y. Drug targeting with nano-sized carrier systems. *J Artif Org* 2005;8:77-84.
111. Parveen S, Sahoo SK. Nanomedicine : clinical applications of polyethylene glycol conjugated proteins and drugs. *Clin Pharmacokinet* 2006;45:965-988.
112. Moghimi SM, Hunter AC, Murray JC. Nanomedicine: current status and future prospects. *Faseb J* 2005;19:311-330.
113. Xiong XB, Huang Y, Lu WL, Zhang X, Zhang H, Nagai T, et al. Enhanced intracellular delivery and improved antitumor efficacy of doxorubicin by sterically stabilized liposomes modified with a synthetic RGD mimetic. *J Control Release* 2005;107:262-275.
114. Xiong XB, Huang Y, Lu WL, Zhang X, Zhang H, Nagai T, et al. Intracellular delivery of doxorubicin with RGD-modified sterically stabilized liposomes for an improved antitumor efficacy: In vitro and in vivo. *J Pharm Sci* 2005;94:1782-1793.

Chapter 2.
Hypotheses and objectives

2.1 Hypotheses

2.1.1 Hypothesis 1

Formulation factors like initial drug loading levels will affect microporosity and hence, the drug release kinetics of polymeric nanoparticles. Nitrogen gas adsorption technique can be used to probe the microporosity of nanoparticles.

2.1.1.1 Justification for studying drug release kinetics

Polymeric nanoparticles (NPs) offer suitable means for delivering various therapeutic agents by either localized or targeted delivery to the tissue of interest [1-9] at a therapeutically optimal rate. Various therapeutic agents such as antibiotics, anti-inflammatory drugs, anticancer agents, proteins and peptides have been encapsulated in polymeric NPs. Since pharmacokinetic properties of these agents are different, drug release rate should be tailored in order to achieve optimum plasma drug concentration and therapeutic effect as per the need. Also, the issue of drug release from nanocarriers still remains central to cancer chemotherapy. It has been shown that stealth liposomes of entrapped cisplatin lack antitumor activity despite of its accumulation in tumor interstitium. This was attributed to the poor and extremely slow release of cisplatin from extravasated liposomes [10]. This underlines the importance of optimizing drug release kinetics from various drug delivery systems.

Drug release from polymeric matrix systems is governed by diffusion of the drug in the matrix as well as the matrix erosion resulting from degradation and dissolution of smaller weight polymer. These processes are affected by physicochemical properties of the drug, polymer and the drug delivery system along with various formulation factors. The pharmaceutical properties of NPs include carrier nature, particle size and size distribution, surface and bulk morphology, surface chemistry, charge, encapsulation efficiency and *in vitro* drug release kinetics. Also, another important issue is the influence of formulation factors including nature and concentration of polymer/s used, type and concentration of emulsifiers, ratio of oil to water phase, effect of centrifugation, lyophilization etc. on the final properties of NPs. Although many of these factors have been investigated in detail to

improve above-mentioned pharmaceutical properties of NPs [11-17], very few studies have undertaken detailed investigation of mechanism of release from NPs [18-26]. Unfortunately, the experiments in this field can only observe the macroscopic behavior of drug release, and the information on the drug diffusion mechanism in polymer at molecular level is still very limited. Knowledge on the diffusion mechanism of drug molecules in polymer matrix and the intermolecular interactions of drug molecules with the polymer chains would help us to understand the diffusion of drug molecules in polymeric nanocarriers and finally, it would guide us to design a controlled release material for a specified drug. Research in this area is still lacking probably due to unavailability of high resolution methods to probe into internal microporous structure of these nanosized materials.

2.1.1.2 Gas adsorption and microstructure of NPs

It is very well known that bulk and surface morphology can have profound effect on release properties on NPs [27]. Although surface morphology of NPs has been studied qualitatively by scanning electron microscope (SEM) [28-30], atomic force microscope (AFM) [28, 29, 31] and transmission electron microscope (TEM) [30-32], there are no reports on the elucidation of bulk morphology of NPs, especially relating to their microporous structure. *Since small pores in few nanometer range can affect matrix hydration, drug diffusion into release medium as well as polymer degradation [33], it is of great importance to gain insight into these small pores (micropores) during NP formation. In the first part of this thesis, we propose to undertake extensive investigation of effect of various formulation variables studied so far on the microstructure of NPs and in turn, on their release kinetics. We hypothesize that formulation factors (e.g. drug loading) will affect the internal structure, especially microporosity of NPs and this will have global effect on release profiles of the encapsulated drugs. We also hypothesize that these changes in microporosity (in few angstroms) will be more important in determining the rate of release from NPs than changes in bigger mesopores. Here, micropores are defined as the pores smaller than 2 nm and mesopores are in the size range of 2-50 nm. It is quite logical to assume that bigger mesopores will either be absent or rarely present in NPs of size 200 nm. Interestingly, in parallel with our studies, there is a recent report on pore size distribution measured by NMR cryoporometry, where Petrov et al [33] have*

correlated pore size distribution in 30-70 nm to the swelling and drug release kinetics. However, it should be noted that the study was carried out on microparticles and not on nanoparticles.

In this regards, *we propose application of gas adsorption technique to investigate microporosity* of NPs of 200 nm in size. This technique allows assessment of a wide range of pore sizes (from 0.35 nm to 100 nm), which includes the complete range of micro- and mesopores, and even (partially) macropores. The analysis of a nitrogen isotherm allows one to obtain parameters such as total pore volume, micropore volume, BET surface area, pore size distribution (PSD) as well as surface fractal dimension. These parameters are commonly used for characterization of zeolites, clays and various catalysts [34-37]. Although these parameters can prove to be very useful in understanding the surface morphology as well as microstructure of NPs, their use in the area of drug delivery is not reported so far. Hence, the initial investigation was planned to verify the usefulness of this technique for characterization of NPs for the first time in the field of NPs, and establish the relationship between microporosity and drug release kinetics.

2.1.2 Hypothesis 2

Molecular architecture (block or graft) of the polymer will define the internal structure as well as the microporosity of nanoparticles during their formation through definite reorganization of different chains. This, in turn, will affect drug release rate.

2.1.2.1 Justification of studying effect of polymer architecture on release kinetics

To further confirm the first hypothesis, PLA homopolymer, and its pegylated copolymers with different molecular architecture (graft or linear block copolymer) were used to prepare NPs. It was hypothesized that polymers would rearrange differently during NP formation depending on their architecture, leading to important change in the internal NP structure, which will consequently affect drug release kinetics.

A poor correlation exists between effect of PEG incorporation into NPs and their release properties. Some authors have reported increased drug release with increased PEG content [14, 20, 21], whereas others reported the reverse trend [38] and some others have

reported no or only slight effect of PEG incorporation on the release rate [39, 40]. It is worthy to mention that various polymer architectures are being synthesized recently for controlled and targeted drug delivery; however, very few studies compare different polymer architectures for their *in vitro* properties [41, 42]. One such recent study includes comparison of diblock, triblock and star-shaped copolymer of PLA and PEG indicating clear differences in their morphology and release properties [41]. This demands further studies on polymer architecture to elucidate differences in properties of drug delivery systems, and more importantly, it would also offer a valuable feedback to properly tune and optimize biopolymers of a new generation for high-quality drug products.

2.1.3 Hypothesis 3

Molecular architecture of the polymer will also affect the surface properties of the NPs due to chain reorganization during nanoparticle formation. This will influence the protein binding ability and cellular interactions of these nanoparticles.

2.1.3.1 Justification for studying surface properties

Today the concept of drug delivery is not limited to prolonging the duration of drug release; instead, it implies at least two strategies for realizing temporal (predetermined drug release kinetics) and spatial distribution control (precisely directing the drug vehicle to the desired site of action) in the body. To achieve this, various nanosystems have been developed using a multidisciplinary approach based on chemistry, material science, bioengineering, biology and medicine. This approach has brought to notice the significance of polymer architecture-property relationships. Polymer architecture markedly influences not only the physicochemical properties of the polymer, but also various aspects of the drug delivery system including drug release rate, biodistribution and even interaction with specific tissues or cells *in vivo* [43]. Thus, optimizing polymer architecture is an intelligent strategy to develop desired pharmaceutical product. Such studies would offer valuable feedback to tune properties of polymer-based drug delivery systems.

In the area of colloidal drug delivery systems, it is a major concern how particles interact when they come in contact with the physiological fluids or tissues. Hence, surface

properties of NPs must be properly designed to maximize the potential for favorable and minimize for unfavorable interactions.

Once the long-circulating carrier reaches the desired tissue, the next step is its intracellular entry. Intracellular trafficking of macromolecules is a very complex phenomenon and has been reviewed recently [44]. It involves different pathways like phagocytosis (for large particles and by specialized cells like macrophages, neutrophils and dendritic cells) and pinocytosis (generally common to all cells) as discussed before in the introduction. Which of these pathways are involved in the uptake mechanism of the carrier will be dependent on its surface properties and will decide the extent of uptake into the cells. *While several studies correlate various physicochemical properties to protein adsorption and/or in vitro phagocytosis of these particles in macrophages, reports focusing on their uptake mechanisms are still lacking in the literature.* Indeed, cellular uptake mechanisms have been studied in detail for various other cell lines including epithelial and cancer cell lines whereas their role in macrophage uptake was seldom studied except few studies like Raynal et al [45]. They have demonstrated scavenger receptor mediated endocytosis of superparamagnetic iron oxide NPs by mouse peritoneal macrophages. It is reported that phagocytosis takes place for particles larger than 500 nm in size; however, it is not yet clear why and how smaller particles are then taken up by macrophages. It is possible that macrophages can effectively take up these 200 nm or smaller particles by mechanisms other than phagocytosis. Although it is shown that presence of PEG on the surface of these NPs reduces their macrophage uptake, whether it is really by reduced phagocytosis or by other mechanisms like endocytosis, macropinocytosis or fluid phase pinocytosis still remains a topic of research. Further, if this reduced macrophage uptake of small size NPs is by reduced endocytosis, the same rule will definitely be extended to other non-phagocytic cells in the body, thus seriously hampering the efficacy of intracellular distribution of pegylated NPs. In fact, incorporation of PEG has demonstrated usefulness in controlling pharmacokinetics of the carriers on one hand while hampering their interaction with the targeted cells and thus, therapeutic efficiency, especially in gene delivery [46-50]. *Hence, in the second part of this thesis, work was undertaken to evaluate effect of diverse molecular architecture of formulated pegylated NPs on their surface properties. Further, efforts were made to find out correlation between these physicochemical properties with their protein adsorption and in vitro*

macrophage uptake. Also, detailed investigation was carried out to shed some light on their uptake mechanism/s by macrophages.

2.2 Objectives

The challenge of modern drug delivery systems is optimization of the activity of drug coupled with the reduction of its side effects *in vivo*. One approach is the use of colloidal drug carriers like nanoparticles (NPs) that can provide site-specific drug delivery combined with optimal drug release profiles. Release kinetics of drug from NPs can be influenced by various factors such as size, drug-polymer interaction, internal structure of the matrix etc. Although majority of factors have been studied previously, the reports on importance of micropores and porosity of NPs are still lacking probably due to the availability of methods with high resolution. Thus, first goal of this study was to gain insight into microporosity of NPs and establish a correlation between microporosity and drug release kinetics. An important objective was to establish whether polymeric NPs possess definite/reproducible internal structure during their formation by emulsion-solvent evaporation method. It was sought to find out the effect of formulation factors like drug loading and polymer architecture on their internal structure and subsequently, on the release kinetics. After optimizing the release rate from NPs, it is equally important to pay attention to properties such as charge, surface chemistry, protein resistant capacity and cytocompatibility for their stability and use *in vivo*. Thus, the second goal was complete characterization of their physicochemical and biological properties along with the study of mechanism of their intracellular uptake to test the feasibility of their use *in vivo* for any therapeutic application.

Thus major objectives were:

1. Synthesis and characterization of biodegradable polyester-based polymers like poly(D,L-Lactide) (PLA), polyethylene glycol grafted on the backbone of PLA (PEG-g-PLA) and multiblock copolymer of PLA and PEG (PLA-PEG-PLA)_n.
2. Optimize the preparation of NPs using these polymers and Propafenone.HCl (Prop), a model drug.

3. Physicochemical characterization of prepared NPs for particle size, drug loading efficiency, differential scanning calorimetry, drug release kinetics, surface morphology by Atomic force microscopy etc.
4. Porosimetry (microporosity, fractal dimension, total pore volume, BET surface area etc.) of prepared NPs and effect of different parameters like polymer type, polymer molecular weight, effect of solvent evaporation method, effect of drug loading etc. on porosimetry of these NPs.
5. Establishment of correlation between microporosity and drug release kinetics of NPs.
6. Chemical surface characterization of NPs using XPS technique
7. Zeta potential measurement and plasma protein adsorption studies using SDS-PAGE on pegylated and non-pegylated NPs
8. Characterization of prepared NPs for their cytotoxicity (along with the safety of blank nanoparticles) and mechanism of their intracellular uptake using murine macrophage cell line (RAW 264.7)

2.3 References

1. Panyam J, Labhasetwar V. Biodegradable nanoparticles for drug and gene delivery to cells and tissue. *Adv Drug Deliv Rev* 2003;55:329-347.
2. Soppimath KS, Aminabhavi TM, Kulkarni AR, Ruzdzinski WE. Biodegradable polymeric nanoparticles as drug delivery devices. *J Control Release* 2001;70:1-20.
3. Moghimi SM, Hunter AC, Murray JC. Long-circulating and target-specific nanoparticles: theory to practice. *Pharmacol Rev* 2001;53:283-318.
4. Brigger I, Dubernet C, Couvreur P. Nanoparticles in cancer therapy and diagnosis. *Adv Drug Deliv Rev* 2002;54:631-651.
5. Sunderland CJ, Steiert M, Talmadge JE, Derfus AM, Barry SE. Targeted nanoparticles for detecting and treating cancer. *Drug Dev Res* 2006;67:70-93.

6. Smith MW, Gumbleton M. Endocytosis at the blood-brain barrier: From basic understanding to drug delivery strategies. *J Drug Target* 2006;14:191-214.
7. Roney C, Kulkarni P, Arora V, Antich P, Bonte F, Wu AM, et al. Targeted nanoparticles for drug delivery through the blood-brain barrier for Alzheimer's disease. *J Control Release* 2005;108:193-214.
8. Couvreur P, Gref R, Andrieux K, Maivy C. Nanotechnologies for drug delivery: Application to cancer and autoimmune diseases. *Prog Solid State Chem* 2006;34:231-235.
9. Yang YY, Wang Y, Powell R, Chan P. Polymeric core-shell nanoparticles for therapeutics. *Clinical and Experimental Pharmacology and Physiology* 2006;33:557-562.
10. Moghimi SM, Hunter AC, Murray JC. Nanomedicine: current status and future prospects. *Faseb J* 2005;19:311-330.
11. Mu L, Feng SS. PLGA/TPGS nanoparticles for controlled release of paclitaxel: effects of the emulsifier and drug loading ratio. *Pharm Res* 2003;20:1864-1872.
12. Yoo HS, Oh JE, Lee KH, Park TG. Biodegradable nanoparticles containing doxorubicin-PLGA conjugate for sustained release. *Pharm Res* 1999;16:1114-1118.
13. Lamprecht A, Ubrich N, Hombreiro Perez M, Lehr C, Hoffman M, Maincent P. Biodegradable monodispersed nanoparticles prepared by pressure homogenization-emulsification. *Int J Pharm* 1999;184:97-105.
14. Matsumoto J, Nakada Y, Sakurai K, Nakamura T, Takahashi Y. Preparation of nanoparticles consisted of poly(L-lactide)-poly(ethylene glycol)-poly(L-lactide) and their evaluation in vitro. *Int J Pharm* 1999;185:93-101.
15. Zambaux MF, Bonneaux F, Gref R, Maincent P, Dellacherie E, Alonso MJ, et al. Influence of experimental parameters on the characteristics of poly(lactic acid) nanoparticles prepared by a double emulsion method. *J Control Release* 1998;50:31-40.
16. Murakami H, Kobayashi M, Takeuchi H, Kawashima Y. Further application of a modified spontaneous emulsification solvent diffusion method to various types of PLGA and PLA polymers for preparation of nanoparticles. *Powder Technol* 2000;107:137-143.

17. Zhang ZP, Feng SS. The drug encapsulation efficiency, in vitro drug release, cellular uptake and cytotoxicity of paclitaxel-loaded poly(lactide)-tocopheryl polyethylene glycol succinate nanoparticles. *Biomaterials* 2006;27:4025-4033.
18. Chia HH, Yang YY, Chung TS, Ng S, Heller J. Auto-catalyzed poly(ortho ester) microspheres: a study of their erosion and drug release mechanism. *J Control Release* 2001;75:11-25.
19. Bittner B, Witt C, Mader K, Kissel T. Degradation and protein release properties of microspheres prepared from biodegradable poly(lactide-co-glycolide) and ABA triblock copolymers: influence of buffer media on polymer erosion and bovine serum albumin release. *J Control Release* 1999;60:297-309.
20. Quellec P, Gref R, Dellacherie E, Sommer F, Tran MD, Alonso MJ. Protein encapsulation within poly(ethylene glycol)-coated nanospheres. II. Controlled release properties. *J Biomed Mater Res* 1999;47:388-395.
21. Lemaire V, Belair J, Hildgen P. Structural modeling of drug release from biodegradable porous matrices based on a combined diffusion/erosion process. *Int J Pharm* 2003;258:95-107.
22. Yang YY, Chung TS, Ng NP. Morphology, drug distribution, and in vitro release profiles of biodegradable polymeric microspheres containing protein fabricated by double-emulsion solvent extraction/evaporation method. *Biomaterials* 2001;22:231-241.
23. Frank A, Rath SK, Venkatraman SS. Controlled release from bioerodible polymers: effect of drug type and polymer composition. *J Control Release* 2005;102:333-344.
24. Gorner T, Gref R, Michenot D, Sommer F, Tran MN, Dellacherie E. Lidocaine-loaded biodegradable nanospheres. I. Optimization Of the drug incorporation into the polymer matrix. *J Control Release* 1999;57:259-268.
25. Chorny M, Fishbein I, Danenberg HD, Golomb G. Lipophilic drug loaded nanospheres prepared by nanoprecipitation: effect of formulation variables on size, drug recovery and release kinetics. *J Control Release* 2002;83:389-400.
26. Sant S, Nadeau V, Hildgen P. Effect of porosity on the release kinetics of propafenone-loaded PEG-g-PLA nanoparticles. *J Control Release* 2005;107:203-214.

27. Feng SS, Chien S. Chemotherapeutic engineering: Application and further development of chemical engineering principles for chemotherapy of cancer and other diseases. *Chem Eng Sci* 2003;58:4087-4114.
28. Dubes A, Parrot-Lopez H, Abdelwahed W, Degobert G, Fessi H, Shahgaldian P, et al. Scanning electron microscopy and atomic force microscopy imaging of solid lipid nanoparticles derived from amphiphilic cyclodextrins. *Eur J Pharm Biopharm* 2003;55:279-282.
29. Mu L, Feng SS. A novel controlled release formulation for the anticancer drug paclitaxel (Taxol): PLGA nanoparticles containing vitamin E TPGS. *J Control Release* 2003;86:33-48.
30. Molpeceres J, Aberturas MR, Guzman M. Biodegradable nanoparticles as a delivery system for cyclosporine: preparation and characterization. *J Microencapsul* 2000;17:599-614.
31. Zhang Y, Zhang J. Surface modification of monodisperse magnetite nanoparticles for improved intracellular uptake to breast cancer cells. *J Colloid Interface Sci* 2005;283:352-357.
32. Panyam J, Sahoo SK, Prabha S, Bargar T, Labhasetwar V. Fluorescence and electron microscopy probes for cellular and tissue uptake of poly(D,L-lactide-co-glycolide) nanoparticles. *Int J Pharm* 2003;262:1-11.
33. Petrov O, Furo I, Schuleit M, Domanig R, Plunkett M, Daicic J. Pore size distributions of biodegradable polymer microparticles in aqueous environments measured by NMR cryoporometry. *Int J Pharm* 2006;309:157-162.
34. Lee JF, Lee CK, Juang LC. Size Effects of Exchange Cation on the Pore Structure and Surface Fractality of Montmorillonite. *J Colloid Interface Sci* 1999;217:172-176.
35. El Shafei GM, Philip CA, Moussa NA. Fractal analysis of hydroxyapatite from nitrogen isotherms. *J Colloid Interface Sci* 2004;277:410-416.
36. Wang CC, Juang LC, Lee CK, Hsu TC, Lee JF, Chao HP. Effects of exchanged surfactant cations on the pore structure and adsorption characteristics of montmorillonite. *J Colloid Interface Sci* 2004;280:27-35.
37. Wang CC, Juang LC, Hsu TC, Lee CK, Lee JF, Huang FC. Adsorption of basic dyes onto montmorillonite. *J Colloid Interface Sci* 2004;273:80-86.

38. Peracchia MT, Gref R, Minamitake Y, Domb A, Lotan N, Langer R. PEG-coated nanospheres from amphiphilic diblock and multiblock copolymers: Investigation of their drug encapsulation and release characteristics. *J Control Release* 1997;46:223-231.
39. Ameller T, Marsaud V, Legrand P, Gref R, Barratt G, Renoir JM. Polyester-poly(ethylene glycol) nanoparticles loaded with the pure antiestrogen RU 58668: physicochemical and opsonization properties. *Pharm Res* 2003;20:1063-1070.
40. Gref R, Quellec P, Sanchez A, Calvo P, Dellacherie E, Alonso MJ. Development and characterization of CyA-loaded poly(lactic acid)poly(ethylene glycol)PEG micro- and nanoparticles. Comparison with conventional PLA particulate carriers. *Eur J Pharm Biopharm* 2001;51:111-118.
41. Jie P, Venkatraman SS, Min F, Freddy BYC, Huat GL. Micelle-like nanoparticles of star-branched PEO-PLA copolymers as chemotherapeutic carrier. *J Control Release* 2005;110:20-33.
42. Pistel KF, Bittner B, Li Y, Koll G, Witner G, Kissel T. Biodegradable rh EPO loaded microspheres prepared from linear and star-branched block copolymers: influence of encapsulation technique and polymer composition on particle characteristics. *J Control Release* 1999;59:309-325.
43. Qiu LY, Bae YH. Polymer architecture and drug delivery. *Pharm Res* 2006;23:1-30.
44. Omidi Y, Gumbleton M. Biological Membranes and Barriers. In: Mahato R, editor. *Biomaterials for Delivery and Targeting of Proteins and Nucleic Acids*. Boca Raton: CRC Press; 2005. p. 232-273.
45. Raynal I, Prigent P, Peyramaure S, Najid A, Rebuzzi C, Corot C. Macrophage endocytosis of superparamagnetic iron oxide nanoparticles: mechanisms and comparison of ferumoxides and ferumoxtran-10. *Invest Radiol* 2004;39:56-63.
46. Deshpande MC, Davies MC, Garnett MC, Williams PM, Armitage D, Bailey L, et al. The effect of poly(ethylene glycol) molecular architecture on cellular interaction and uptake of DNA complexes. *J Control Release* 2004;97:143-156.
47. Behrens I, Pena AIV, Alonso MJ, Kissel T. Comparative uptake studies of bioadhesive and non-bioadhesive nanoparticles in human intestinal cell lines and rats: The effect of mucus on particle adsorption and transport. *Pharm Res* 2002;19:1185-1193.

48. Kaul G, Amiji M. Long-circulating poly(ethylene glycol)-modified gelatin nanoparticles for intracellular delivery. *Pharm Res* 2002;19:1061-1067.
49. Zhang Y, Kohler N, Zhang MQ. Surface modification of superparamagnetic magnetite nanoparticles and their intracellular uptake. *Biomaterials* 2002;23:1553-1561.
50. Hatakeyama H, Akita H, Kogure K, Oishi M, Nagasaki Y, Kihira Y, et al. Development of a novel systemic gene delivery system for cancer therapy with a tumor-specific cleavable PEG-lipid. *Gene Ther* 2006;14:68-77.

PRESENTATION OF MANUSCRIPTS

CHAPTER 3.
EFFECT OF POROSITY ON THE RELEASE
KINETICS OF PROPAFENONE-LOADED PEG-G-
PLA NANOPARTICLES

**EFFECT OF POROSITY ON THE RELEASE KINETICS OF
PROPAFENONE-LOADED PEG-g-PLA NANOPARTICLES**
[*Journal of Controlled Release*,107(2): 203-214, 2005]*

Shilpa Sant, Véronique Nadeau and Patrice Hildgen **

Faculty of Pharmacy, University of Montreal, Montreal (QC) CANADA H3C 3J7

**To whom correspondence should be addressed: Faculty of Pharmacy, University of Montreal, C.P. 6128, Succ. Centre-ville, Montreal (Qc) CANADA H3C 3J7, Tel: +1(514) 343-6448, Fax: +1(514) 343-6871, Email: [REDACTED]

*Reproduced with the permission of Elsevier

3.1 Abstract

Nanoparticle preparation by emulsification-solvent evaporation method is a complex phenomenon. Various formulation factors can affect the internal structure and release of drug from nanoparticles (NPs). Aim of the present study is to optimize NPs of PEG-g-PLA polymer and study the effect of various factors on the porosity as well as release profile of drug-loaded NPs. Propafenone hydrochloride (Prop. HCl), a model drug, was encapsulated in the NPs using different amounts of triethylamine (TEA) and initial drug loading levels. NPs were also prepared without TEA by using propafenone base (Prop). All the formulations were characterized for surface morphology, size and size distribution, encapsulation efficiency, thermal analysis, porosimetry and *in vitro* release studies. Encapsulation efficiency of Prop ranged between 10-43 % and was dependent on initial drug loading as well as amount of TEA added. Porosity studies revealed that use of TEA altered the pore size distribution compared to formulations without TEA. Formulations with higher drug loading showed greater volume contribution of small pores, higher fractal dimension suggesting more complex pore structure and slower drug release, probably due to decrease in the effective diffusion coefficient of Prop. Results suggest that formulation factors play an important role affecting the porosity and release rate of NPs.

Also, fractal dimension could be one of the most important factors in determining the release behavior of NPs.

Keywords: Nanoparticles, Porosity, Fractal dimension, Release, Grafted polymer

3.2 Introduction

In recent years, issues in targeted drug delivery are gaining importance with the availability of more potent and specific drugs and in-depth understanding of pathophysiology and cellular mechanisms underlying the disease conditions. All the therapeutic agents could be benefited by targeting to specific tissues without reducing their therapeutic efficacy. Nanoparticles (NPs), because of their versatility, sustained release properties, sub-cellular size and biocompatibility appear to be a promising system to achieve these important objectives. Nanoparticulate systems have great potential, being able to convert poorly soluble, poorly absorbed and labile biologically active substances into promising drugs. However, uptake of conventional NPs by reticuloendothelial systems after intravascular administration limits their use [1]. Therefore, the concept of long-circulating NPs using amphiphilic copolymers has emerged. Such carriers can provide a long circulating drug reservoir from which the drug can be released into a vascular compartment in a continuous and controlled manner [1-3].

Drug release from NPs is interplay of various factors including nature of polymer, physicochemical properties of drug and formulation factors. Although release of bioactive molecules from nano- or microparticles has been the focus of many investigations [4-13], effect of these factors on the microstructure of NPs remains to be explored. It has to be pointed out that the composition and manufacturing procedure of nano- or microparticles can strongly affect the underlying release mechanisms [14]. Additives used in the formulation may change the characteristics of the final drug delivery system. It is well known that the NP preparation by o/w emulsion-solvent evaporation is a complex process in which, the organic solvent generates pores in the structure during its evaporation. This

may lead to changes in the microstructure of NPs significant enough to affect their physical properties, especially the release kinetics.

The porous structure of a material is important in both natural phenomena and practical applications such as dissolution, adsorption and diffusion of drugs [15]. Lemaire et al suggested that, during release, a drug molecule located inside a pore would naturally diffuse towards one of the end-points of the pore and eventually reach outside. If a drug molecule is present within the network of micropores, it will have to diffuse towards the closest pore to be released outside. The movement of such molecule in the micropore network is highly restricted due to the limited space available [16]. Thus, in other words, the effective pore diffusion coefficient will be smaller than the diffusivity in a straight cylindrical pore as a result of the random orientation of pores leading to longer diffusion path. This effective restricted diffusion coefficient of the drug in the porous media is a function of the diffusivity of drug, porosity (ϵ) and tortuosity (τ) of the matrix. The tortuosity in turn depends on the pore structure, pore size and shape distributions [17].

Pore size measurements can provide information about pore diameter and volume. It can be determined by gas adsorption and mercury porosimetry. From nitrogen adsorption isotherms, some basic structural information such as BET surface area, mean pore size, pore size distribution and total pore volume can be obtained. Additional information can be obtained about fractal geometry, which suggests that the surfaces of most materials are fractal at molecular level due to atom packing arrangements and defects. This surface fractal dimension (D) can be calculated from the adsorption and desorption data [18]. The value of D for solid surfaces can vary from 2 (smooth, regular surface) to 3 (very rough surface). Recently, Neimark et al [19, 20] proposed a thermodynamic method for calculating surface fractal dimension from adsorption isotherm data based on the relationship between the surface area of the adsorbed film and the average pore radius. Use of fractal dimensions in pharmaceutical sciences has been proposed since more than a decade [21], however, it has been used mostly to study dissolution behavior of granules and powders [22-26]. The authors have used surface fractal dimension suggesting that the dissolution would be faster for high value of D due to rougher surface of particles. In addition to the surface heterogeneity, the structural heterogeneity of the given solid, generated by the existence of pores of different sizes (i.e. micro and mesopores), can

contribute significantly to D [27]. Greater the value of D suggests more complex pore structure and restricted diffusion of the drug molecule within the pore network.

The aim of the present study was to optimize stealth NPs of a novel polymer, PEG-g-PLA encapsulating a model drug, propafenone hydrochloride. The second objective was to study the effect of triethylamine (TEA) and drug loading on the physicochemical properties of NPs including porosity and surface morphology. In this article, we also address the effect of these different variables on the microstructure and thus, on the release kinetics of NPs by introducing fractal dimension as a new parameter.

3.3 Materials and Methods

3.3.1. Materials

D,L- Lactide, poly(ethylene glycol) methyl ether (2,000 Da), Allyl glycidyl ether, tetraphenyltin, Polyvinyl alcohol (PVA, average M_w 9,000-10,000 Da, 80% hydrolyzed) and triethylamine (TEA, 99.5%) were purchased from Aldrich chemical company Inc., Milwaukee, USA. Propafenone hydrochloride (Prop.HCl) was obtained from Sigma chemical company, St. Louis, USA. Sodium hydroxide pellets were purchased from Anachemia Canada Inc. and dichloromethane (DCM) was purchased from Laboratoire Mat Inc., Montreal, Quebec, Canada.

Propafenone base (Prop) was obtained from Prop.HCl by addition of TEA. Briefly, excess TEA was added to 100 mg of Prop.HCl in DCM. The TEA.HCl was removed by extraction into water and Prop was collected after evaporation of the organic layer.

3.3.2. Synthesis of polymer

The polymer, polyethylene glycol grafted randomly on poly-(D,L) lactic acid (PEG-g-PLA) (M_w 29,000 Da, PEG M_w 2,000 Da) was synthesized in our lab as reported earlier [28]. Briefly, D,L-lactide (21.5 g, 99 mol %) was polymerized in presence of allyl glycidyl ether (0.343 g, 1 mol %) with tetraphenyltin as a catalyst (1:10,000 moles with regard to

lactide) at 180°C for 6 h under argon. Polylactic acid with allyl groups was purified by dissolving in ethyl acetate and precipitating in water. The allyl groups were converted to hydroxyl group by hydroboration with equimolar quantity of borane in tetrahydrofuran followed by oxidation in the presence of hydrogen peroxide under alkaline conditions (1.5 moles of 3 M sodium hydroxide). Hydroxyl group was oxidized to carboxylic acid group using Jones reagent, which was further converted to an acid chloride using thionyl chloride (1:1000 M). Finally, methoxy-PEG was grafted onto the polymer backbone by the reaction between acid chloride and the hydroxyl group of methoxy-PEG (2,000 Da) in presence of pyridine. Subsequently, the final polymer was purified by evaporating pyridine and washing with distilled water.

¹H NMR spectra were recorded on Bruker ARX 400 spectrometer. Chemical shift (δ) was measured in ppm using tetramethylsilane (TMS) as an internal reference. Size exclusion chromatography was performed on Water associate chromatography system with a differential refractometer as detector and Phenomenex Phenogel 5 μ as column. Polystyrene standards were used for calibration with chloroform as mobile phase at a flow rate of 0.6 mL/min. Chemical structure of polymer and NMR spectrum is shown in figure 3.1.

3.3.3. Preparation of Nanoparticles (NPs)

NPs were prepared by emulsion-solvent evaporation method. PEG-g-PLA polymer (300 mg) was dissolved in 10 mL of DCM and emulsified in 50 mL of 0.5 % w/v PVA solution as an external aqueous phase using high-pressure homogenizer (Emulsiflex C30, Avestin, Ottawa, Canada) at a pressure of 10,000 psi for 3 min. The emulsion was collected by washing with another 50 mL of 0.5 % PVA. The DCM was evaporated under reduced pressure with constant stirring to obtain nanoparticles. Finally, the particles were collected by centrifugation at 35,000 g for 45 min (Sorval[®] Evolution_{RC}, Kendro, USA). The PVA present in the supernatant was detected by a colorimetric method described in the section 2.4.4. When no PVA was detected in the supernatant, the nanoparticle suspension was lyophilized (Freeze Dry System, Lyph.Lock 4.5, Labconco) and stored at 4°C until further use. Drug-loaded nanoparticles of either Prop.HCl or Prop were prepared in the similar

manner using initial loading levels of 5 or 10% w/w of polymer. Prop.HCl was dissolved in DCM using different ratios of triethylamine (TEA) whereas for Prop, no TEA was added. TEA added in case of Prop.HCl transformed the drug into free base, which dissolved in DCM without any precipitation. Summary of different formulations is given in table 3.1. For the convenience, formulations are labeled such that the number denotes the loading level used and the suffix in italics denotes the ratio of Prop: TEA; for example, 5_{1:1} means the batch prepared with 5% initial drug loading and 1:1 Prop.HCl: TEA ratio and 5₀ indicates batch prepared with 5% initial loading with no TEA added.

3.3.4. Characterization of NPs

3.3.4.1. Particle size distribution

Nanoparticle size and size distribution was measured by dynamic light scattering (DLS) (N4 Plus, Coulter Electronics, Miami, FL, USA) both before and after lyophilization. For all the batches, fresh NPs suspensions (0.1 mL) or 1 mg of dry NPs were diluted 10-100 times and size measurements were performed at 25°C and 90° scattering angle for 180 seconds. The mean particle diameter was calculated using differential size distribution processor (SDP) intensity analysis program.

3.3.4.2. Morphology

Surface morphology of NPs before and after resuspension was studied using Nanoscope IIIa Dimension 3100 atomic force microscope (Digital Instruments, Santa Barbara, CA, USA). Samples were prepared by deposition of particles on freshly cleaved mica followed by air-drying. Images were obtained using TappingMode™ etched silicon probes (TESP7) with spring constant of 20-100 N/m and resonant frequency of 200-400 kHz. Cantilever length was 125 μm.

3.3.4.3. Encapsulation Efficiency (EE)

NPs were suspended in 1N NaOH for 1 h to which ethanol was added followed by acidification with 1N HCl. Amount of drug entrapped was then measured by spectrophotometry at 305 nm (U-2001 UV/Visible spectrophotometer, Hitachi). Percent encapsulation efficiency (% EE) was calculated as the ratio of amount of drug entrapped to

the total amount of drug added initially. For all the formulations, % EE is expressed in terms of the propafenone base (Prop).

3.3.4.4. Determination of Residual PVA

The amount of PVA remaining in the NPs was determined by a colorimetric method based on the formation of a colored complex between two adjacent hydroxyl groups of PVA and an iodine molecule [4]. Briefly, 2 mg of lyophilized NPs were dissolved in 1 mL of 0.5 N NaOH, neutralized by 1 N HCl and the volume was made up to 5 mL with distilled water. To this, 3 mL of saturated solution of boric acid and 0.5 mL of 0.1 N Iodine was added, and the volume was made up to 10 mL with distilled water. The absorbance was measured at 660 nm on Hitachi 2000 spectrophotometer. The amount of PVA was calculated by using the calibration curve of PVA prepared under the same conditions.

3.3.4.5. Differential Scanning Calorimetry (DSC)

The thermal properties of the polymer and drug in the physical mixture and NPs were characterized by DSC analysis (DSC Q1000, V9.0, build 275, Universal 4.1 D, TA Instruments, USA). Unless otherwise specified, measurements were done (n=2) on polymer, Prop.HCl, Prop (pure base), polymer: Prop.HCl, polymer: Prop physical mixture and drug-loaded NPs. Physical mixture was prepared by triturating polymer and Prop.HCl or Prop in the ratio similar to the highest drug loaded NPs (48: 2 w/w respectively). In brief, weighed samples were sealed in crimped aluminum pans with lids and heated at the rate of 10°C/min from -40 to 200°C. The samples were purged with pure dry nitrogen at a flow rate of 50 mL/min. The DSC was calibrated for temperature with indium (Goodfellow, 99.999% Pure), and tin (NIST SRM 2000). The instrument was calibrated for heat flow with indium (Goodfellow, 99.999% Pure).

3.3.4.6. Porosity measurements

Total surface area and porosity of the NPs were measured by nitrogen adsorption using a porosimeter (Quantachrome instruments, Autosorb-1™, Gas sorption system, ON, Canada). Briefly, weighed amounts of NPs were placed in the glass cells and outgassed with nitrogen at 25°C for 3 h before analysis. Subsequently, the sample and the reference cells were immersed in liquid nitrogen at -196°C and adsorption isotherm was obtained

from the volume of nitrogen (cc/g) adsorbed onto the surface of nanoparticles as a function of relative pressure. Total surface area was calculated by Brunauer-Emmette-Teller (BET) method using five adsorption points in the P/P_0 range of 1 – 3. Pore size distribution (PSD) was calculated according to Horvath-Kawazoe (HK) method in the pore size range of 0 –20 Å and surface fractal dimension was obtained by Neimark-Kiselev (NK) method using the Autosorb-1™ software. Mathematical details of HK and NK methods could be found in details elsewhere [29,30] and [19,27], respectively.

3.3.4.7. *In vitro* release study

All the 6 formulations prepared using different amount of TEA and drug loading levels were tested for *in vitro* release in triplicate in PBS, pH 7.4. Fifty mg of NPs were suspended in 2.5 mL PBS in a dialysis tubing (Spectra Por 1 membrane, 6-8 kDa cut-off). This dialysis tubing was placed in a screw-capped tube containing 10 mL PBS. The tubes were shaken at 200 rpm on a horizontal water bath shaker (Orbit Shaker Bath, Labline) maintained at $37 \pm 1^\circ\text{C}$. At predetermined time intervals, the whole medium in the tube was withdrawn and replaced by fresh PBS to maintain sink conditions. The aliquots were assayed for the amount of Prop released by spectrophotometry at 305 nm.

3.4 Results and Discussion

3.4.1. Characterization of polymer

^1H NMR spectrum of PEG-*g*-PLA polymer is shown in fig. 3.1 along with the structure. Multiplets corresponding to lactic acid –CH could be observed at 5.17 ppm. Overlapping doublets at 1.56 ppm were due to the methyl groups of D- and L-lactic acid repeat units. A peak at 3.64 could be attributed to the methylene groups of polyethylene glycol. Molecular weight and molecular weight distribution of the polymer were determined by size exclusion chromatography. The number average and weight average molecular weights of the polymer were found to be 20,600 and 29,000 Da, respectively. Polydispersity was 1.4. Unimodal mass distribution ruled out the possibility of presence of untreated methoxy PEG or Poly (D,L- lactide).

3.4.2. Morphology and particle size measurements

Particle size distribution by DLS showed unimodal distribution for freshly prepared as well as resuspended NPs. Different formulations showed similar particle size in the range of 178-192 nm (Table 3.1). Thus, drug loading levels as well as amount of TEA used had no apparent effect on the particle size, suggesting that the size was largely controlled by the emulsification process during nanoparticle preparation. However, the particle size for all the batches was increased almost 1.5 times after resuspension in spite of the use of Tween 80 (0.01%) or probe sonication (1-5 min) for resuspended NPs (data not shown). AFM revealed that NPs were spherical with smooth surface and displayed their aggregating tendency (Fig. 3.2). Therefore, the increase in particle size found by DLS might be due to aggregation of the particles. Thus, it should be noted that the results of particle size distribution by light scattering method should be supplemented with some visual methods like AFM.

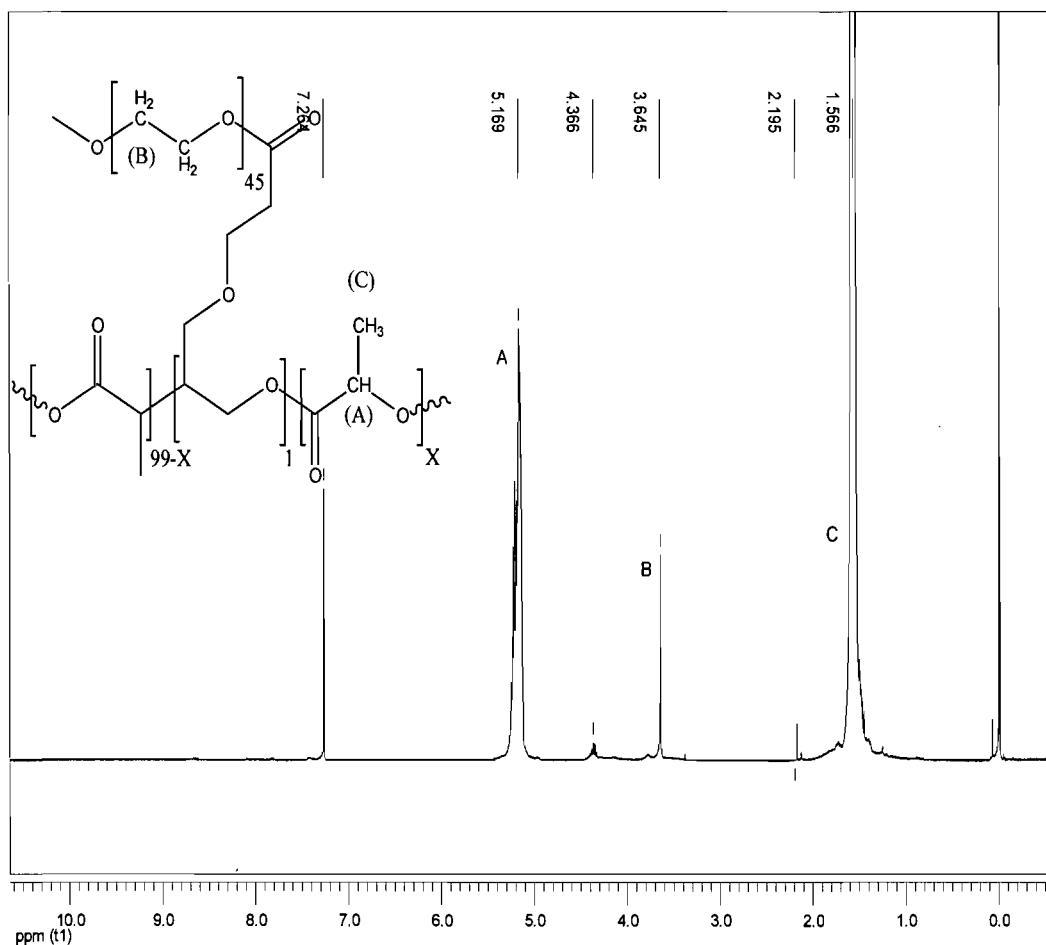


Figure 3.1. Chemical structure and NMR spectrum of the polymer, PEG-g-PLA

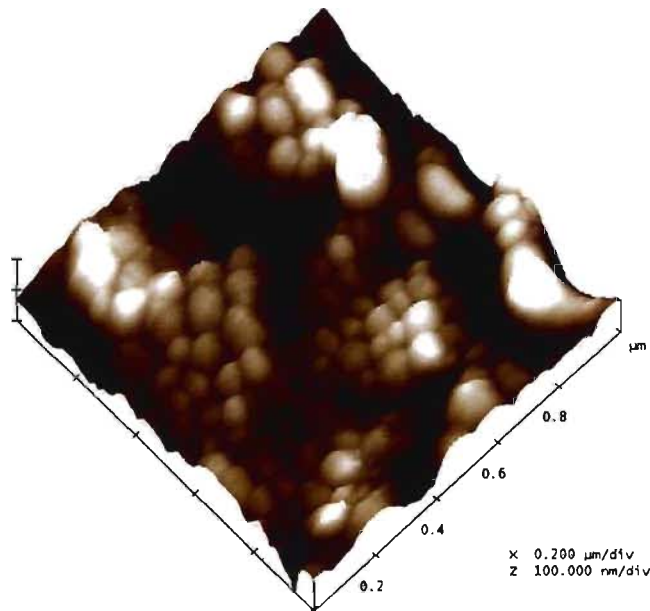


Figure 3.2. Surface morphology of NPs (formulation 10:1) by AFM.

3.4.3. Encapsulation efficiency (EE)

As seen from the table 3.1, EE of Prop.HCl was very low (10%) for formulation prepared without TEA. However, it increased from 10 % to 43 % with use of TEA. This could be due to the fact that TEA scavenges hydrochloride from Prop.HCl, thus, setting free the pure hydrophobic base (Prop). This allows efficient physical entrapment of Prop in the hydrophobic PLA core of the polymer, resulting in the improved encapsulation efficiency. To further support this, pure base was isolated from its hydrochloride salt and incorporated in NPs. It was observed that EE of formulations prepared with pure base was comparable with those prepared with 1:1 Prop.HCl: TEA ratio at the same loading levels. With increase in the amount of TEA, EE further increased by 1.5 times. Kohori et al [31] also showed increased incorporation of adriamycin (ADR) into micelles with increased level of TEA (1:2.4 molar ratio of ADR.HCl: TEA) attributing it to the effective removal of hydrochloride and more efficient physical entrapment. Also, EE was always more at 5% initial loading than 10% for the same Prop:TEA ratio. It is noteworthy to mention that the increase in the EE is not accompanied by any increase in the particle size. However, the reason for observed increase in EE with higher molar ratio above 1:1 is not known. There are many reports citing the interaction between the carboxylic groups of PLA and amino groups of basic drugs like leuprorelin acetate [32, 33]. The authors have reported that

degree of interaction between the drug and the polymer determines the entrapment efficiency. Thus, we propose that addition of TEA more than stoichiometric ratio probably favors removal of hydrochloride more efficiently *in situ* favoring the ionic interaction between the carboxylic groups of PLA and basic amino groups of Prop, which finally results in the improved encapsulation efficacy.

Table 3.1. Summary of different formulations and their characterization

Formulation	Form of drug	Loading (% w/w)	Prop:TEA (M)	Size (nm) ^a	PI	PVA (% w/w)	EE (%) ^b
5 ₀	Prop	5	0	180 ± 20.8	0.235	6.71 ± 0.41	28.03 ± 6.0
5 _{1:1}	Prop.HCl	5	1:1	188 ± 50.1	0.104	6.38 ± 0.83	29.57 ± 5.3
5 _{1:2}	Prop.HCl	5	1:2	192 ± 40.8	0.101	6.05 ± 0.53	42.75 ± 3.7
10 ₀	Prop	10	0	190 ± 38.3	0.009	6.81 ± 0.59	23.66 ± 1.0
10 _{1:1}	Prop.HCl	10	1:1	184 ± 33.8	0.222	7.18 ± 0.60	21.63 ± 0.7
10 _{1:2}	Prop.HCl	10	1:2	178 ± 20.8	0.053	6.78 ± 0.44	40.75 ± 2.2
VII	Prop.HCl	10	0	184 ± 45.2	0.143	nd	9.81 ± 1.8

All values indicate ± S. D. for n= 3 independent experiments

^a: Median

^b: Mean

PI: Polydispersity, EE: Encapsulation efficiency, nd: not determined

3.4.4. Residual PVA

It is widely reported that surfactant remaining on the surface of the NPs alters their properties such as particle size, hydrophilicity, release kinetics, cellular uptake etc. [4]. Therefore, it is important to know the amount of surfactant associated with the final lyophilized NPs. Our basic purpose to determine the residual PVA was to confirm that the difference in release kinetics of NPs was not due to presence of different amount of PVA. It was observed that a fixed amount of PVA (6-7 % w/w) remained on the surface of all the formulations even after 4-5 washings (Table 3.1). An attempt was made to evaluate whether PVA was present either inside the polymeric matrix or on the surface of the particles. To determine the surface-associated PVA, NPs were suspended in distilled water (data not shown), whereas for total amount of PVA associated with the particles (amount entrapped as well as present on the surface), NPs were digested in 0.5 N NaOH. The same amount of PVA (6-7 %w/w) was present in the given NP formulation by both assays confirming that the amount of PVA was solely associated with the surface of the particles

(Table 3.1). This might be the reason of the observed aggregating tendency of NPs. Our results are in accordance with other authors. Sahoo et al [4] have reported 6.15% w/w PVA remaining with DCM as solvent and 5% PVA solution as external aqueous phase for PLGA NPs. Zambaux et al have also reported 5-6 % w/w PVA associated with PLA NPs after 3 washings when 1 % PVA was used as an external aqueous phase [34]. There was no significant difference in the amount of PVA associated with the different formulations probably because the same solvent and same polymer was used for the preparation of all the formulations. Thus, the possibility of residual PVA playing any role towards difference in the release kinetics could be ruled out.

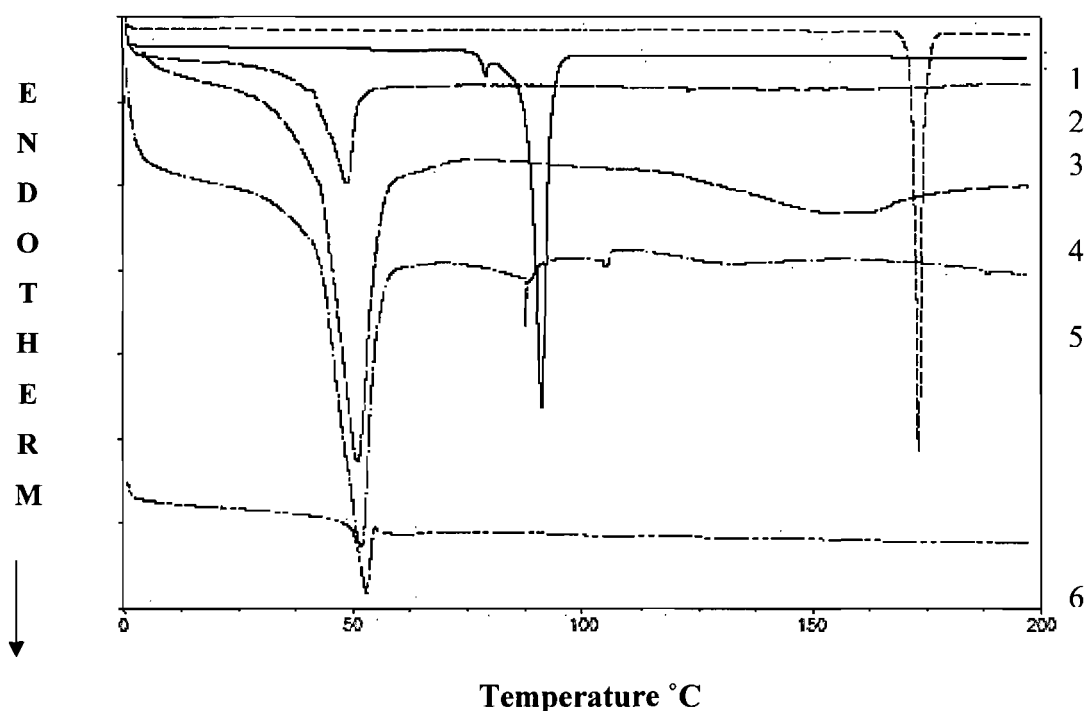


Figure 3.3. DSC curves of (1) Prop.HCl; (2) base (Prop); (3) Polymer; (4) Physical mixture of Prop.HCl: Polymer; (5) Physical mixture of Prop: Polymer and (6) Drug loaded NPs (10_{1:2})

3.4.5. Thermal analysis

DSC was used to detect possible drug crystallization inside the NPs as well as any possible interaction between the drug and the polymeric matrix. As shown in the fig. 3.3, DSC curve of PEG-g-PLA showed an endothermic peak corresponding to the glass transition (T_g) at $\sim 48^\circ\text{C}$. The melting peak of the Prop.HCl crystals and Prop (base) appeared at ~ 173 and 91°C respectively. This melting endotherm could also be detected in

the drug: polymer physical mixtures (2:48, respectively); however, there was broadening of this peak. As seen from fig. 3.3, T_g of polymer was also shifted by 2-3°C in both the physical mixtures, indicating some interaction between drug and polymer. After encapsulation of Prop.HCl in the NPs, T_g of the polymer further shifted to ~ 54 °C, which might be due to the effect of process or formulation variables. Also, melting point endotherm of drug disappeared (Fig. 3.3) indicating presence of drug in the amorphous or solid dispersion state in the polymer matrix [35]. Our results are in accordance with Miyajima et al [36] who have reported increase in T_g of copoly (lactic/glycolic acid) after incorporation of basic drugs. This may be because of interaction between the polymer carboxyl residues and amino group of drug as suggested by the authors [36].

3.4.6. Surface area, pore size distribution and fractal dimension

Table 3.2. Porosity measurements for different formulations

No	Prop:TEA (M)	L_t (%w/w)	Lr (% w/w)	Total pore vol (cc/g)	Micropore SA (m ² /g)	BET SA (m ² /g)	D
5 ₀	0	5	1.40±0.3	0.34±0.06	18.2 ± 6.3	25.2±5.3	2.538±0.04
5 _{1:1}	1:1	5	1.48±0.3	0.31±0.09	15.8 ± 5.0	23.2±4.9	2.529±0.05
5 _{1:2}	1:2	5	2.14±0.2	0.33±0.09	16.0 ± 5.4	23.1±4.9	2.516±0.01
10 ₀	0	10	2.37±0.1	0.38±0.03	22.4 ± 0.5	28.4±6.1	2.582±0.1
10 _{1:1}	1:1	10	2.16±0.1	0.37±0.06	18.3± 3.2	24.9±5.3	2.572±0.01*
10 _{1:2}	1:2	10	4.08±0.2	0.35±0.05	18.1 ± 3.1	24.6±4.8	2.577±0.01*

All values indicate Mean ± S. D. for n=3 independent observations,

L_t : Theoretical loading, Lr: Real loading, SA: surface area, D: fractal dimension,

*: $P < 0.05$, Student's paired t-test

In order to find out the microstructure of the particles, PSD was measured using nitrogen adsorption porosimetry. According to IUPAC definition, pores with a diameter below 40 Å are micropores and that between 40 to 1000 Å are mesopores. As seen from table 3.2, there was no significant difference between total pore volume, micropore surface area and BET surface area for different formulations. PSD also followed the similar pattern

above 20 Å for all the formulations. However, there was difference between the formulations depending on the drug loading for PSD below 20 Å.

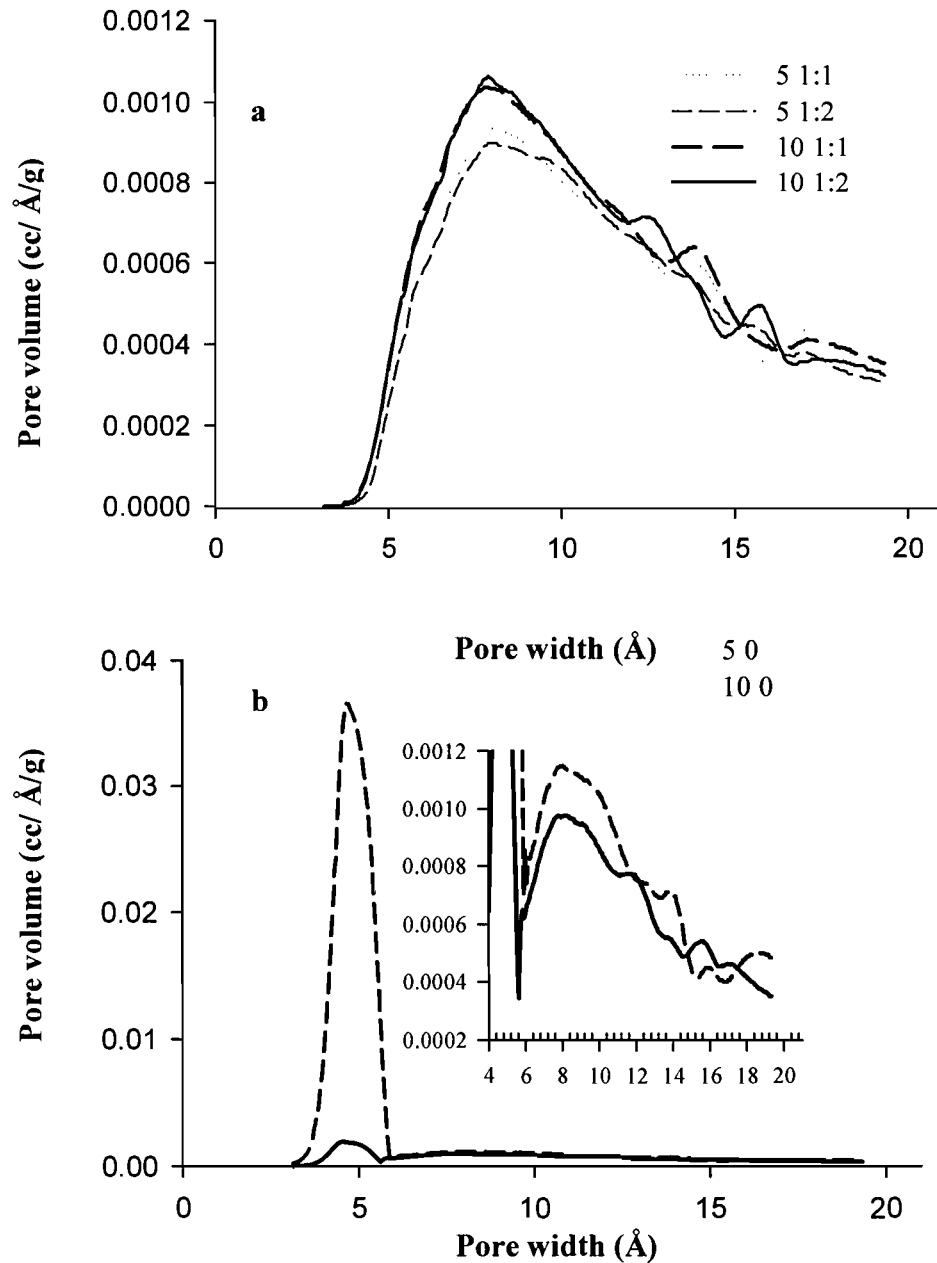


Figure 3.4. Pore size distribution for various formulations with (a) or without (b) TEA. All values are mean \pm S. D. for $n=3$, Inset in fig b shows the pore size distribution on the same scale as Fig. 3.4 a.

As shown in fig. 3.4, formulations with 10 % drug loading had greater volume contribution of smaller pores as compared to those with 5 % drug loading. Also, it should

be noted that different amount of TEA at the same drug loading level exhibited same PSD. It seems logical to assume that if higher amount of drug were initially available to be accommodated in the same size of NPs, it would lead to the formation of a heterogeneous matrix as suggested by Gorner et al [5]. This would lead to more compact internal structure increasing number of smaller pores for formulations with 10% loading.

As shown in fig. 3.4 a, all the formulations prepared with different amounts of TEA had larger pores with peak at around 8-9 Å (formulations 5_{1:1}, 5_{1:2} and 10_{1:1}, 10_{1:2}) whereas those prepared without TEA (formulations 5₀ and 10₀), showed additional pore population towards smaller micropores at around 4.7 Å (Fig 3.4 b). This may be a complex effect of drug loading and TEA, and could be explained as follows. TEA added during preparation of NPs increased the drug loading due to hydrophobic interaction between the drug and polymer masking the smaller pores with peak around 4.7 Å which was present in the formulations without TEA. At the same time, escaping TEA.HCl soluble in the aqueous external phase would have also contributed to larger pores along with evaporating organic solvent, thus shifting the PSD slightly towards larger pores (8 Å). In other words, formulation prepared in the presence of TEA showed only one peak due to escaping TEA.HCl whereas those prepared without TEA showed both the peaks. It is noteworthy that all the four formulations with TEA followed similar pattern of PSD emphasizing some control exercised by TEA in pore formation.

The observed difference in the PSD was also reflected on the surface fractal dimension (D), which is related to the surface irregularities created by the pores open at the surface. Thus, it can reflect the pore size distribution. Generally, the value of D is high when the volume of the small pores is important and decreases when the contribution of smaller pores decreases [27, 37]. These pores can be more complex from inside, thus creating tortuous matrix. As seen from the table 3.2, D was similar for formulations with same theoretical drug loading because all of them showed similar PSD. Formulations with 10% loading always had higher proportion of smaller pores (Fig. 3.4 a and b) and greater value for D. Thus, it can be seen that the initial loading level influenced the PSD and fractal dimension of NPs.

3.4.7. *In vitro* Release

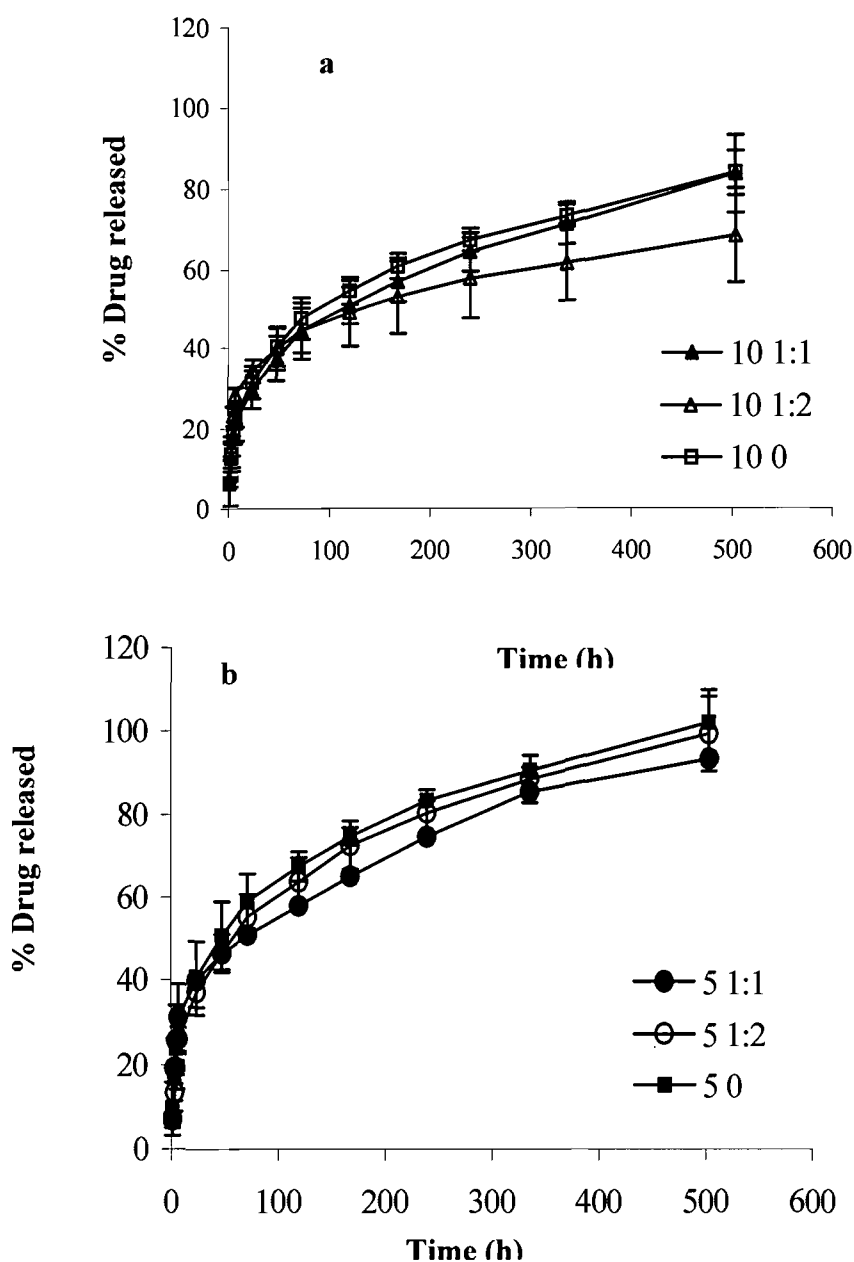


Figure 3.5. Effect of TEA (0, 1:1, 1:2) on the release profile of NPs at different drug loading levels, a; 10 % and b; 5 %. Error bars indicate mean \pm S. D. for n= 3

Drug release from microdisperse system is a complex phenomenon affected by various factors including the drug loading, additives and the internal structure of the NPs. There are many reports on the factors affecting the release behavior of the drug from the NPs; nevertheless, the effect of porosity on the release behavior of the drug from NPs has been rarely addressed.

For all the formulations, the initial burst release was 20-30% followed by the sustained release over next 28 days. The identical burst of 20-30% suggests that the same amount of drug was present at or near the surface, irrespective of real loading. It was observed that TEA added had no apparent effect on release pattern of the different formulations with same theoretical drug loading although it changed the real loading inside the particles (Table 3.1, Fig 3.5). When different parameters including mean micropore width, micropore volume, micropore surface area, BET surface area, and total surface area obtained from the porosimetry of these formulations were compared, there was very small difference in all these parameters (Table 3.2). PSD of the formulations at the same drug loading was similar (Fig. 3.4) irrespective of amount of TEA used. This could be the reason why all these formulations with same theoretical drug loading but different amount of TEA exhibited apparently same release kinetics (Fig. 3.5). As shown in fig 3.6, release profiles of formulation with different theoretical drug loadings showed difference in their release behavior (e. g. 5₀ Vs 10₀, 5_{1:1} Vs 10_{1:1} and 5_{1:2} Vs 10_{1:2}). It was found that the release of the drug from NPs with 5% theoretical drug loading was always faster than 10% loading irrespective of amount of TEA added. From the DSC results, it is clear that the drug was present in the form of solid dispersion even in case of NPs with the highest drug loading. Thus, the dissolution of the drug before diffusion into the release media would not be a rate limiting step as suggested by Gerner et al [5]. As the same polymer was used for all formulations, difference in the polymer degradation might not be significant to affect the release kinetics [8]. This implies that the factors affecting the drug diffusivity from the polymeric matrix would then control the release behavior.

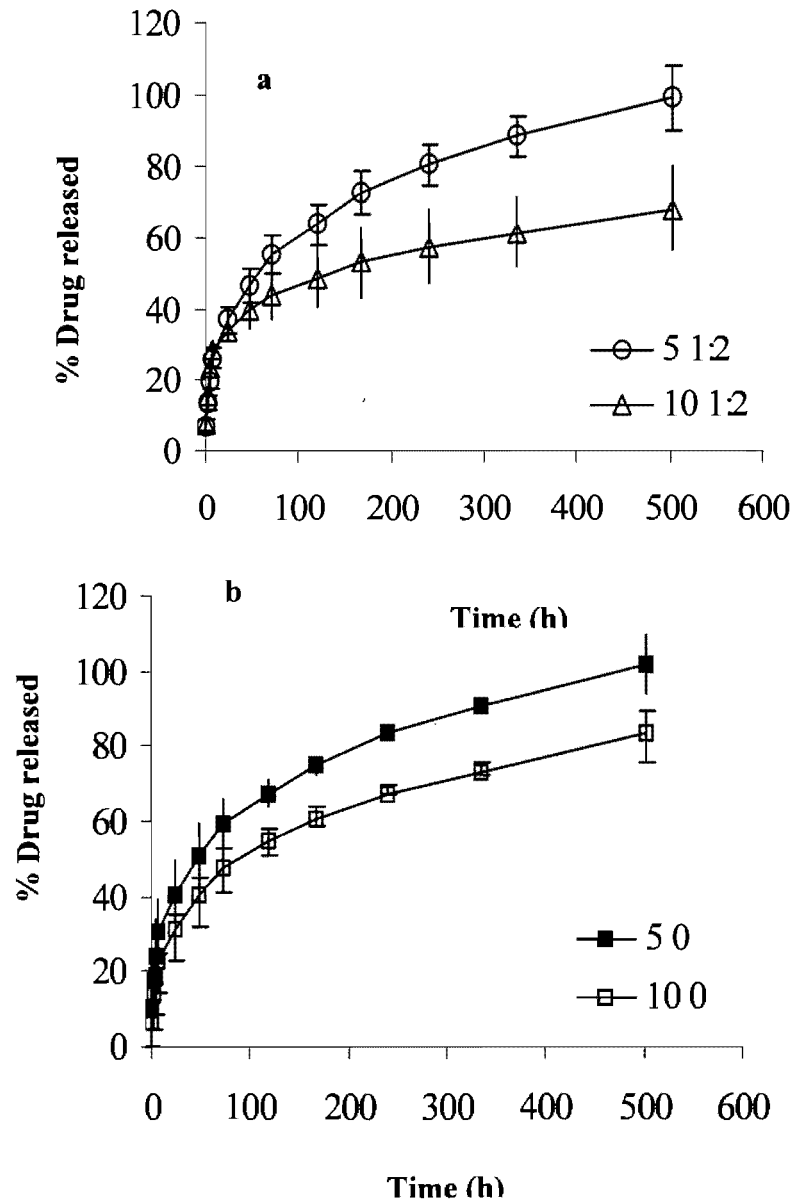


Figure 3.6. Effect of initial drug loading level on the release profile of NPs in the presence (a, 1:2 M Prop: TEA) or absence (b) of TEA. Error bars indicate mean \pm S. D. for n= 3

It was observed that PSD and fractal dimension were the most critical parameters determining the release behavior, whereas other parameters related to total and external surface area played minor role. Our results are in accordance with the model recently proposed by Lemaire et al [16] where authors suggested that the effective diffusion coefficient of the drug molecule in the wetted polymer, the average pore length and the initial pore diameter are the most critical parameters influencing the release kinetics. The

drug molecule located in the network of micropores will first diffuse towards the closest pore; however, this diffusion in the micropore network is slow due to the limited space available. In our study also, fractal dimension (D) seemed to play a key role in determining the rate of release. Higher value of D indicates more complex pore structure, lower effective diffusion coefficient of the drug due to random orientation of pores and increased tortuosity [16] from such a system. As shown in table 3.2, formulations with 5% drug loading always showed smaller D and hence, greater effective diffusion coefficient and thus faster release profile (Fig. 3.6). Also, volume contribution of smaller pores for 10₀, 10_{1:1} and 10_{1:2} was always more than 5₀, 5_{1:1} and 5_{1:2} (Fig. 3.4). This effect was more prominent especially in the formulation 5₀ and 10₀ (Fig. 3.4 b) and was also reflected in their release kinetics (Fig. 3.6 b). As seen from fig. 3.4 b and table 3.2, formulation 5₀ with lowest volume contribution of smaller pores and low value for D showed the fastest release rate whereas formulation 10₀ with highest volume contribution of smaller pores and highest value of D exhibited the slowest release. PSD towards smaller pores may mean more compact, tortuous internal structure, thus, decreasing the rate of drug diffusion.

Presence of higher amounts of drug and/or TEA in the initial polymeric phase enhanced actual drug loading. However, the drug loading mechanism for both these factors seems to be different as can be seen from the effect on release kinetics and PSD. When PSD curves were compared, it was observed that change in drug loading resulted in change in PSD and thus, release kinetics. However, different amounts of TEA at same drug loading level did not change the PSD significantly and thus, the release kinetics. Interestingly, formulations 5_{1:2} and 10_{1:1} (with same drug levels inside the NPs) did show difference in PSD irrespective of the same amount of drug being loaded inside the NPs. This further supports our hypothesis that the mechanism by which the drug loading ratio and TEA increase the real loading might be different. Further studies will clarify this issue.

3.5 Conclusion

In the present study, stealth NPs of PEG-g-PLA were optimized for their encapsulation efficiency using TEA and characterized for porosimetry in addition to other conventional physicochemical properties. The results obtained show a correlation between the release kinetics and PSD. Higher drug loading ratios led to more compact structure

creating smaller pores, showed higher value of fractal dimension and more complex pore structure, resulting in slower drug release. On the other hand, TEA apparently did not have much effect on the release as it was counteracted by higher drug loading. Although the exact mechanism of the effect of drug loading and TEA on PSD and the drug release remains to be elucidated, it can be concluded that formulation factors certainly affect the internal structure of NPs and may play a major role in influencing the release behavior. Further studies are underway to characterize these formulations for their stealth behavior including resistance to protein adsorption and macrophage phagocytosis.

3.6 References

- [1] S. M. Moghimi, A. C. Hunter, J. C. Murray, Long-circulating and target-specific nanoparticles: theory to practice, *Pharmacol Rev* 53(2) (2001) 283-318.
- [2] P. Quellec, R. Gref, L. Perrin, E. Dellacherie, F. Sommer, J. M. Verbavatz, M. J. Alonso, Protein encapsulation within polyethylene glycol-coated nanospheres. I. Physicochemical characterization, *J Biomed Mater Res* 42(1) (1998) 45-54.
- [3] Y. Li, Y. Pei, X. Zhang, Z. Gu, Z. Zhou, W. Yuan, J. Zhou, J. Zhu, X. Gao, PEGylated PLGA nanoparticles as protein carriers: synthesis, preparation and biodistribution in rats, *J Control Release* 71(2) (2001) 203-211.
- [4] S. K. Sahoo, J. Panyam, S. Prabha, V. Labhasetwar, Residual polyvinyl alcohol associated with poly (D,L-lactide-co-glycolide) nanoparticles affects their physical properties and cellular uptake, *J Control Release* 82(1) (2002) 105-114.
- [5] T. Gorner, R. Gref, D. Michenot, F. Sommer, M. N. Tran, E. Dellacherie, Lidocaine-loaded biodegradable nanospheres. I. Optimization Of the drug incorporation into the polymer matrix, *J Control Release* 57(3) (1999) 259-268.
- [6] M. Chorny, I. Fishbein, H. D. Danenberg, G. Golomb, Lipophilic drug loaded nanospheres prepared by nanoprecipitation: effect of formulation variables on size, drug recovery and release kinetics, *J Control Release* 83(3) (2002) 389-400.
- [7] Y. Y. Yang, T. S. Chung, N. P. Ng, Morphology, drug distribution, and in vitro release profiles of biodegradable polymeric microspheres containing protein fabricated by double-emulsion solvent extraction/evaporation method, *Biomaterials* 22(3) (2001) 231-241.

- [8] G. Ruan, S. S. Feng, Preparation and characterization of poly(lactic acid)-poly(ethylene glycol)-poly(lactic acid) (PLA-PEG-PLA) microspheres for controlled release of paclitaxel, *Biomaterials* 24(27) (2003) 5037-5044.
- [9] T. Ameller, V. Marsaud, P. Legrand, R. Gref, G. Barratt, J. M. Renoir, Polyester-poly(ethylene glycol) nanoparticles loaded with the pure antiestrogen RU 58668: physicochemical and opsonization properties, *Pharm. Res.* 20(7) (2003) 1063-1070.
- [10] A. Lamprecht, N. Ubrich, M. Hombreiro Perez, C. Lehr, M. Hoffman, P. Maincent, Biodegradable monodispersed nanoparticles prepared by pressure homogenization-emulsification, *Int J Pharm* 184(1) (1999) 97-105.
- [11] J. Matsumoto, Y. Nakada, K. Sakurai, T. Nakamura, Y. Takahashi, Preparation of nanoparticles consisted of poly(L-lactide)-poly(ethylene glycol)-poly(L-lactide) and their evaluation in vitro, *Int J Pharm* 185(1) (1999) 93-101.
- [12] M. T. Peracchia, R. Gref, Y. Minamitake, A. Domb, N. Lotan, R. Langer, PEG-coated nanospheres from amphiphilic diblock and multiblock copolymers: Investigation of their drug encapsulation and release characteristics, *J Control Release* 46(1997) 223-231.
- [13] B. Bittner, C. Witt, K. Mader, T. Kissel, Degradation and protein release properties of microspheres prepared from biodegradable poly(lactide-co-glycolide) and ABA triblock copolymers: influence of buffer media on polymer erosion and bovine serum albumin release, *J Control Release* 60(2-3) (1999) 297-309.
- [14] J. Siepmann, N. Faisant, J. Akiki, J. Richard, J. P. Benoit, Effect of the size of biodegradable microparticles on drug release: experiment and theory, *J Control Release* 96(1) (2004) 123-134.
- [15] K. A. Mehta, M. S. Kislalioglu, W. Phuapradit, A. W. Malick, N. H. Shah, Effect of formulation and process variables on porosity parameters and release rates from a multi unit erosion matrix of a poorly soluble drug, *J Control Release* 63(1-2) (2000) 201-211.
- [16] V. Lemaire, J. Belair, P. Hildgen, Structural modeling of drug release from biodegradable porous matrices based on a combined diffusion/erosion process, *Int J Pharm* 258(1-2) (2003) 95-107.
- [17] S. R. Veith, E. Hughes, G. Vuataz, S. E. Pratsinis, Restricted diffusion in silica particles measured by pulsed field gradient NMR, *J Colloid Interface Sci* 274(1) (2004) 216-228.

- [18] J. F. Lee, C. K. Lee, L. C. Juang, Size Effects of Exchange Cation on the Pore Structure and Surface Fractality of Montmorillonite, *J Colloid Interface Sci* 217(1) (1999) 172-176.
- [19] A. V. Neimark, K. K. Unger, Method of discrimination of surface fractality, *J Colloid Interface Sci* 158(1993) 412-419.
- [20] A. V. Neimark, M. Hanson, K. K. Unger, Fractal analysis of the distribution of high viscosity fluids in porous supports, *J Phys Chem* 97(1993) 6011-6015.
- [21] H. P. Koch, The concept of fractals in the pharmaceutical sciences, *Pharmazie* 48(9) (1993) 643-659.
- [22] B. Albertini, C. Cavallari, N. Passerini, D. Voinovich, M. L. Gonzalez-Rodriguez, L. Magarotto, L. Rodriguez, Characterization and taste-masking evaluation of acetaminophen granules: comparison between different preparation methods in a high-shear mixer, *Eur J Pharm Sci* 21(2-3) (2004) 295-303.
- [23] A. Fini, G. Fazio, M. J. Fernandez-Hervas, M. A. Holgado, A. M. Rabasco, Fractal analysis of sodium cholate particles, *J Pharm Sci* 85(9) (1996) 971-975.
- [24] A. Fini, M. A. Holgado, L. Rodriguez, C. Cavallari, Ultrasound-compacted indomethacin/polyvinylpyrrolidone systems: effect of compaction process on particle morphology and dissolution behavior, *J Pharm Sci* 91(8) (2002) 1880-1890.
- [25] A. Fini, M. Garuti, G. Fazio, J. Alvarez-Fuentes, M. A. Holgado, Diclofenac salts. I. Fractal and thermal analysis of sodium and potassium diclofenac salts, *J Pharm Sci* 90(12) (2001) 2049-2057.
- [26] T. Li, K. Park, Fractal analysis of pharmaceutical particles by atomic force microscopy, *Pharm Res* 15(8) (1998) 1222-1232.
- [27] N. Rizkalla, P. Hildgen, R. Thibert, Influence of the Fractal Character of Model Substances on their Reactivity at Solid-Liquid Interfaces, *J Colloid Interface Sci* 215(1) (1999) 43-53.
- [28] G. Leclair, R. Quesnel, M. Bocar, P. Hildgen. Synthesis and characterization of a novel class of versatile grafted biopolymers. *Proc. Int. Symp. Control. Release Bioact. Mater.*; 2003; Scotland; 2003.
- [29] F. Rouquerol, J. Rouquerol, K. Sing, Assessment of microporosity, *Adsorption by powders and porous solids: Principles, methodology and applications*, Academic Press, San Diego, 1999, pp. 231-232.

- [30] G. Horvath, K. Kawazoe, Method for the calculation of effective pore size distribution in molecular sieve carbon, *J Chem Eng Japan* 16(5) (1983) 470-475.
- [31] F. Kohori, M. Yokoyama, K. Sakai, T. Okano, Process design for efficient and controlled drug incorporation into polymeric micelle carrier systems, *J Control Release* 78(1-3) (2002) 155-163.
- [32] H. Okada, Y. Doken, Y. Ogawa, H. Toguchi, Preparation of three-month depot injectable microspheres of leuporelin acetate using biodegradable polymers, *Pharm Res* 11(8) (1994) 1143-1147.
- [33] H. Okada, H. Yamamoto, T. Heya, Y. Inoue, S. Kamei, Y. Ogawa, H. Toguchi, Drug delivery using biodegradable microspheres, *J Control Release* 28(1994) 121-129.
- [34] M. F. Zambaux, F. Bonneaux, R. Gref, P. Maincent, E. Dellacherie, M. J. Alonso, P. Labrude, C. Vigneron, Influence of experimental parameters on the characteristics of poly(lactic acid) nanoparticles prepared by a double emulsion method, *J Control Release* 50(1-3) (1998) 31-40.
- [35] L. Mu, S. S. Feng, PLGA/TPGS nanoparticles for controlled release of paclitaxel: effects of the emulsifier and drug loading ratio, *Pharm Res* 20(11) (2003) 1864-1872.
- [36] M. Miyajima, A. Koshika, J. Okada, A. Kusai, M. Ikeda, The effects of drug physico-chemical properties on release from copoly (lactic/glycolic acid) matrix, *Int J Pharm* 169(1998) 255-263.
- [37] G. M. El Shafei, C. A. Philip, N. A. Moussa, Fractal analysis of hydroxyapatite from nitrogen isotherms, *J Colloid Interface Sci* 277(2) (2004) 410-416.

LINK BETWEEN FIRST AND SECOND ARTICLE

The results of the first article have demonstrated usefulness of gas adsorption technique for studying microporosity of NPs. Also, differences in microporosity, although marginal, seemed to offer adequate explanation for differences in the release kinetics of propafenone hydrochloride (Prop) from NPs of PEG-g-PLA [1], which could not be explained otherwise by differences in drug loading or thermal properties of these NPs. It was thought that microporosity of NPs reflected the polymer interchain spacing and void spaces or free volume. Hence, it was speculated that change in the molecular structure of the polymer will lead to significant differences in the internal microporous structure of NPs fabricated of these polymers. As mentioned in the introduction of this thesis, reports on mechanisms of NP formation and their microporosity/microstructure are scarce in the literature. Thus, in continuation with this first study, further studies were planned to explore effect of polymer architecture as well as drug loading on the microporous structure of NPs. In this second manuscript, an attempt was made to apply gas adsorption technique to blank NPs prepared from 4 different polymers to unravel the mechanism of polymer chain organization inside NPs.

It was also evident from the review of literature that results of the drug release profiles from pegylated particulate systems are controversial regardless of many studies being conducted in this area. Some studies have reported enhanced release rates with presence of PEG [2] whereas others have reported the opposite trend [3]. Hence, one can safely assume the role of internal structure of NP matrix to influence drug release behavior. In fact, it can be speculated that the microporous structure of these reported systems might have been different leading to contradictory results. Thus, the work in the second manuscript focuses on the effect of molecular architecture of pegylated polymers on the microporous structure and drug release properties of NPs.

References:

1. Sant S, Nadeau V, Hildgen P. Effect of porosity on the release kinetics of propafenone-loaded PEG-g-PLA nanoparticles. *J Control Release* 2005;107(2):203-214.

2. Matsumoto J, Nakada Y, Sakurai K, Nakamura T, Takahashi Y. Preparation of nanoparticles consisted of poly(L-lactide)-poly(ethylene glycol)-poly(L-lactide) and their evaluation in vitro. *Int J Pharm* 1999;185(1):93-101.
3. Peracchia MT, Gref R, Minamitake Y, Domb A, Lotan N, Langer R. PEG-coated nanospheres from amphiphilic diblock and multiblock copolymers: Investigation of their drug encapsulation and release characteristics. *J Control Release* 1997;46:223-231.

CHAPTER 4.
MICROPOROUS STRUCTURE AND DRUG
RELEASE KINETICS OF POLYMERIC
NANOPARTICLES

MICROPOROUS STRUCTURE AND DRUG RELEASE KINETICS OF POLYMERIC NANOPARTICLES *

Shilpa Sant, Matthias Thommes and Patrice Hildgen **

¹Faculty of Pharmacy, University of Montreal, C. P. 6128 succ. Centre-ville, Montreal, QC, H3C 3J7

²Quantachrome Instruments, 1900 Corporate Drive, Boynton Beach, FL 33426

**To whom correspondence should be addressed: Faculty of Pharmacy, University of Montreal, C.P. 6128, Succ. Centre-ville, Montreal (Qc) CANADA H3C 3J7, Tel: +1(514) 343-6448, Fax: +1(514) 343-6871, Email: XXXXXXXXXX

***: Received the comments for minor revision from Langmuir**

4.1 Abstract

Aim of the present study was to characterize the pegylated nanoparticles (NPs) for their microporosity and study its effect on drug release kinetics. Blank and drug-loaded NPs were prepared from three different pegylated polymers, namely, poly(ethylene glycol)_{1%}-*graft*-poly(D,L lactide), poly(ethylene glycol)_{5%}-*graft*-poly(D,L lactide) and multiblock copolymer; (poly(D,L lactide)-*block*-poly(ethylene glycol)-*block*-poly(D,L lactide))_n. These NPs were characterized for their microporosity using nitrogen adsorption isotherm. NPs of multiblock copolymer showed least microporosity and BET surface area, and that of PEG_{1%}-*g*-PLA showed the maximum. Based on these results, structural organization of PLA and PEG chains inside the NPs was proposed and validated with DSC and XPS surface analysis. *In vitro* drug release study revealed that PEG_{1%}-*g*-PLA NPs exhibited slower release despite of their higher surface area and microporosity. This was attributed to the presence of increased microporosity forming tortuous internal structure, thereby hindering drug diffusion from the matrix. Thus, it was concluded that microporous structure of NPs, which is affected by molecular architecture of polymers, determines the release rate of the encapsulated drug.

Keywords: Pegylated Nanoparticles, Nitrogen adsorption, Microporosity, Drug release kinetics, Internal structure

4.2 Introduction

Intensive research has been done in past few decades in the development of polymeric nanoparticles (NPs) as an effective drug delivery system for controlled release and targeting¹⁻³. The therapeutic success of such a system is determined by its drug release kinetics, which is a function of structural and physicochemical properties of the NPs. Thus, it is a complex interplay of various factors such as properties of polymer and drug⁴, their interaction with each other⁵, drug load^{6, 7}, drug distribution inside the carrier, size and morphology of the carrier^{6, 7}. Although majority of above-mentioned factors have been studied previously, reports on the importance of microporosity of NPs are lacking due to the unavailability of methods with high resolution. Small pores in a few nanometre range can affect matrix hydration, drug diffusion into release medium and polymer degradation⁸. It has been documented that macroscopic properties of solid materials, like drug release, permeability are closely connected to their microporous structure⁹⁻¹¹. This microstructure is usually characterized by density, surface area and porosity. While the evolution of porosity during microparticle formation has been a focus of research for many years^{8, 12}, studies on underlying mechanisms of NP formation and the factors affecting their microporosity are scarce in the literature. Many techniques like pycnometry, gas adsorption, X-ray diffraction, calorimetry have been used to characterize porous solids^{13, 14}. Gas adsorption is more popular because it allows the assessment of a wide range of pore sizes (from 0.35 nm to 100 nm), which includes the complete range of micro- and mesopores, and even (partially) macropores. In addition, gas adsorption techniques are convenient to use, and are less cost intensive than other methods.

Analysis of a nitrogen adsorption isotherm allows one to obtain parameters such as total pore volume, micropore volume, BET surface area, pore size distribution (PSD) as well as the surface fractal dimension. These parameters are commonly used for the characterization of zeolites, clays and various catalysts¹⁵⁻¹⁸. Although these parameters can prove to be very useful in understanding the surface morphology as well as microporous structure of NPs, their use in the area of drug delivery is not reported so far. Recently, we

have shown that formulation factors affect the internal structure and fractal dimension of NPs and thus, release kinetics of encapsulated drugs¹⁹. This study is an attempt to understand the effect of polymer architecture and drug loading on microporous structure of NPs. It is shown that arrangement of polymer chains inside the matrix during NP formation is dependent on the molecular architecture of the polymer.

It was also noted that results of the drug release profiles from pegylated particulate systems are controversial regardless of many studies being conducted in this area. Some studies have reported enhanced release rates with presence of PEG²⁰ whereas others have reported the opposite trend²¹. Hence, one can safely assume the role of internal structure of NP matrix to influence drug release behavior. In fact, it can be speculated that the microporous structure of these reported systems might have been different leading to contradictory results. Hence, another purpose of this study was to shed some light on the role of microporous internal structure on the diffusion of drug molecules from pegylated NPs.

4.3 Materials and methods

4.3.1. Materials

D,L- Lactide, poly(ethylene glycol) methyl ether (MePEG; 2,000 Da), poly(ethylene glycol) (PEG, 1500 Da), allyl glycidyl ether, tetraphenyltin, polyvinyl alcohol (PVA, average M_w 9,000-10,000 Da, 80% hydrolyzed) and propafenone hydrochloride (Prop) were purchased from Aldrich chemical company Inc., Milwaukee, USA. Dichloromethane (DCM) was purchased from Laboratoire Mat Inc., Montreal, Quebec, Canada.

4.3.2. Synthesis of the polymers

Homopolymer, poly(D,L)lactide (PLA) was synthesized by ring-opening polymerization of dilactide in argon atmosphere, using tetraphenyltin as catalyst. Briefly, dilactide was crystallized from toluene solution and dried under vacuum before use. Weighed amount of purified dilactide was then placed in round bottom flask and purged

thoroughly with argon. Bulk polymerization was carried at 180°C for 6 h. The polymer thus obtained was dissolved in acetone and was purified by precipitating in water.

Polymers with polyethylene glycol grafted poly-(D,L) lactide (PEG-*g*-PLA) (PEG M_w 2,000 Da) were synthesized in the laboratory and the detailed procedure can be found as reported earlier^{19,22}. PEG grafting was performed at 2 different grafting densities; viz. 1% and 5 % (mole/mole of lactic acid monomer). D,L-lactide (21.5 g, 99 mol %) was polymerized in presence of allyl glycidyl ether (0.343 g, 1 mol %) with tetraphenyltin as a catalyst (1:10,000 moles with regards to D, L-lactide) at 180°C for 6 h under argon. Polylactic acid with allyl groups was purified by dissolving in ethyl acetate and precipitating in water. The allyl groups were converted to hydroxyl group by hydroboration with equimolar quantities of borane in tetrahydrofuran, followed by oxidation in the presence of hydrogen peroxide under alkaline conditions (1.5 moles of 3 M sodium hydroxide). Pendent hydroxyl group was oxidized to carboxylic acid group using Jones reagent, which was further converted to an acid chloride using thionyl chloride (1:1000 M). Finally, methoxy-PEG was grafted onto the polymer backbone by the reaction between acid chloride and the hydroxyl group of methoxy-PEG (2,000 Da) in presence of pyridine. Final polymer was purified by evaporating pyridine and washing with distilled water. For 5% PEG-grafted polymer, concentrations of D,L-Lactide and allyl glycidyl ether were 95 mol % and 5 mol % respectively, remaining synthesis procedure being the same.

Multiblock copolymer, (PLA-PEG-PLA)_n was synthesized as reported earlier²³ using PEG with M_n of 1500 and succinic acid was used as condensing agent to link the triblock copolymers.

¹H NMR spectra were recorded on Bruker ARX 400 spectrometer (Bruker Biospin, Billerica, MA, USA). Chemical shift (δ) was measured in ppm using tetramethylsilane (TMS) as an internal reference. Size exclusion chromatography (SEC) was performed on Water associate chromatography system (Waters, Milford, MA, USA) equipped with refractive index detector and Phenomenex Phenogel 5 μ column. Polystyrene standards were used for calibration with chloroform as mobile phase at a flow rate of 0.6 mL/min.

4.3.3. Preparation of Nanoparticles (NPs)

Blank NPs of PLA, PEG_{1%}-g-PLA, PEG_{5%}-g-PLA and (PLA-PEG-PLA)_n were prepared by emulsion-solvent evaporation method¹⁹. NPs could not be prepared using multiblock copolymer alone due to its low molecular weight; hence, 1:1 mixture of PLA and multiblock copolymer was used for preparation of NPs in this case. Each polymer (1 g) was dissolved in 10 mL of DCM containing 1:2 M triethylamine (TEA) and emulsified in 50 mL of 0.5% w/v PVA solution as an external aqueous phase using high-pressure homogenizer (Emulsiflex C30, Avestin, Ottawa, Canada) at a pressure of 10,000 psi for 3 min. The emulsion was collected by washing with additional 50 mL of 0.5% PVA solution. Then, DCM was evaporated under reduced pressure with constant stirring to obtain NPs. Finally, the particles were collected by centrifugation at 35,000 g for 45 min (Sorvall Evolution[®] RC, Kendro, Newton, CT, USA). NP suspension was then lyophilized (Freeze Dry System, Lyph.Lock 4.5, Labconco Corporation, MO, USA) to get dry NPs and stored at 4°C until further use. Prop-loaded NPs were prepared in similar manner using 1:2 M TEA and initial loading level of 7.5 % w/w of polymer.

4.3.4. Characterization of NPs

4.3.4.1 Particle size distribution

Size and size distribution was measured by photon correlation spectroscopy (PCS) (N4 Plus, Coulter Electronics, Miami, FL, USA) at 25°C and 90° scattering angle for 180 seconds. The mean particle diameter was calculated using differential size distribution processor (SDP) intensity analysis program.

4.3.4.2 Encapsulation efficiency (EE)

NPs were suspended in 1N NaOH for 1 h and ethanol was added followed by acidification with 1N HCl. Amount of Prop entrapped was then measured by spectrophotometry at 305 nm (U-2001 UV/Visible spectrophotometer, Hitachi, Tokyo, Japan). Percent encapsulation efficiency (% EE) was calculated as the ratio of amount of drug entrapped to the total amount of drug added initially.

4.3.4.3 Differential scanning calorimetry (DSC)

The thermal properties of pure polymer and blank NPs were characterized by DSC analysis (DSC Q1000, V9.0, build 275, Universal 4.1 D, TA Instruments, Grimsby, ON, Canada). Weighed samples of pure polymers were sealed in crimped aluminum pans with lids and were heated from -50°C to 220°C (2 runs) at the rate of $10^{\circ}\text{C}/\text{min}$, while NP samples were heated from -50 to 70°C at the rate of $10^{\circ}\text{C}/\text{min}$, held at 70°C for 1 min and cooled again to -50°C . This cycle was repeated 3 times to ensure that NP structure was not destroyed. The samples were purged with pure dry nitrogen at a flow rate of 50 mL/min. The DSC was calibrated for temperature with indium (Goodfellow, 99.999% pure), and tin (NIST SRM 2000). The instrument was calibrated for heat flow with indium (Goodfellow, 99.999% pure). The analyses of the obtained DSC thermograms were done using Universal analysis 2000, version 14.0C, TA instruments, Grimsby, ON, Canada.

4.3.4.4. Porosity measurements

Nitrogen adsorption experiments and porosity measurements were done using microporosimeter (Autosorb-1 MP, Quantachrome Instruments, Boynton Beach, FL, USA) as described by Sant et al¹⁹. Weighed amounts of NPs were placed in glass cells and the effect of degassing was studied for upto 68 h. Finally, all the samples were degassed under identical conditions before analysis. The sample and reference cells were immersed in liquid nitrogen at -196°C and high resolution nitrogen adsorption isotherm (relative pressure 10^{-6} to 1) was obtained from the volume of nitrogen (cc/g) adsorbed onto the surface of NPs as a function of relative pressure. Krypton was also used in BET region to validate the nitrogen data.

4.3.4.5. XPS analysis

XPS analysis of blank NP samples was performed on VG ESCALAB MK II (VG Scientific, Crawley, UK) using Mg $K\alpha$ X-rays (hv 1253.6 eV) and an electron take off angle of 0° . A single survey scan spectrum (0-1000 eV) and narrow scans for C1s (210-305 eV) and O1s (525-550 eV) were recorded for each sample with a pass energy of 1 eV and 0.5 eV, respectively. Acquisition and data analysis were performed by a VGS 5000 data system. Peak fitting of the C1s envelope was as described by Shakesheff et al²⁴. Chemical shifts were referenced to hydrocarbon at 285 eV.

4.3.5 *In vitro* release study

Prop-loaded NPs of PEG_{1%}-g-PLA and (PLA-PEG-PLA)_n were tested for *in vitro* release in triplicate in phosphate buffered saline (PBS), pH 7.4. Fifty mg NPs were suspended in 2.5 mL PBS in a dialysis tubing (6-8 kDa, Spectra Por 1 membrane, Spectrum Laboratories, CA, USA). This dialysis tubing was placed in a screw-capped tube containing 10 mL PBS. The tubes were shaken at 200 rpm on a horizontal water bath shaker (Orbit Shaker Bath, Labline) maintained at $37 \pm 1^\circ\text{C}$. At predetermined time intervals, whole medium in the tube was withdrawn and replaced by fresh PBS to maintain sink conditions. The aliquots were assayed for the amount of Prop released by spectrophotometry at 305 nm.

4.4 Results and Discussion

4.4.1. Characterization of polymers

¹H NMR spectroscopy and size exclusion chromatography (SEC) were used to measure molecular number average (M_n) and weight average (M_w) distribution of polymers. Polydispersity was calculated by the ratio of M_w to M_n . The results are summarized in Table 4.1. ¹H NMR spectra and chemical structures of all polymers are shown in Fig. 4.1. Typical spectra were obtained with peaks at 5.2 ppm corresponding to the tertiary PLA proton (m, -CH), peak at 3.6 ppm for the protons of the repeating units in PEG chain (m, OCH₂-CH₂O), peak at 4.3 ppm for the PEG connecting unit to the PLA block (m, CH₂-OCO), and peak at 1.5 ppm for the pendent methyl group of the PLA chain (m, -CH₃). For the multiblock copolymer, additional peak could be seen at around 2.7 ppm corresponding to the protons of succinic acid group (m, CH₂-COO). Final PEG grafting percentage was close to the feed ratio of PEG as shown in Table 4.1. Multiblock copolymer showed highest PEG content of 17.8 mol %.

In addition to molar mass and polydispersity, the thermal properties of polymers are influenced by their molecular structure. PLA showed glass transition (T_g) at 41.2°C (Table 4.1, Fig. 4.2a). Random grafting PEG (1%) on PLA backbone resulted in increased T_g value (by about 6°C) due to enhanced chain rigidity (Fig. 4.2b, Table 4.1). Merino et al²⁵ has reported similar increase in T_g for hyperbranched polymers and dendrimers over their linear

chain analogues. However, further increasing PEG grafting density to 5% showed a decrease in T_g of PEG_{5%}-g-PLA polymer (Fig. 4.2c, Table 4.1). This can be attributed to enhanced segmental mobility of PLA chains caused by plasticization effect of increasing PEG concentration, as reported earlier²⁶. Thus, for low PEG grafting percentage, effect of branching was predominant whereas increasing PEG concentration led to predominant plasticizer effect. Similar effect was seen on T_g of multiblock copolymer (Fig. 4.2d). Very low T_g value ($\sim 15^\circ\text{C}$) of multiblock copolymer can be due to their very high PEG content (17.8 mol %) and/or low molecular weight as compared to grafted polymers (Table 4.1). At the same time, melting peak of PEG was present in PEG_{5%}-g-PLA and multiblock copolymer, which could not be seen in PEG_{1%}-g-PLA, possibly due to its lower PEG concentration.

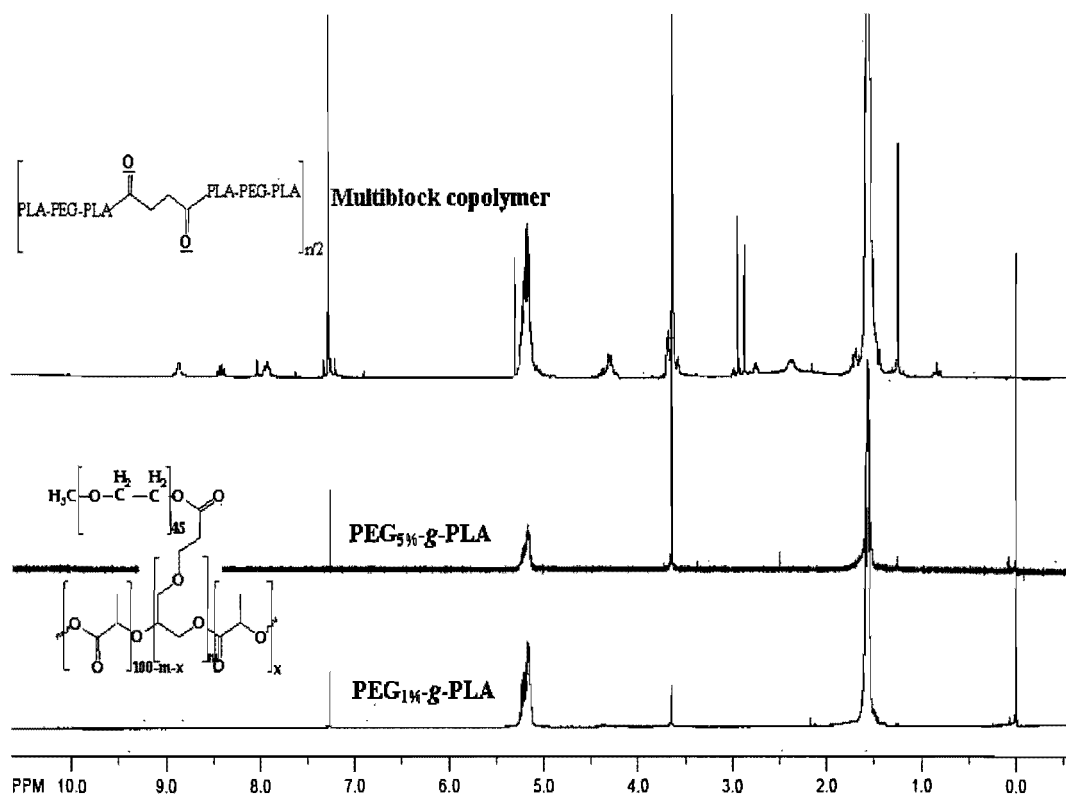


Figure 4.1. ^1H NMR spectra and chemical structures of multiblock copolymer, PEG_{1%}-g-PLA ($m = 1$) and PEG_{5%}-g-PLA ($m = 5$).

Table 4.1. Polymer characterization by ^1H NMR and Size Exclusion Chromatography and DSC

Polymer	M_n	M_w	M_w/M_n	PEG ^a (mol %)	T_g ^b
Poly(D,L)Lactide	18222	24844	1.36	-	41.17
PEG _{1%} -g-PLA	9753	15059	1.54	1.2	47.32
PEG _{5%} -g-PLA	9245	14363	1.55	7.0	34.82
(PLA-PEG-PLA) _n	5250	6120	1.16	17.8	15.27

^a: Calculated from peak intensity ratios of PEG (3.6 ppm) and PLA (5.2 ppm) by ^1H NMR

^b: Glass transition temperature calculated as half extrapolated tangents from second run of the DSC thermograms of respective polymers

4.4.2. Particle size distribution and encapsulation efficiency (EE)

Blank and Prop-loaded NPs were found to be monodispersed having diameter of 180 to 210 nm as determined by PCS (Supporting information, Fig. S3, Table 4.2 and 4.3). Prop loading slightly increased the particle size for each type of polymer (Table 4.3). EE was found to be between 40 to 65% w/w depending on the polymer type (Table 4.3). Grafted polymers showed better EE than multiblock copolymer, which could be attributed to enhanced steric hindrance of PEG chains in case of grafted copolymers, thus reducing premature diffusion of Prop into the external aqueous phase during solidification of NPs.

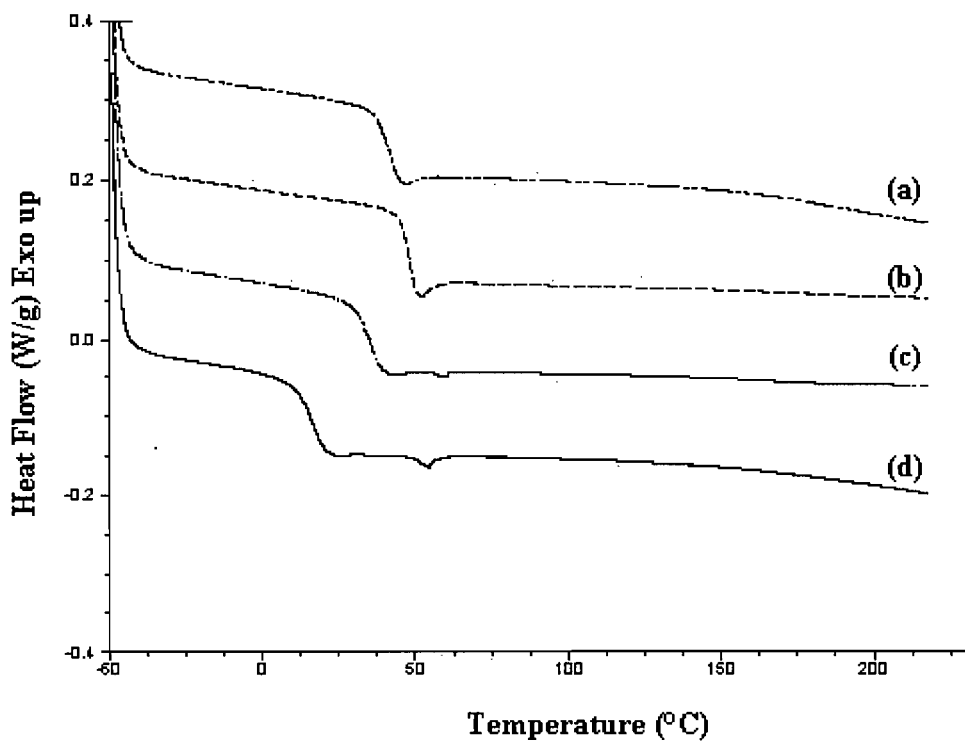


Figure 4.2. DSC thermograms of 4 different polymers heated at the rate of 10°C/min from -50 to 220°C, PLA (a), PEG_{1%}-g-PLA (b), PEG_{5%}-g-PLA (c), and (PLA-PEG-PLA)_n (d)

Table 4.2. Characterization of blank NPs

NP Formulation	Size (nm)	Polydispersity	S _{BET, N₂} ^b (m ² /g)	T _g ^c	% PEG ^d
PLA-Blank	185 ± 3	0.359	18.47±1.39	51.40	-
Peg1-Blank	180 ± 4	0.078	28.29±0.09 ^a	49.21	5.5
Peg5-Blank	184 ± 8	0.22	14.45±1.50 ^a	43.90	9.1
Multi-Blank	192 ± 7	0.019	7.88±0.69 ^a	33.35	3.7

Multi: multiblock copolymer + PLA (1:1), PLA: Poly(D,L-lactide), Peg1: PEG_{1%}-g-PLA, Peg5: PEG_{5%}-g-PLA;

Blank: Blank NPs, e. g., Multi-Blank: Blank NPs prepared from multiblock copolymer + PLA (1:1)

^a: Values are significantly different as compared to PLA-Blank at $p < 0.05$ by Student's paired t-test

^b: $S_{\text{BET}, \text{N}_2}$: surface area determined by nitrogen gas adsorption

^c: Glass transition temperature calculated as half extrapolated tangents from second run of the DSC thermograms of respective NPs

^d: % surface PEG coverage determined by XPS analysis; Relative monomer % was calculated taking into consideration areas under the curve for respective C1s peaks

All values are mean \pm S.D. of $n=3$

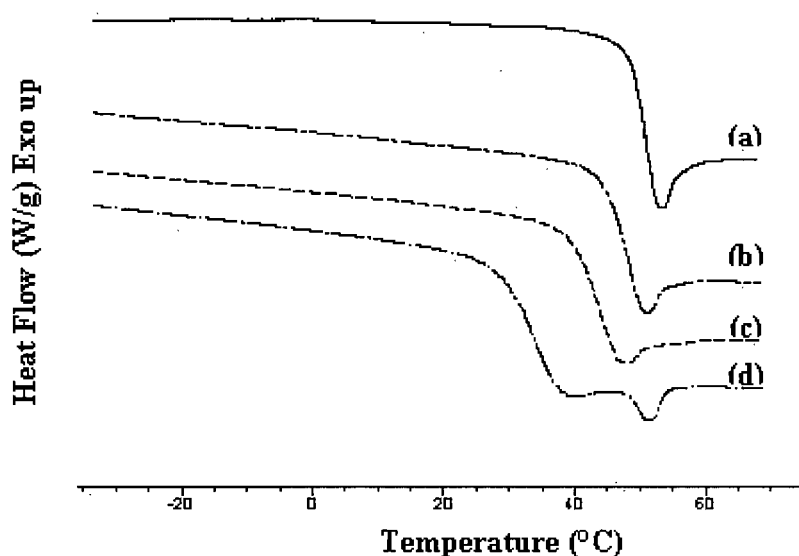


Figure 4.3. Second run of DSC thermograms of blank NPs heated at the rate of $10^{\circ}\text{C}/\text{min}$ from -50 to 70°C , PLA (a), $\text{PEG}_{1\%}\text{-g-PLA}$ (b), $\text{PEG}_{5\%}\text{-g-PLA}$ (c), and $(\text{PLA-PEG-PLA})_n$ (d)

4.4.3. Thermal properties of NPs

The three consecutive DSC scans of all the NPs were superimposable except the sharp peak of enthalpy of polymer chain relaxation in the first scan was less prominent in

the subsequent scans (Supporting information, Fig. S1). This confirms that the structure of NPs was conserved during the experiment. Further, it was noted that all NPs had higher T_g as compared to respective polymers (Table 4.1 and 4.2), elucidating compromised polymer chain mobility when formulated as NPs. Also, all pegylated NPs including PEG_{1%}-g-PLA showed reduction in T_g as compared to PLA NPs indicative of presence of some PEG chains inside the core of PLA. This decrease in T_g (18°C) was more important for multiblock copolymer NPs. Also, melting endotherm was evident only in the multiblock copolymer NPs at 51.5°C in all three runs (Fig. 4.3d and Supporting information, S1-D).

4.4.4. Porosity measurements and XPS analysis of blank NPs

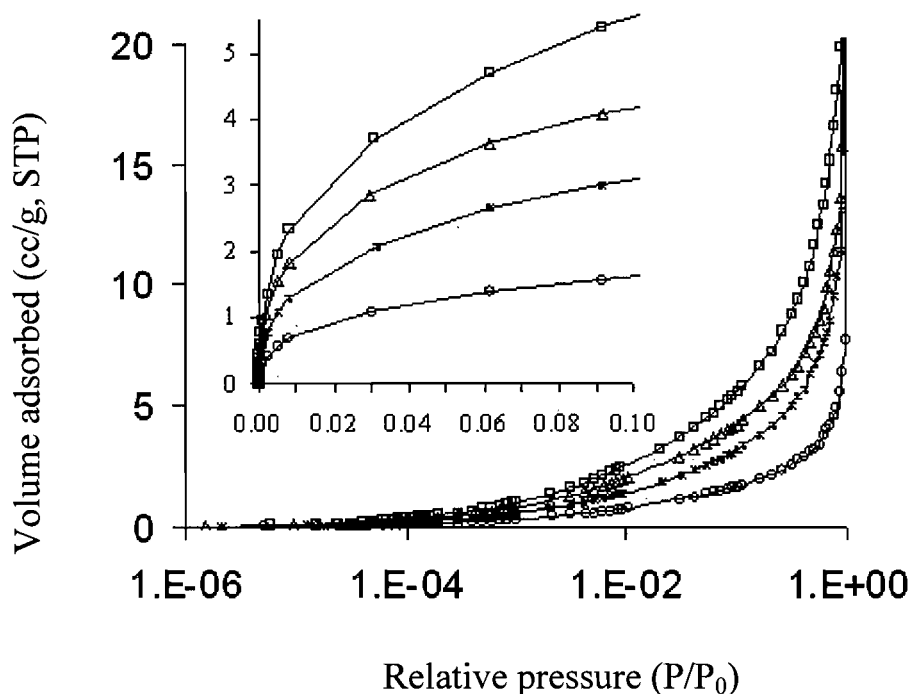


Figure 4.4. High resolution nitrogen adsorption isotherms of blank NPs of PEG_{1%}-g-PLA (\square), PLA (\triangle), PEG_{5%}-g-PLA ($*$) and (PLA-PEG-PLA)_n (\circ). Inset shows magnified region between 0-5 cc/g on y-axis to reveal the detailed adsorption behavior of nitrogen in relative pressure range 10^{-6} to 10^{-1} .

Fig. 4.4 shows high resolution nitrogen isotherms of blank NPs prepared from 4 different polymers, in the relative pressure range 10^{-6} to 1. Logarithmic scale is used to reveal the detailed adsorption behaviour in the microporous region. BET surface area was

calculated using five adsorption points in the relative pressure range of 0.1 – 0.3. Cumulative micropore volume was calculated according to Horvath-Kawazoe (HK) method^{27, 28} in the relative pressure range of 10^{-6} -0.1/0.01 to include the pore size range of 0 – 20 Å. The HK method is based on slit-shaped pore model. Even though this pore model may not be appropriate for NPs, it was applied here since it would still allow comparison between samples as the measurements were done under identical conditions. NPs of PEG_{1%}-g-PLA showed highest nitrogen uptake and that of multiblock copolymer showed the lowest. A comparison of cumulative micropore volumes for different NPs is shown in Fig. 4.5. It was seen that micropore volume for blank NPs of different polymers were in the order of PEG_{1%}-g-PLA > PLA > PEG_{5%}-g-PLA > (PLA-PEG-PLA)_n. BET surface area followed the same trend (Table 4.2). Thus, differences in isotherms correlated extremely well with the changes in BET surface area and micropore volume. These results confirm that changes in the BET surface area of NPs were indeed due to microporosity, and this can further be attributed to the molecular structure of the polymers as described below.

Based on the DSC studies of polymers and blank NPs as well as their microporosity data, following hypothesis (Fig. 4.6) is proposed to explain the polymer chain organization of these structurally diverse polymers during NPs formation. In case of PLA NPs, PLA will undergo rapid phase separation into polymer-rich/polymer-poor phase because of its hydrophobic nature. This leads to polymer gelation and precipitation (Fig. 4.6a) even with the slightest of organic solvent extraction into external aqueous phase, preventing further entry of water inside the embryonic particles. In such a case, it is reasonable to refer the microporosity to that created due to individual chain folding and/or efficient packing of several such chains creating void spaces in a nanoparticle. Indeed, it has long been recognized that polymers can possess large amount of void space, referred to as free volume^{9, 10}. It is suggested that above a certain amount of free volume, the voids would be interconnected and polymer would behave as a microporous material⁹.

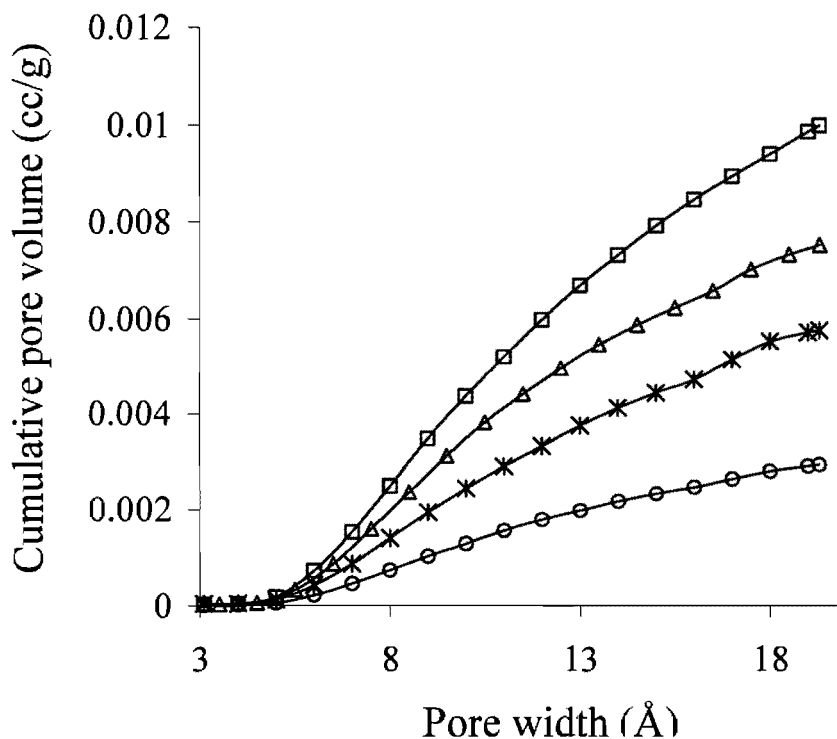


Figure 4.5. Effect of molecular structure of polymer on microporosity of blank NPs of PEG_{1%}-g-PLA (□), PLA (Δ), PEG_{5%}-g-PLA (*) and (PLA-PEG-PLA)_n (○)

In case of grafted polymers, hydrophilic PEG chains are covalently linked to hydrophobic PLA. The immiscibility of these two blocks should result in microphase separation of components, the ease of which would depend on the chemistry of the polymer²⁹. It is hypothesized that, due to the peculiar polymer structure, phase separation in grafted polymers will be facilitated as PLA backbone can collapse easily in water (non-solvent for PLA) leaving PEG on the external surface of the emulsion droplet facing aqueous phase (good solvent for PEG). Thus, grafted copolymers NPs will have hydrophobic PLA core surrounded by hydrophilic PEG shell (Fig. 4.6b). Higher T_g value of pure PEG_{1%}-g-PLA compared to homopolymer PLA (Table 4.1) signifies higher rigidity of the polymer backbone due to random grafting of PEG chains. Similar behaviour has been reported for PLA-PEG diblock and triblock copolymers, where these copolymers exhibited less flexibility, high T_g value and phase separation due to poor miscibility of PEG and PLA

blocks³⁰. Further it should be noted that DSC studies of NPs revealed depression in T_g for PEG_{1%}-g-PLA NPs over PLA NPs (Table 4.2). This suggests presence of few PEG chains miscible in the PLA core. Thus, higher microporosity of PEG_{1%}-g-PLA NPs can be attributed to the rigidity of polymer chain in accordance with Mckeown et al³¹. They have recently suggested that highly rigid molecular structure leads to increase in the microporosity of polymer.

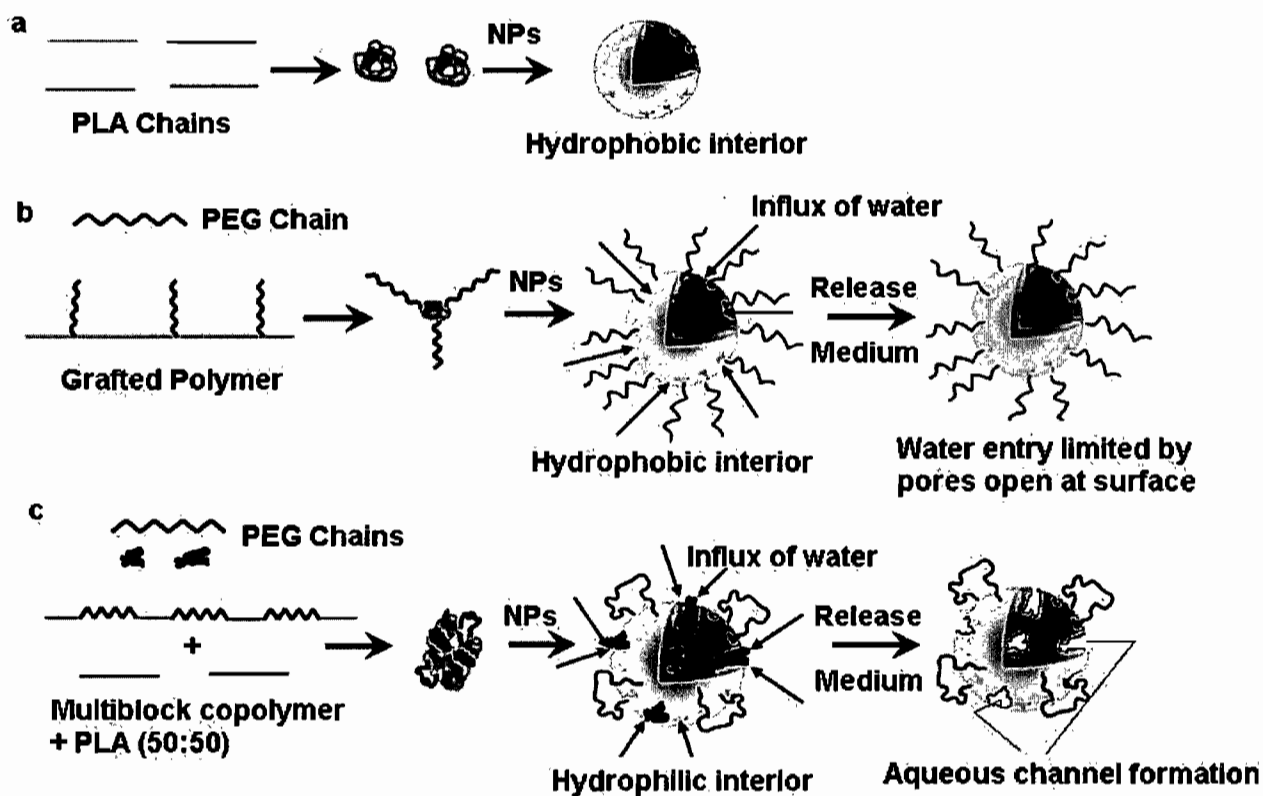


Figure 4.6. Schematic representation of arrangement of polymer chains inside NPs and mechanism of drug release; PLA (a), grafted polymers (b) and multiblock copolymer (c)

On the contrary, PEG_{5%}-g-PLA NPs resulted in decrease in microporosity compared to PLA homopolymer. Why? It is worthy to note that PEG_{5%}-g-PLA polymer and NPs, both resulted in greater decrease in T_g (6-7°C) as compared to PLA homopolymer and NPs respectively, emphasizing improved flexibility of the polymer backbone and presence of more PEG chains in the PLA core of NPs as compared to PEG_{1%}-g-PLA. This additional

PEG chains penetrating inside the core of NPs will block some of the pores. This explains the decreased microporosity of PEG_{5%-g}-PLA NPs.

In case of (PLA-PEG-PLA)_n multiblock copolymer, although it has both hydrophobic PLA and hydrophilic PEG domains, microphase separation of polymer itself might not be as easy as grafted copolymers. This is due to the fact that covalent linkage of PEG chain with two neighboring PLA chains will significantly hamper its spatial mobility. Indeed, Wang et al.³⁰ have shown absence of phase separation in multiblock copolymers of PLA and PEG due to enhanced miscibility of two blocks and increased hydrophilicity. Very high depression in T_g (25.9°C, Table 4.1) of multiblock copolymer clearly supports their enhanced miscibility. Thus, faster gelation of the polymeric phase during solvent evaporation will not allow all the PEG chains to phase-separate inhibiting their migration to the surface. In such a case, higher amount of PEG chains, which could not come out on the surface during polymer gelation would be forced to accommodate themselves in between PLA chains (Fig. 4.6c). Large shift in T_g of these NPs clearly supports this hypothesis. According to this hypothesis, NPs prepared with mixture of multiblock copolymer/PLA should result in more important pore blocking effect because of interpenetration of PEG chains in the PLA core thereby exhibiting reduced microporosity as is evident from the microporosity results. Also, presence of melting endotherm of PEG in these NPs (Fig. 4.3) clearly suggests existence of PEG microdomains which was not the case with any of the grafted copolymer NPs.

Further support to the suggested internal structure of NPs comes from XPS analysis of surface chemistry of these NPs. Relative PEG concentrations at NP surfaces were found to be 5.5%, 9.1% and 3.7% for PEG_{1%-g}-PLA, PEG_{5%-g}-PLA and multiblock copolymer NPs respectively (Table 4.2). It is evident that proportionate enrichment of the surface with PEG could not be seen on increasing grafting percentage from 1% to 5%, further supporting penetration of some PEG chains inside the core of PEG_{5%-g}-PLA NPs reducing their microporosity. NPs of multiblock copolymer showed least amount of PEG present at the surface despite its highest total PEG content (Table 4.1). These XPS results confirm incorporation of substantial amount of PEG chains in the PLA core of multiblock copolymer NPs, rendering higher hydrophilicity to the cores of these NPs.

4.4.5. Microporosity measurements of Prop-loaded NPs

Table 4.3. Characterization of Prop-loaded NPs

NP Formulation	Size (nm)	Actual loading (% w/w)	% EE	S _{BET, N₂} ^c (m ² /g)	S _{BET, Kr} ^d (m ² /g)	T _g ^e
Multi-Prop	211 ± 6	3.01	40.10	3.79±0.62 ^{a,b}	3.69	36.64
Peg1-Prop	205 ± 10	4.13	55.07	20.4±1.10 ^a	19.12	48.14

Multi: multiblock copolymer + PLA (1:1), Peg1: PEG_{1%}-g-PLA; Peg5: PEG_{5%}-g-PLA;

Prop: Propafenone.HCl-loaded NPs of respective polymers, e. g., Multi-Prop: Prop-loaded NPs of 1:1 mixture of multiblock copolymer + PLA

EE: Encapsulation efficiency, calculated by ratio of drug encapsulated in NPs to the initial drug added × 100

Actual loading = mg of drug encapsulated per 100 mg of NPs

^a: p < 0.05 as compared to respective blank NPs (student's paired t-test)

^b: p < 0.001 as compared to prop-loaded PEG_{1%}-g-PLA NPs (student's paired t-test)

^c: S_{BET, N₂}: surface area measured by nitrogen gas

^d: S_{BET, Kr}: surface area measured by krypton gas

^e: Glass transition temperature calculated as half extrapolated tangents from second run of the DSC thermograms of respective NPs

All values are mean ± S.D. of n=3

Above-mentioned results have demonstrated dependence of internal structure of NPs on the molecular structure of polymer. These changes in the microstructure of NPs are expected to reflect in their drug release properties. Indeed, extensive studies have shown dependence of gas permeability properties of various polymers on their microporosity^{9, 32}. Such research was rarely applied to the field of controlled release polymers, to the best of our knowledge. It is evident from the literature that drug release profiles from pegylated particulate systems are still controversial regardless of many studies being conducted in this area. Some studies have reported enhanced release rates with presence of PEG²⁰ whereas others have reported the opposite trend²¹. Hence, one can safely assume the role of nanoparticle internal structure to influence their drug release behaviour. Previously, we

have successfully used microporosity to explain release kinetics of propafenone hydrochloride (Prop) from NPs of PEG-*g*-PLA¹⁹, which could not have been otherwise explained by their drug loading differences or thermal properties. To further probe into release mechanism from pegylated polymers with different molecular structure, drug-loaded NPs were prepared using Prop as a model drug.

Some of the properties of Prop-loaded NPs are enlisted in Table 4.3. High resolution nitrogen isotherms, BET surface area as well as micropore volume plots of all Prop-loaded NPs followed the same trend as blank NPs, with NPs of PEG_{1%}-*g*-PLA having the highest and that of multiblock copolymer having the least microporosity (Supporting information, Fig. S2).

Given the fact that all NPs showed similar particle size distribution (Fig. S3, supporting information), changes in BET surface area would then be due to differences in texture, which can be caused by different crystal faces, local crystalline disorder, surface roughness or the presence of impurities. However, most frequently it has its source in the presence of micropores³³. We have confirmed the N₂- BET surface area of multiblock copolymer and PEG_{1%}-*g*-PLA polymer NPs by krypton adsorption at -196°C in the relative pressure range of 0.05 to 0.3. Krypton has a much smaller saturation pressure (1.63 torrs) compared to nitrogen (760 torrs) at -196°C, which allows to increase the sensitivity of the manometric adsorption measurements significantly¹⁴. In other words, krypton adsorption allows to obtain accurate surface areas for materials with small specific surface areas (< 0.05 m²/g), or if only a very small amount of sample is available (as is the case here, i.e. the total surface area provided for the measurements was for most samples around 0.5 m²). As indicated, the specific surface area measured by krypton was found to be in excellent agreement with that measured with nitrogen (3.69 Vs 3.79 m²/g for multiblock copolymer and 19.12 Vs 20.4 m²/g for PEG_{1%}-*g*-PLA) (Table 4.3).

4.4.6. *In vitro* drug release

The main purpose of this study was to compare and study the effect of microporosity on drug release profiles of pegylated NPs. NPs of PLA and PEG_{5%}-*g*-PLA polymers showed very marginal differences in their microporosity as compared to PEG_{1%}-*g*-PLA NPs (Supporting information, Fig. S2). Also, actual drug loading in PLA NPs was

very low (only 0.45% w/w) as compared to NPs of pegylated polymers (3-5% w/w). This would also affect the release pattern from PLA NPs. Hence, multiblock copolymer and PEG_{1%}-g-PLA NPs showing clear differences in microporosity were selected for *in vitro* release studies (Fig. 4.7). Multiblock copolymer NPs showed the faster drug release than PEG_{1%}-g-PLA NPs. It can be clearly seen that NPs followed reverse trend of release kinetics (multiblock copolymer > PEG_{1%}-g-PLA) as compared to microporosity (PEG_{1%}-g-PLA > multiblock copolymer). It is also worthy to mention here that *in vitro* drug release curve of PEG_{5%}-g-PLA NPs was in between PEG_{1%}-g-PLA and multiblock copolymer NPs (Data not shown as no statistical difference was found between the groups) as could be predicted from its microporosity data.

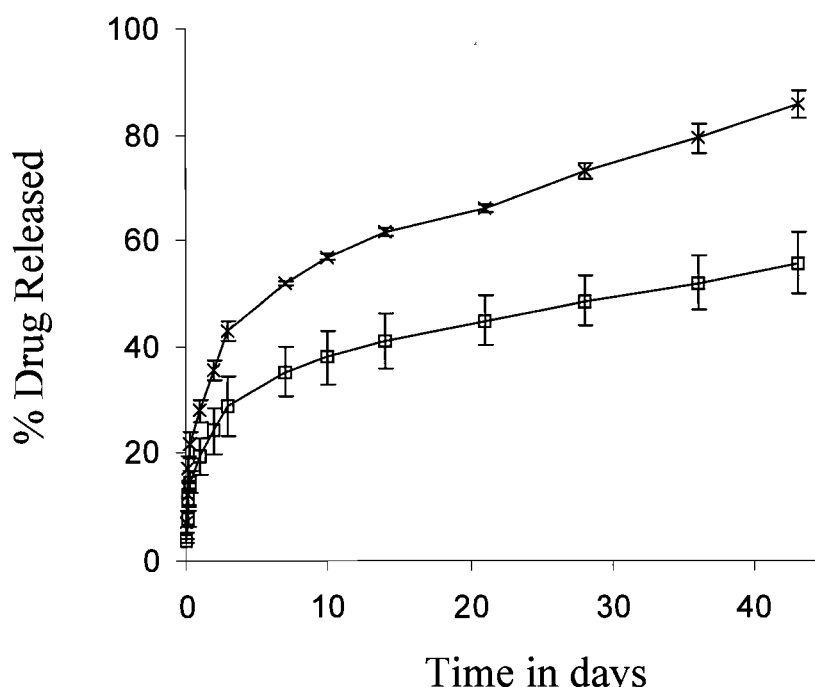


Figure 4.7. Effect of polymer type on *in vitro* release profile of Prop-loaded NPs; values are represented as mean \pm S. D. of 3 independent experiments. PEG_{1%}-g-PLA (□), (PLA-PEG-PLA)_n (×)

It is well known that diffusion of the drug into the release medium depends on its effective diffusion coefficient through polymer matrix, which in turn, depends on the porosity and tortuosity of matrix³⁴. It should be borne in mind that we are dealing with

nanosized particles in the range of 180-200 nm and not microparticles which have been shown to possess very big pores in the range of few micrometers. Unfortunately, various experiments in the field of nanoparticles have been limited to the macroscopic behaviour of drug release, and the information about a molecular-level mechanism underlying the diffusion of drug molecules through the polymer matrix is still poorly understood. For nanosized particles, it is not the big pores, but the micropores (pores smaller than 2 nm) will be important in the diffusion process. These micropores having smaller or similar size of drug molecules would act differently than the bigger pores, actually restricting the diffusion of drug molecules through the polymer matrix. In other words, these small pores would create compact structure due to limited cavities for the movement of drug molecules. Thus, increased microporosity eventually renders the polymer matrix more compact and tortuous unlike the big pores. This would decrease the effective diffusion coefficient of the drug and thus, slow down drug release process. Hence, in our case, higher microporosity of grafted copolymer NPs hindered movement of big drug molecules like propafenone (1.6 nm as calculated from Chemoffice 8.0) through the aqueous channels further reducing its effective diffusion coefficient and thus, the final rate of release³⁵.

Recently, Zhao et al³⁶, studied the mechanism of diffusion of aspirin molecules in polymer matrix by molecular dynamics simulation and again, it is to be emphasized that wriggling of the polymer chain and free volume of the polymer matrix were proposed to be the diffusion mechanisms. In this work, authors have emphasized importance of the size of cavities available in polymer matrix for the diffusion of drug molecules. When these cavities are small (for instance, micropores in our case), the drug molecules cannot jump from one cavity to other and have to depend on the wriggling of the polymer chain (short irregular movements of polymer chains up and down or from side to side). Surprisingly, in accordance with our work, the authors³⁶ also found that diffusion coefficient of aspirin increases with increase in the PEG concentration in polymer matrix. If we carefully observe our results and schematics in Figure 4.6, multiblock copolymer NPs have more PEG entrapped in the polymer matrix and hence, the faster diffusion and consequently, faster release of Prop from this polymer matrix. Thus, this work again confirmed the results corroborated in our first study¹⁹ that microporosity really plays an important role in drug release kinetics. In fact, it should be noted that these findings are experimental proof of the results obtained by molecular dynamic simulation³⁶.

The NPs of PEG_{1%}-g-PLA and multiblock copolymer were also subjected to gel permeation chromatography (GPC) during *in vitro* release study in order to determine the polymer degradation rate. The molecular weight reduction of PLA core was much faster in case of multiblock copolymer NPs in contrast to the negligible change in case of PEG_{1%}-g-PLA NPs (Supporting information, Fig. S4). These results emphasize that rapid core wetting in multiblock copolymer due to PEG entrapment enhances the polymer degradation rate after 21 days and in turn, the porosity increasing drug release rate.

Above results of *in vitro* drug release and NP degradation provide additional support to the hypothesis of polymer chain organization during NPs formation as proposed in fig. 4.6 and pore blocking effect exhibited by multiblock copolymer NPs. It is widely established that hydrophilicity of the matrix is one of the major driving forces in its hydration and in turn, the drug release kinetics^{37, 38}. In case of multiblock copolymer NPs, a major portion of PEG is entrapped in the core during NP formation (Fig. 4.6c). In addition to enhancing hydrophilicity of core, this PEG will result in pore blocking and reduced microporosity of NPs in dry state as measured by gas adsorption. Once these NPs are placed in release medium, hydrophilic PEG chains will draw water and swell rapidly into the core leading to formation of water channels. This will also result into opening of the blocked pores in the core of multiblock copolymer NPs. This in turn, is translated into rapid drug release. Indeed, multiblock copolymers of PEG and PLLA have been reported to be more hydrophilic than their PLLA homopolymer resulting in faster drug release^{39, 40}. Core of grafted copolymer NPs will be predominantly hydrophobic due to the presence of major fraction of PLA in the core (Fig. 4.6b). Thus, the rate limiting factor in drug release from these cores will be amount and accessibility of surface pores, wetting and effective diffusion coefficient. Thus, higher microporosity as well as hydrophobicity of the core justifies slower drug release from the NPs of grafted copolymers.

4.5 Conclusion

In conclusion, the nitrogen adsorption technique has been successfully used to gain insight into microporosity at angstrom level. Porosity data thus obtained, also pointed out to the fact that the polymers with diverse chemistry and architecture rearranged differently during NP formation. This decided the internal microstructure of NPs and determined the

kinetics of drug release. Rate of drug release from NPs correlated well with the changes in microporosity. In a nutshell, this study clearly showed the important effect of microporosity of nanoparticles on the drug release kinetics.

4.6 Acknowledgements

Authors are grateful to Natural Sciences and Engineering Research Council of Canada (NSERC) for funding this project and award of Postgraduate Scholarship to Shilpa Sant during her Ph. D. Authors wish to thank Dr. Christian Pellerin, Professor Adjoint, Department of Chemistry, University of Montreal along with Julie Boivin and Sylvain Esseimbre, Research agents, Department of Chemistry, University of Montreal for their help in the design and data analysis of DSC experiments.

4.7 Supporting information available

Detailed thermal properties, cumulative micropore volume after drug loading, size distribution profile and SEC analysis data after degradation of NPs. This additional information is available free of charge via the internet at <http://pubs.acs.org>.

4.8 References

1. Panyam, J.; Labhasetwar, V., *Adv Drug Deliv Rev* 2003, 55, (3), 329-47.
2. Sunderland, C. J.; Steiert, M.; Talmadge, J. E.; Derfus, A. M.; Barry, S. E., *Drug Dev Res* 2006, 67, (1), 70-93.
3. Brigger, I.; Dubernet, C.; Couvreur, P., *Adv Drug Deliv Rev* 2002, 54, (5), 631-51.
4. Frank, A.; Rath, S. K.; Venkatraman, S. S., *J Control Release* 2005, 102, (2), 333-344.
5. Quellec, P.; Gref, R.; Dellacherie, E.; Sommer, F.; Tran, M. D.; Alonso, M. J., *J Biomed Mater Res* 1999, 47, (3), 388-95.
6. Gorner, T.; Gref, R.; Michenot, D.; Sommer, F.; Tran, M. N.; Dellacherie, E., *J Control Release* 1999, 57, (3), 259-68.
7. Chorny, M.; Fishbein, I.; Danenberg, H. D.; Golomb, G., *J Control Release* 2002, 83, (3), 389-400.

8. Petrov, O.; Furo, I.; Schuleit, M.; Domanig, R.; Plunkett, M.; Daicic, J., *Int J Pharm* 2006, 309, (1-2), 157-162.
9. McKeown, N. B.; Budd, P. M., *Chem Soc Rev* 2006, 35, (8), 675-683.
10. Budd, P. M.; McKeown, N. B.; Fritsch, D., *J Mater Chem* 2005, 15, (20), 1977-1986.
11. Wang, D.; Zhu, G.; Zhang, Y.; Yang, W.; Wu, B.; Tang, Y.; Xie, Z., *New J Chem* 2005, 29, (2), 272-274.
12. Yang, Y.-Y.; Chung, T.-S.; Bai, X.-L.; Chan, W.-K., *Chem Eng Sci* 2000, 55, (12), 2223-2236.
13. Rouquerol, J.; Avnir, D.; Fairbridge, C. W.; Everett, D. H.; Haynes, J. H.; Pernicone, N.; Ramsay, J. D. F.; Sing, K. S. W.; Unger, K. K., *Pure Appl Chem* 1994, 66, (8), 1739-1758.
14. Lowell, S.; Shields, J. E.; Thomas, M. A.; Thommes, M., *Characterization of Porous Solids and Powders: Surface Area, Pore Size and Density*. Kluwer Academic Publishers: Dordrecht, 2004.
15. Lee, J. F.; Lee, C. K.; Juang, L. C., *J Colloid Interface Sci* 1999, 217, (1), 172-176.
16. El Shafei, G. M.; Philip, C. A.; Moussa, N. A., *J Colloid Interface Sci* 2004, 277, (2), 410-6.
17. Wang, C. C.; Juang, L. C.; Lee, C. K.; Hsu, T. C.; Lee, J. F.; Chao, H. P., *J Colloid Interface Sci* 2004, 280, (1), 27-35.
18. Wang, C. C.; Juang, L. C.; Hsu, T. C.; Lee, C. K.; Lee, J. F.; Huang, F. C., *J Colloid Interface Sci* 2004, 273, (1), 80-86.
19. Sant, S.; Nadeau, V.; Hildgen, P., *J Control Release* 2005, 107, (2), 203-214.
20. Matsumoto, J.; Nakada, Y.; Sakurai, K.; Nakamura, T.; Takahashi, Y., *Int J Pharm* 1999, 185, (1), 93-101.
21. Peracchia, M. T.; Gref, R.; Minamitake, Y.; Domb, A.; Lotan, N.; Langer, R., *J Control Release* 1997, 46, 223-231.
22. Nadeau, V.; Leclair, G.; Sant, S.; Rabanel, J.-M.; Quesnel, R.; Hildgen, P., *Polymer* 2005, 46, (25), 11263-11272.
23. Quesnel, R.; Hildgen, P., *Molecules* 2005, 10, (1), 98-104.
24. Shakesheff, K. M.; Evora, C.; Soriano, I.; Langer, R., *J Colloid Interface Sci* 1997, 185, (2), 538.

25. Merino, S.; Brauge, L.; Caminade, A. M.; Majoral, J. P.; Taton, D.; Gnanou, Y., *Chem-A Eur J* 2001, 7, (14), 3095-3105.
26. Kulinski, Z.; Piorkowska, E.; Gadzinowska, K.; Stasiak, M., *Biomacromolecules* 2006, 7, (7), 2128-2135.
27. Horvath, G.; Kawazoe, K., *J Chem Eng Japan* 1983, 16, (5), 470-475.
28. Dombrowski, R. J.; Lastoskie, C. M.; Hyduke, D. R., *Colloids Surfaces A Physicochem Eng Asp* 2001, 187, 23-39.
29. Shin, D.; Shin, K.; Aamer, K. A.; Tew, G. N.; Russell, T. P.; Lee, J. H.; Jho, J. Y., *Macromolecules* 2005, 38, (1), 104-109.
30. Wang, S.; Cui, W.; Bei, J., *Anal Bioanal Chem* 2005, 381, (3), 547-556.
31. Pakunlu, R. I.; Wang, Y.; Saad, M.; Khandare, J. J.; Starovoytov, V.; Minko, T., *J Control Release* 2006, 114, (2), 153-162.
32. Ilinitch, O. M.; Fenelonov, V. B.; Lapkin, A. A.; Okkel, L. G.; Terskikh, V. V.; Zamaraev, K. I., *Microporous Mesoporous Mater* 1999, 31, (1-2), 97-110.
33. Cejka, J.; Zilkova, N.; Rathousky, J.; Zukal, A.; Jagiello, J., *Langmuir* 2004, 20, (18), 7532-7539.
34. Veith, S. R.; Hughes, E.; Vuataz, G.; Pratsinis, S. E., *J Colloid Interface Sci* 2004, 274, (1), 216-28.
35. Lemaire, V.; Belair, J.; Hildgen, P., *Int J Pharm* 2003, 258, (1-2), 95-107.
36. Zhao, Z. J.; Wang, Q.; Zhang, L.; Liu, Y. C., *Journal of Physical Chemistry B* 2007, 111, (17), 4411-4416.
37. Roy, D. S., *Eur J Pharm Sci* 2002, 16, (3), 193-199.
38. Sung, K. C., *Int J Pharm* 1998, 172, (1-2), 17-25.
39. Luo, W.; Li, S. M.; Bei, J. Z.; Wang, S. G., *J Appl Polym Sci* 2002, 84, (9), 1729-1736.
40. Chen, W.; Luo, W.; Wang, S.; Bei, J., *Polym Adv Technol* 2003, 14, (3-5), 245-253.

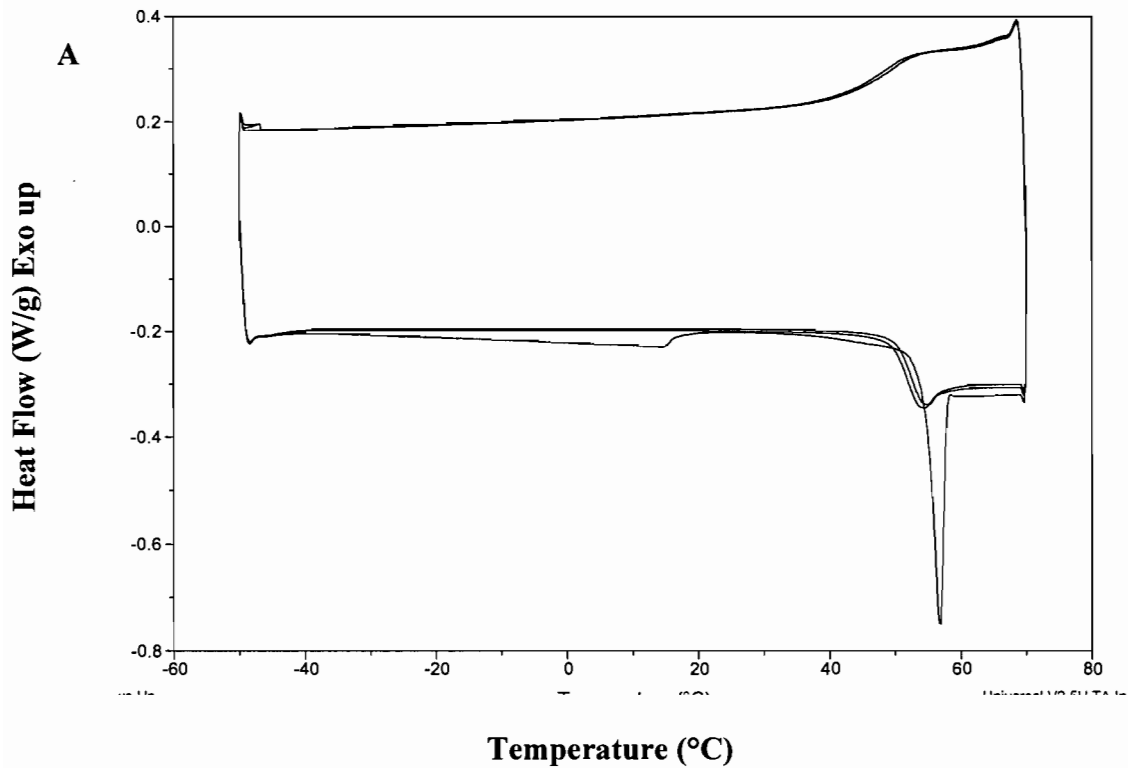
3.1 Supporting information

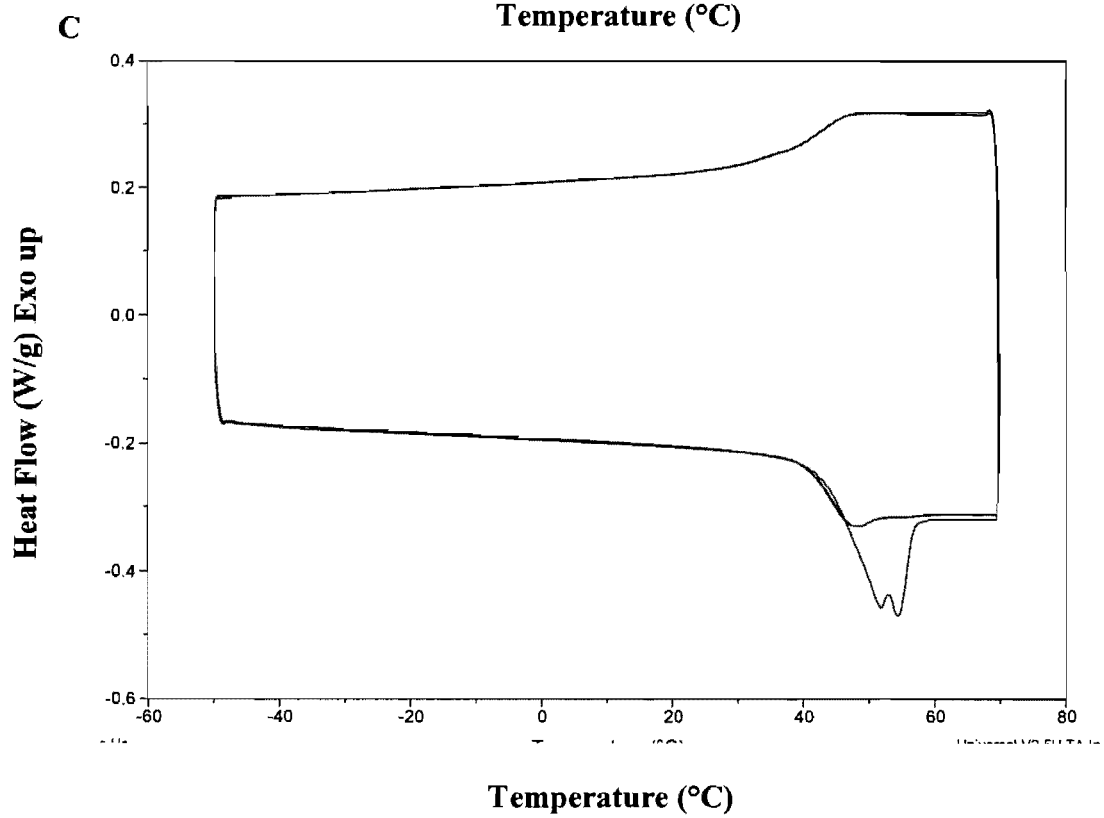
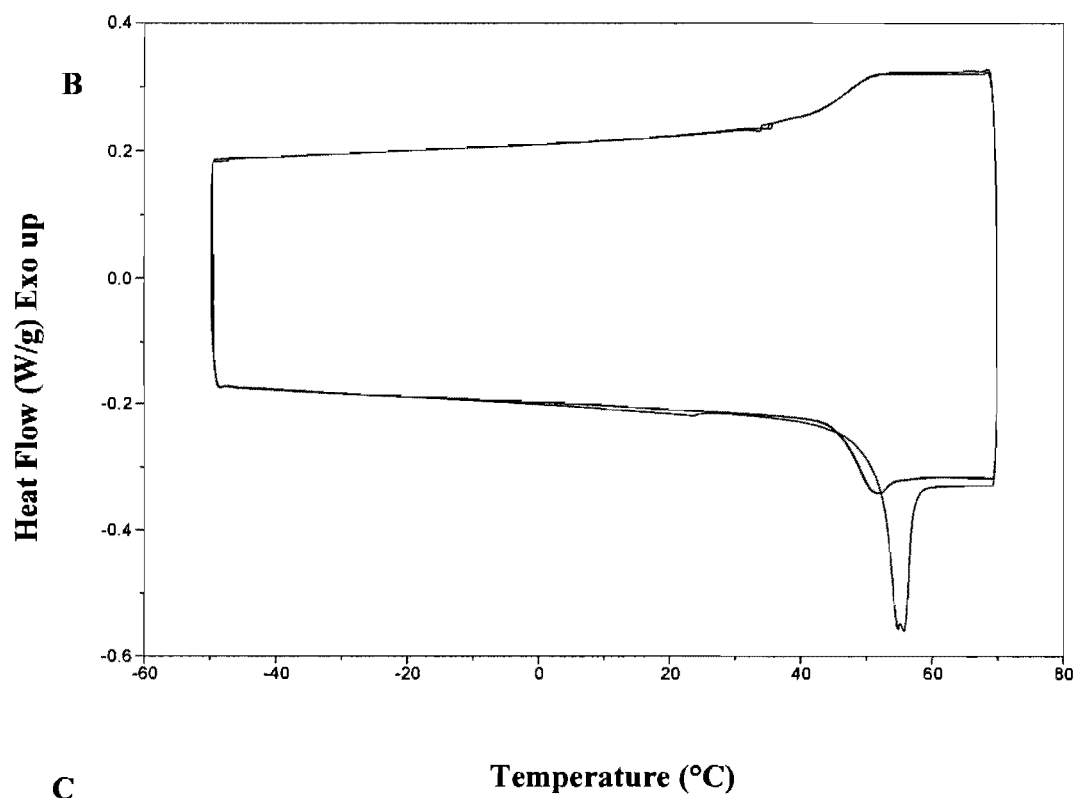
MICROPOROUS STRUCTURE AND DRUG RELEASE KINETICS OF POLYMERIC NANOPARTICLES *

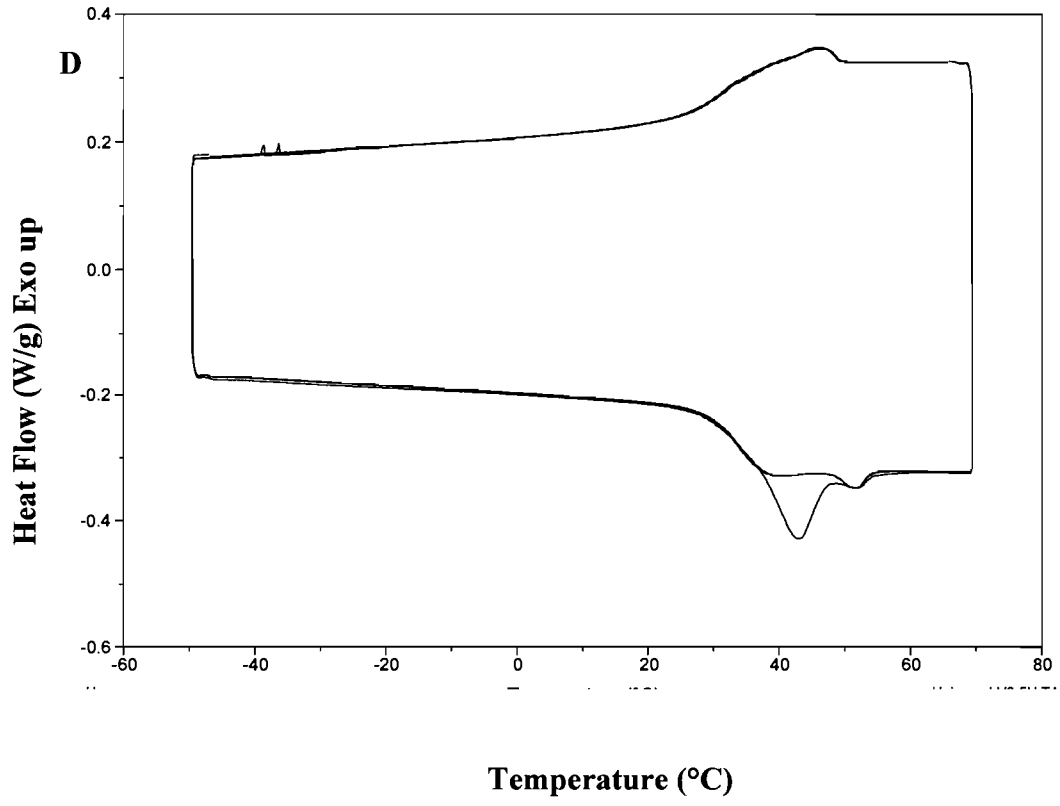
DSC Studies on blank NPs

Figure S1

Three subsequent DSC thermograms of respective NPs heated at the rate of 10°C/min from -50 to 70°C, PLA (A), PEG_{1%}-g-PLA (B), PEG_{5%}-g-PLA (C), and (PLA-PEG-PLA)_n (D)







Microporosity of Prop-loaded pegylated NPs

Figure S2

Microporosity of Prop-loaded NPs of PEG_{1%}-g-PLA (■), PEG_{5%}-g-PLA (+) and (PEG-PLA-PEG)_n (●).

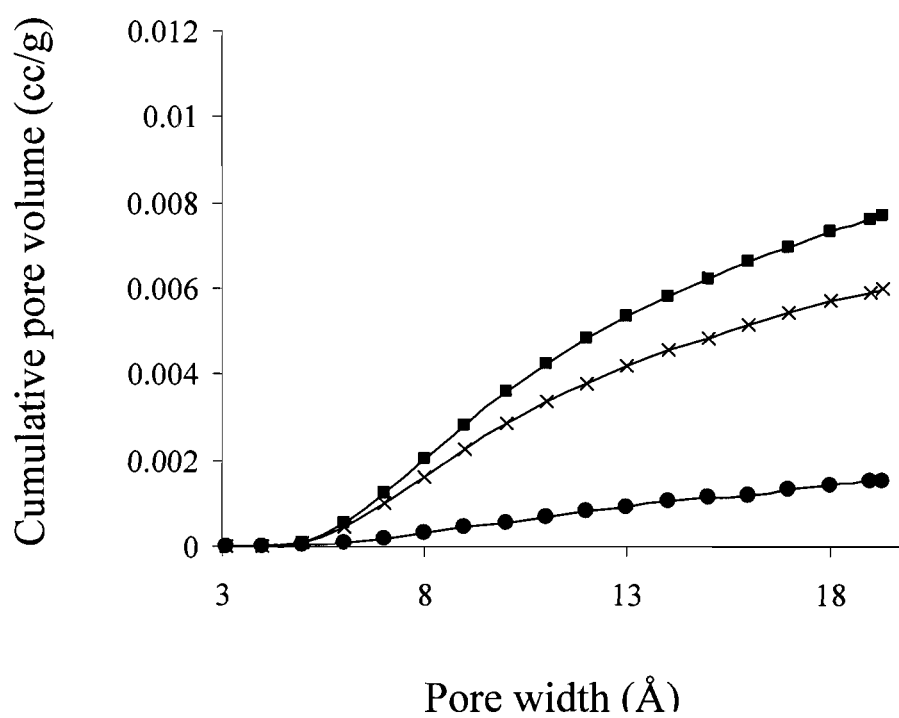


Figure S3**Particle size distribution of prop-loaded NPs**

Particle size distribution for Prop-loaded NPs; PEG_{1%}-g-PLA (□), PEG_{5%}-g-PLA (▲), (PLA-PEG-PLA)_n (×)

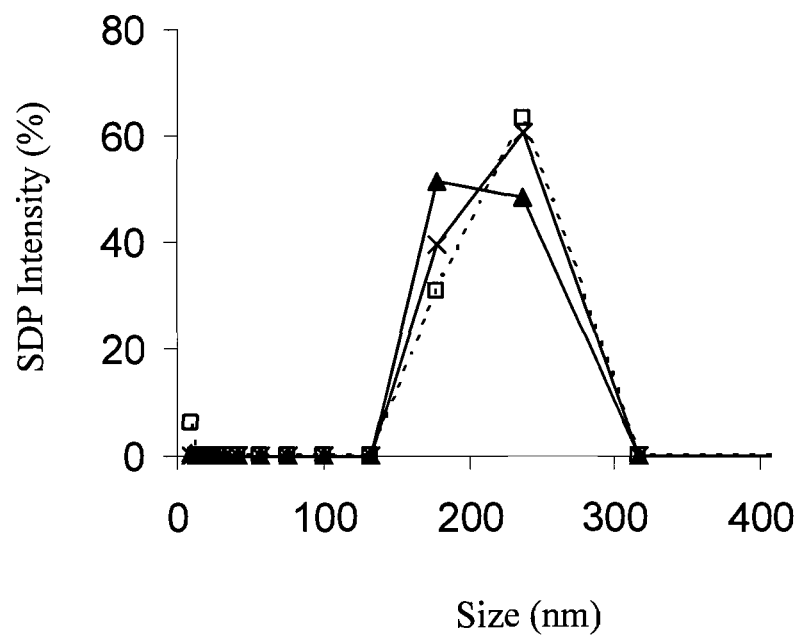
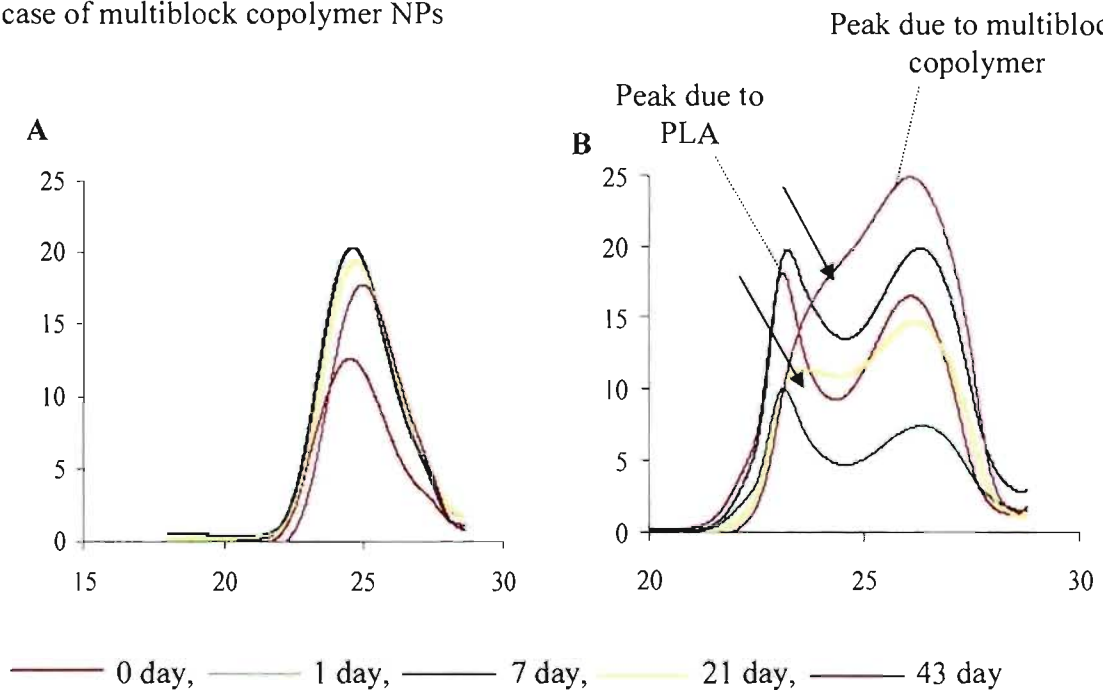


Figure S4**Gel permeation chromatography of NPs at various intervals of time during release studies**

Degradation studies of (A) PEG_{1%}-g-PLA and (B) multiblock copolymer NPs by GPC NPs were suspended in PBS, pH 7.4 at 37°C in shaking water bath. The study was terminated at 0, 1, 7, 21, and 43 days, NPs were lyophilized and molecular weight distribution was determined by gel permeation chromatography using polystyrene standards and tetrahydrofuran as mobile phase. The arrows indicate disappearing peak for PLA cores in case of multiblock copolymer NPs



LINK BETWEEN SECOND AND THIRD ARTICLE

In the first part of this thesis, we have explored polymer architecture, drug loading and other formulation factors affecting the microporosity and internal structure of NPs. This, in turn, had global effect on drug release kinetics. However, just tailoring to the need of release properties is not sufficient to achieve the best results with any colloidal drug carriers.

It is well documented that surface properties of vectors are crucial in deciding their *in vivo* behavior. For successful drug delivery vehicle, it should be stable in biological milieu and further, reach the target site (e.g. tissue/cell) or even its intracellular target (e.g. cytoplasm/nucleus). Thus, to further exploit formulated nanoparticulate system to target to various cancers or inflammatory diseases or even to brain, the next important issue was their protein resistant ability, cytocompatibility and cellular interaction properties. The major concern was how the polymer architecture affected PEG density at the surface of these vectors and whether this surface PEG could be effective in rendering these NPs protein-resistant and reduce their uptake by macrophages. Hence, further experiments were designed to study the surface properties of these vectors with respect to morphology, charge & PEG density. Also, efforts were directed to understand their impact on protein binding, cellular interaction and uptake mechanisms.

CHAPTER 5.
EFFECT OF POLYMER ARCHITECTURE ON
SURFACE PROPERTIES, PLASMA PROTEIN
ADSORPTION AND CELLULAR INTERACTIONS OF
PEGYLATED NANOPARTICLES

EFFECT OF POLYMER ARCHITECTURE ON SURFACE PROPERTIES, PLASMA PROTEIN ADSORPTION AND CELLULAR INTERACTIONS OF PEGYLATED NANOPARTICLES *

Shilpa Sant¹, Suzie Poulin² and Patrice Hildgen^{1**}

¹Faculty of Pharmacy, University of Montreal, C. P. 6128 succ. Centre-ville, Montreal, QC, H3C 3J7

²: École Polytechnique, C.P.6079, Succ. Centre-ville, Montréal, QC, H3C 3A7

** To whom correspondence should be addressed: Faculty of Pharmacy, University of Montreal, C.P. 6128, Succ. Centre-ville, Montreal (Qc) CANADA H3C 3J7, Tel: +1(514) 343-6448, Fax: +1(514) 343-6871, Email [REDACTED]

* : Accepted with minor revision in Journal of Biomedical Materials Research: Part A

5.1 Abstract

Aim of the present study was to evaluate the cellular interaction of nanoparticles (NPs) prepared from different pegylated polymers and elucidate the effect of polymer architecture, for instance, grafted versus block copolymer on their cellular uptake. Fluorescein-labeled NPs of 4 different polymers, viz., poly(D,L lactide) (PLA), poly(ethylene glycol)_{1%}-*graft*-poly(D,L lactide) (PEG_{1%}-*g*-PLA), poly(ethylene glycol)_{5%}-*graft*-poly(D,L lactide) (PEG_{5%}-*g*-PLA) and (poly(D,L lactide)-block-poly(ethylene glycol)-block-poly(D,L lactide))_n multiblock copolymer (PLA-PEG-PLA)_n were prepared. These NPs were characterized for size, zeta potential and surface morphology. XPS studies revealed possibility of chemical interaction between PLA-COOH groups and PVA-OH groups, thus making it difficult to be washed off from the NP surface completely. Grafted polymer NPs showed more surface PEG coverage than (PLA-PEG-PLA)_n despite of their comparatively lower PEG content. The results of surface properties were translated into protein binding showing least amount of proteins bound to grafted copolymer NPs as against multiblock copolymer NPs. NPs showed no toxicity to RAW 264.7 cells. Cellular uptake of NPs was temperature and concentration-dependent as well as involved clathrin-

mediated processes. Thus, this study confirms the importance of polymer architecture in determining the surface properties and hence, protein binding and cellular interactions of NPs. Also, it was shown that grafted copolymer NPs reduced macrophage uptake as compared to multiblock copolymer although mechanisms different than phagocytosis were involved.

Keywords: Polymer architecture, Pegylated polymers, Surface properties, Protein binding, Phagocytosis, AFM phase imaging

5.2 Introduction

The ultimate goal of controlled release drug delivery system is to maximize therapeutic activity while minimizing the negative side effects of the drug. In this regard, versatile nanoscale delivery vehicles like nanoparticles (NPs) are being designed based on novel biomaterials. Once administered intravenously, these NPs are recognized by mononuclear phagocytic system (MPS) due to opsonization. Size and surface characteristics of NPs both play an important role in the blood opsonization and clearance kinetics¹⁻⁴. Larger particles (200 nm and above) and those with hydrophobic surfaces are more efficient in activating human complement system and cleared faster from the blood than their smaller counterparts. Hence, precision surface engineering with synthetic polymers is often required to control NP interaction and their fate within the biological system.

Among various approaches described, surface stabilization of NPs and liposomes with poly (ethylene glycol) (PEG) has proved to be one of the most successful strategy for suppressing macrophage recognition and prolonging circulation times of such colloidal particles^{3,5,6}. The efficiency of this process depends on the polymer type, surface stability, reactivity and physics (surface density and conformation)^{7,8}. Despite the identification of various physicochemical parameters like surface charge, PEG chain length, its molecular weight, PEG layer thickness, density and conformation of PEG layer^{2,9-12}, effect of molecular architecture of copolymers on their protein resistance ability remains to be adequately addressed. Indeed, polymer architecture markedly influences not only the physicochemical properties of the polymer, but also various facets of drug delivery systems including drug release rate, biodistribution and even interaction with specific tissues or

cells *in vivo*⁸. Thus, optimizing polymer architecture is an intelligent strategy to develop desired pharmaceutical product. Such studies would offer valuable feedback to tune properties of polymer-based drug delivery systems.

Once the long-circulating carrier reaches the desired tissue, next step is its intracellular entry. Intracellular trafficking of macromolecules is very complex phenomenon and has been reviewed recently¹³. It involves different pathways like phagocytosis (for large particles and by specialized cells like macrophages, neutrophils and dendritic cells) and pinocytosis (generally common to all cells). Pinocytosis can be receptor/ligand-mediated (e.g. clathrin- and caveole-mediated) or constitutive (e.g. adsorptive or fluid phase endocytosis). Now, which of these pathways are involved in the uptake mechanism of the carrier will be dependent on its surface properties and will decide the extent of uptake into the cells. Several studies have correlated physicochemical properties of particles to protein adsorption and/or *in vitro* phagocytosis in macrophages¹⁴⁻¹⁸. However, reports focusing on their uptake mechanisms in macrophages are still lacking in literature. Indeed, cellular uptake mechanisms have been studied in detail for various epithelial and cancer cell lines whereas their role in macrophages was seldom studied according to the best of our knowledge. It is reported that phagocytosis takes place for particles larger than 500 nm in size, however, why smaller particles are taken up by macrophages and by which mechanisms remains to be addressed. It is possible that macrophages can effectively take up these 200 nm or smaller particles by mechanisms other than phagocytosis. Although it is shown that presence of PEG on the surface of these NPs reduces their macrophage uptake, whether it is really by reduced phagocytosis or by other mechanisms like endocytosis, macropinocytosis or fluid phase pinocytosis still remains a topic of research. Further, if this reduced macrophage uptake of small size NPs is by reduced endocytosis, the same rule will definitely be extended to other non-phagocytic cells in the body, thus seriously hampering the efficacy of intracellular distribution of pegylated NPs. In fact, it is already reported that incorporation of PEG was useful in controlling pharmacokinetics of the nanocarriers on one hand, while hampering their interaction with the targeted cells and thus, therapeutic efficiency, especially in gene delivery¹⁹⁻²³. Hence, the present study was undertaken to evaluate effect of diverse molecular architecture (block versus graft copolymers) on surface properties and macrophage uptake of pegylated NPs. Further, efforts were made to find out correlation

between the physicochemical properties of NPs with their surface protein adsorption and *in vitro* macrophage uptake. Also, detailed investigation was carried out to shed some light on their uptake mechanism/s by macrophages.

5.3 Materials and methods

5.3.1 Materials

D,L- Lactide, poly(ethylene glycol) methyl ether (2,000 Da), allyl glycidyl ether, tetraphenyltin, polyvinyl alcohol (PVA, average M_w 9,000-10,000 Da, 80% hydrolyzed), fluorescein, and ethyl carbodiimide were purchased from Aldrich chemical company Inc., Milwaukee, USA. Dichloromethane (DCM) was purchased from Laboratoire Mat Inc., Montreal, QC, Canada. All materials for cell culture were purchased from Invitrogen (Burlington, ON, Canada).

5.3.2 Synthesis of polymers

Poly(D,L)lactide (PLA) homopolymer was synthesized by ring-opening polymerization of dilactide under argon using tetraphenyltin as catalyst. Dilactide was crystallized from toluene solution and dried under vacuum before use. Weighed amount of purified dilactide was placed in round bottom flask and purged thoroughly with argon to displace air present in the sample. Bulk polymerization was carried out under argon at 180°C for 6 h. The polymer thus obtained was dissolved in acetone and purified by precipitation in water.

Polymers with polyethylene glycol grafted poly-(D,L) lactide (PEG-g-PLA) (PEG M_w 2,000 Da) were synthesized in our laboratory as reported earlier^{24,25}. Multiblock copolymer, (PLA-PEG-PLA)_n was synthesized as reported²⁶ using PEG with M_n of 1500, and succinic acid was used as condensing agent to link triblock copolymers.

Synthesized polymers were characterized by ¹H NMR, gel permeation chromatography (GPC) and differential scanning calorimetry (DSC). ¹H NMR spectra were recorded on Bruker ARX 400 spectrometer (Bruker Biospin, Billerica, MA, USA).

Chemical shift (δ) was measured in ppm using tetramethylsilane (TMS) as an internal reference. Mole % of PEG was calculated with respect to PLA from ^1H NMR data.

GPC was performed on Water Associate Chromatography System (Waters, Milford, MA, USA) equipped with refractive index detector and Phenomenex Phenogel 5 μ column. Polystyrene standards were used for calibration with chloroform as mobile phase at a flow rate of 0.6 mL/min.

The thermal properties of pure polymers were characterized by DSC analysis (DSC Q1000, V9.0, build 275, Universal 4.1 D, TA Instruments, Grimsby, ON, Canada). Weighed samples were sealed in crimped aluminum pans with lids and were heated at the rate of 10°C/min from -50°C to 220°C (2 runs) The samples were purged with pure dry nitrogen at a flow rate of 50 mL/min. The DSC was calibrated for temperature with indium (Goodfellow, 99.999% pure), and tin (NIST SRM 2000). The instrument was calibrated for heat flow with indium (Goodfellow, 99.999% pure). The analyses of the obtained DSC thermograms were done using Universal analysis 2000, version 14.0C, TA instruments, Grimsby, ON, Canada. Results of polymer characterization are enlisted in Table 5.1.

5.3.3 Preparation of nanoparticles (NPs)

Blank NPs of PLA, PEG_{1%}-g-PLA, PEG_{5%}-g-PLA and (PLA-PEG-PLA)_n were prepared by emulsion-solvent evaporation method ²⁵. Each polymer (500 mg) was dissolved in 5 mL of DCM and emulsified in 50 mL of 0.5 % w/v PVA solution as an external aqueous phase using high-pressure homogenizer (Emulsiflex C30, Avestin, Ottawa, Canada) at a pressure of 10,000 psi for 3 min. The emulsion was collected by washing with another 50 mL of 0.5% PVA solution. DCM was evaporated under reduced pressure with constant stirring to obtain NPs. NPs were collected by centrifugation at 35,000 g for 45 min (Sorval[®] Evolution_{RC}, Kendro, Newton, CT, USA). NP suspension was then lyophilized (Freeze Dry System, Lyph.Lock 4.5, Labconco) to get dry NPs and stored at 4°C until further use. 1:1 (w/w) mixture of PLA and multiblock copolymer was used for preparing multiblock copolymer NPs due to its low molecular weight.

5.3.4 Fluorescence labeling of blank NPs

Blank NPs (100 mg) of PLA, PEG_{1%}-g-PLA, PEG_{5%}-g-PLA and (PLA-PEG-PLA)_n were suspended in PBS. Fluorescein (5 mg) was added to this suspension followed by ethyl carbodiimide and the suspension was stirred for 3 days in dark. Labeled particles were then dialysed (6-8 kDa, Spectra Por 1 membrane, Spectrum Laboratories, CA, USA) against distilled water for 5 days until no fluorescence was detected in the dialysate. Dry particles were obtained by lyophilization.

5.3.5 Characterization of NPs

5.3.5.1 Particle size distribution

NP size and size distribution was measured by photon correlation spectroscopy (PCS) (N4 Plus, Coulter Electronics, Miami, FL, USA) at 25°C and 90° scattering angle for 180 seconds. The mean particle diameter was calculated using differential size distribution processor (SDP) intensity analysis program.

5.3.5.2 Zeta potential measurement

NPs were suspended in 0.22 µm filtered 0.25% w/v saline solution and zeta potential was measured in triplicate on Malvern ZetaSizer Nanoseries ZS (Malvern Instruments, Worcestershire, UK).

5.3.5.3 Surface morphology and phage image analysis

Freshly cleaved mica surface was dipped in poly-L-lysine solution (4 mg/mL) for 45 minutes followed by thorough washing of the surface with 0.22 µm filtered Mili-Q water to remove excess of poly-L-lysine. The surfaces were then dipped vertically in respective NP suspension for 30 minutes. Excessively deposited NPs were washed off with 0.22 µm filtered Mili-Q water followed by air-drying. Topography and phase images of these samples were captured simultaneously using Nanoscope IIIa Dimension 3100 atomic force microscope (Digital Instruments, Santa Barbara, CA, USA). All Images were acquired using 125 µm TappingMode™ etched silicon probes (TESP7) with tip radius of 5-10 nm, spring constant of 20-100 N/m and resonance frequency of 200-400 kHz. A set-point ratio

(ratio of engaged oscillation amplitude to free air oscillation amplitude) between 0.6 and 0.8 was used for all topographic and phase images unless otherwise stated.

5.3.5.4 XPS analysis

XPS analysis of powdered NP samples was performed on VG Scientific ESCALAB MK II using Mg K α X-rays (hv 1253.6 eV) and an electron take off angle of 0°. A single survey scan spectrum (0-1000 eV) and narrow scans for C1s (210-305 eV) and O1s (525-550 eV) were recorded for each sample with a pass energy of 1 eV and 0.5 eV, respectively. Acquisition and data analysis were performed by a VGS 5000 data system. Peak fitting of the C1s envelope was as described by Shakesheff et al²⁷. Chemical shifts were referenced to hydrocarbon at 285 eV.

5.3.5.5 Plasma protein binding

NPs (5 mg) were incubated with 100 μ L whole human serum for 18 h at 37°C with gentle agitation. Loosely bound protein fraction was removed by thorough washing with Milli-Q water. Adsorbed proteins were desorbed by incubating with Laemmli sample buffer (Sigma, St. Louis, USA) and then, analysed by SDS-PAGE on 10% polyacrylamide gel performed on a Mini Vertical Gel System (Fisher Biotech, Canada). The gel was run at 150 V for 1 h and then developed with silver stain. Briefly, the gel was shaken gently by soaking in 50% methanol followed by freshly prepared staining solution (1 mL 0.2 g/mL silver nitrate added to solution of 5.2 mL 0.36% NaOH and 0.35 mL of 14.8 M ammonium hydroxide, volume was made upto 25 mL) for 10-15 min. The gel was further washed with deionized water twice for 5 min and then developed for 5-10 min in a development solution containing 0.5 mL of 1% w/v citric acid and 50 μ L of 37% formaldehyde in 100 mL water. After washing once in deionized water, the gel was destained in a mixture of 45% v/v methanol and 5% v/v acetic acid. Revealed gels were scanned by exposition to UV light using a ChemiImager 5500 imaging system (Alpha Innotech Corp., San Leandro, CA).

5.3.6 Cell culture

Macrophage cell line, RAW 264.7 was a kind gift from Dr. Jean-Christophe Leroux, (Faculty of Pharmacy, University of Montreal, QC, Canada). The cells were grown in Dulbecco's modified Eagle cell culture medium (DMEM) containing 10% (v/v) heat-

inactivated fetal bovine serum, 100 U/mL penicillin-G and 100 mg/mL streptomycin (Invitrogen, Burlington, ON, Canada) in an atmosphere of 5% CO₂ and 95% relative humidity. The cells were routinely passaged at 90–95% confluence.

5.3.6.1 Evaluation of cellular toxicity of blank NPs

Inhibition of cell proliferation was assessed by tetrazolium salt 3-(4,5-dimethylthiazol-2-yl)-2,5-diphenyl tetrazolium bromide (MTT) assay. Briefly, 5×10^5 RAW 264.7 cells were seeded in 96-well flat bottom plates (Costar, Corning, NY) and allowed to grow for 24 h. The cells were then incubated with increasing concentrations of blank NPs for 24 h. Cell layers were washed with cold PBS and further incubated with 10 μ L of MTT solution (5 mg/mL in PBS) for 4 h at 37°C. Formazan crystals formed were then dissolved along with the cell layers and absorbance was measured on microplate reader at 570 nm. Cell viability was calculated with respect to PBS as control.

5.3.6.2 Cellular interaction with RAW 264.7

RAW 264.7 cells (1×10^5 cells/ well) were plated in 96-well flat bottom plates (Costar, Corning, NY) and allowed to adhere overnight in DMEM with 10% serum. Next day, the medium was removed and replaced by RPMI 1640 without serum. The cells were then incubated with different concentrations of fluorescein-labeled PLA or pegylated NPs for 3 h at 37°C. The cell monolayers were washed with cold PBS (pH 7.4) and then lysed with 0.2% Triton-X 100 in 0.2 N NaOH solution. The fluorescence was measured on microplate reader at excitation and emission wavelength of 494 nm and 520 nm, respectively. The amount of NPs phagocytosed was calculated from calibration curve of NPs under the same conditions. To find the mechanism of cellular entry, cell monolayers were incubated with endocytic and metabolic inhibitors as described by Huang et al²⁸. First, the cell monolayers were incubated with different inhibitors for 1 h, followed by NPs (160 μ g/mL) for another 3 h. Cell monolayers were then washed four times with cold PBS (pH 7.4) followed by 100 μ L 5 mM EDTA (pH 5.0) and then lysed with 0.2% Triton-X 100 in 0.2 N NaOH solution. The fluorescence was measured on microplate reader at excitation and emission wavelength of 494 nm and 520 nm, respectively.

5.4 Results and Discussion

5.4.1 Polymer characterization

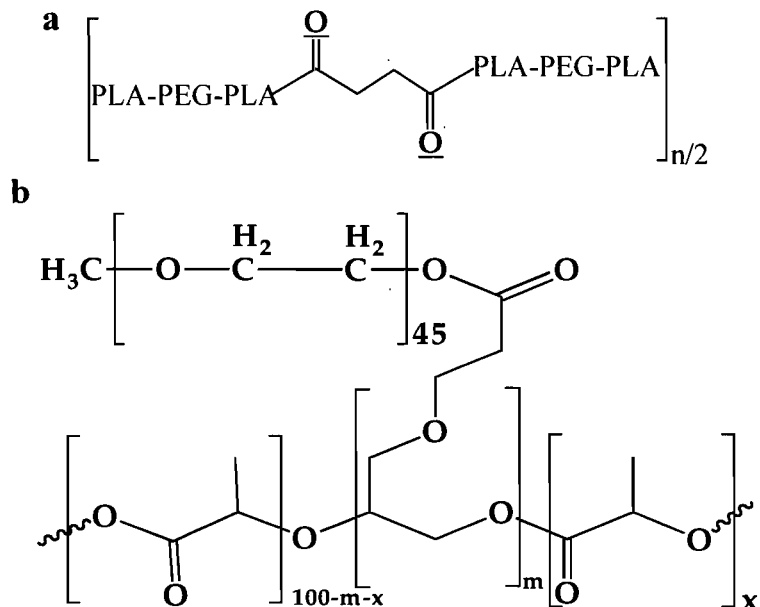


Figure 5.1. Chemical structures of multiblock copolymer (a) and grafted copolymers (b) where $m=1$ and 5 for PEG_{1%}-g-PLA and PEG_{5%}-g-PLA.

Table 5.1. Polymer characterization by gel permeation chromatography, ¹H NMR and DSC

Polymer	M_n	M_w	M_w/M_n	PEG* (mol %)	T_g °C**
Poly(D,L)Lactide	18222	24844	1.36	-	41.2
PEG1%-g-PLA	9753	15059	1.54	1.2	47.3
PEG5%-g-PLA	9245	14363	1.55	7.0	34.8
(PLA-PEG-PLA) _n	5250	6120	1.16	17.8	15.7

*: Calculated by NMR

** : Calculated from second run of DSC

Chemical structures of the polymers are shown in Fig. 5.1. The measured molecular weight, polydispersity, and thermal properties of synthesized polymers are summarized in Table 5.1. Polymers with well defined composition and low polydispersities were obtained using the employed synthesis route.

5.4.2 Size and charge of NPs

Table 5.2 shows the particle size distribution and zeta potential data of NPs. Mean diameter of all NPs was in the range of 180-195 nm. Zeta potential measurements revealed that PLA NPs had lowest negative zeta potential (-2.5 mV) and multiblock copolymer had the most negative zeta potential of -22.7 mV (Table 5.2). Zeta potential results of PLA NPs are in agreement with Zambaux et al²⁹ who obtained the value of -4 mV for PLA NPs prepared with PVA. This low zeta potential for PLA NPs could be attributed to presence of PVA on the surface of these NPs. In case of NPs of grafted polymers, lower zeta potential can be correlated to the arrangement of PEG groups on the surface of NPs. On the other hand, high negative zeta potential of multiblock copolymer NPs was attributed to the presence of ester bonds in the structure on the multiblock copolymer where the delocalization of negative charges was possible as suggested by Quaglia et al³⁰. This may also mean presence of insufficient amount of PEG and/or unprotected surfaces on these NPs.

Table 5.2. Characterization of NPs

Formulation	Size (nm)	Polydispersity	Zeta potential (mV)
PLA	185	0.359	-2.5 ± 0.61
PEG _{1%} -g-PLA	180	0.078	-5.97 ± 0.83
PEG _{5%} -g-PLA	184	0.22	-7.72 ± 1.69
(PLA-PEG-PLA) _n	192	0.019	-22.72 ± 2.06

5.4.3 Surafec morphology and phase analysis

Tapping mode atomic force microscopy (TM-AFM) is a versatile technique, which allows probing soft samples such as biological and polymeric materials^{31,32}. One recent development in TM-AFM is the use of the changes in the phase angle of the cantilever probe to produce phase image. This image often provides more contrast than the topographic image and has been shown to be sensitive to material surface properties such as stiffness, viscoelasticity and chemical composition^{31,33,34}. In general, changes in the phase angle during scanning are related to energy dissipation during tip-sample interaction^{31,34}. It has been shown previously that phase contrast images recorded in moderate tapping force ($r_{sp} = 0.5-0.7$) can be related to such properties as viscoelasticity or stiffness^{33,34}. Although AFM has been widely used to study the topography of NPs/micelles³⁵⁻³⁷, phase image analysis has not yet been reported to study the surface of NPs to the best of our knowledge. We report phase image AFM studies of NP samples to explore the possibility of detection of PEG on the surface of pegylated NPs due to viscoelastic and/or hydrophilicity differences between PLA and PEG chains.

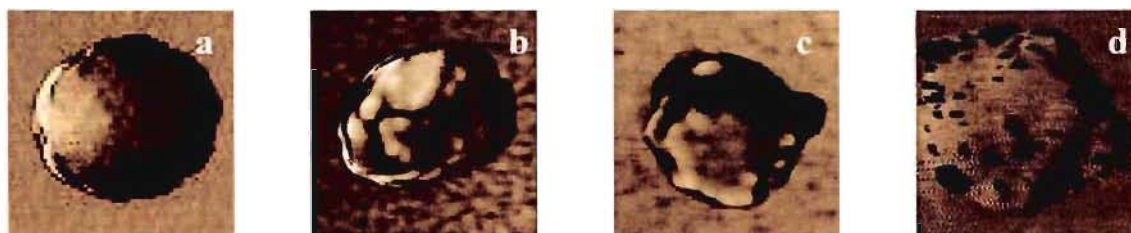


Figure 5.2. Tapping mode AFM phase images of NPs. all images are acquired in air. Scan size: 250×250 (nm \times nm): PLA (a), PEG_{1%}-g-PLA (b), PEG_{5%}-g-PLA (c), PLA-PEG-PLA)_n (d)

The TM-AFM phase images of PLA, grafted and multiblock copolymer NPs acquired at moderate tapping force are shown in Fig. 5.2. It can be seen that PLA particles had homogenous surface without any phase separation (Fig. 5.2 a). This may suggest that residual PVA coated the surface of PLA NPs very homogeneously, in turn, masking negative surface charge (Table 5.2). On the other hand, all pegylated NPs showed the presence of sharp phase contrast (Fig. 5.2 b-d). As PEG has smaller Young's modulus than PLA³⁸, PEG molecule is softer than PLA resulting into darker regions for PEG in the phase

images due to negative phase shift. This has already been demonstrated for poly(styrene-*b*-ethylene oxide) polymer films where softer PEG segments resulted in darker regions embedded in lighter polystyrene matrix³⁹. Thus, AFM studies gave a direct visible proof for the presence of PEG on the surface of pegylated NPs.

5.4.4 XPS analysis

XPS analysis was carried out to probe into surface composition of these NPs prepared with different polymers and to quantitate PEG/PVA concentration on their surface. XPS spectrum of PEG showed one peak corresponding to ether carbons (286.4 eV, Table 5.3). PVA polymer showed three main peaks corresponding to C-C/C-H (285 eV), C-OH (1.3 eV shift) and O-C=O (4.2 eV shift) environments. For pure PLA polymer, the best envelop fit was obtained using three main peaks corresponding to C-C/C-H (285 eV), C-OH (1.9 eV shift) and O-C=O (4.0 eV shift) environments (Table 5.3). These results are in accordance with Shakesheff et al²⁷.

Table 5.3. Relative peak areas from XPS surface analysis

Functional group	Chemical shift/Atomic percentage						
	Pure materials as reference			Nanoparticles			
	PLA	PVA	PEG	PLA	PEG _{1%}	PEG _{5%}	Multi + PLA (50:50)
C-C (PVA)	-	0.0/48.5	-	0.0/27.3	0.0/14.7	0.0/8.4	0.0/13.9
C-C (PLA)	0.0/38.3	-	-	0.0/7.8	0.0/16.1	0.0/25.6	0.0/25.8
C-O (PVA)	-	1.3/41.5	-	1.3/23.5	1.3/12.7	1.3/7.3	1.3/11.9
C-O (PLA)	1.90/31.0	-	-	1.9/6.3	1.9/13.1	1.9/20.8	1.9/21.0
C-O (PEG)	-	-	1.45/100	-	1.6/5.5	1.5/9.1	1.5/3.7
O-C=O (PVA)	-	4.2/10.1	-	4.2/5.8	4.2/3.1	4.2/1.8	4.2/2.9
O-C=O (PLA)	4.0/30.7	-	-	4.0/6.3	4.0/12.9	4.0/20.6	4.0/20.8
*C-O-C=O	-	-	-	1.0/14.9	1.25/9.3	1.25/1.4	-
C-O-*C=O	-	-	-	2.1/8.2	2.1/12.7	2.1/5.0	-

Primary C 1s chemical shifts (eV) relative to saturated hydrocarbon (C 1s = 285.0 eV)

Interestingly, XPS data of PLA NPs could not be fitted using only 3 peaks observed in PLA polymer sample. Same results were obtained even though analysis was repeated twice and on a different instrument to rule out any sample handling or instrumental error. To get the best envelop fit, two additional peaks had to be added corresponding to C-O-*C=O (2.1 eV shift) and *C-O-C=O (1.0 to 1.25 eV shift) (Table 5.3). These additional peaks obtained in PLA NPs could be the result of chemical interaction between PLA –COOH end groups and PVA –OH groups during NP formation. It is well-known that a fraction of PVA remains associated with the NPs despite of repeated washings and this has been attributed to the hydrophobic interactions between vinyl acetate segment of PVA and PLA/PLGA core^{40,41}. Presence of two additional peaks corresponding to *C-O-C=O and C-O-*C=O in the XPS spectrum of PLA NPs indicate the possibility of chemical interaction between PLA and PVA. This explains the surface homogeneity of PLA NPs as revealed by AFM and also supports effective masking of negative charge of these NPs.

Analysis of NPs prepared from grafted polymers showed similar results where best envelop fit was obtained by addition of two more peaks as that found for PLA NPs, again suggesting the similar reaction taking place between available PLA –COOH and PVA –OH groups (Table 5.3). This interaction became weaker with increasing PEG grafting percentage (total contribution of additional peaks were 22% and 6.4% for PEG_{1%}-g-PLA and PEG_{5%}-g-PLA NPs, respectively, Table 5.3). Although multiblock copolymer NPs showed presence of PVA, these peaks were absent indicating no chemical reaction between the polymer and PVA. This seems logical as synthesis of multiblock copolymer has been realized by polymerization between PLA –COOH and PEG –OH groups, first resulting in triblock copolymers which are then condensed to form multiblock copolymers. Thus, it is clear that number of free –COOH end groups available for reaction with PVA-OH groups are much less in multiblock copolymer NPs in contrast to PLA homopolymer and grafted polymers. Whatever may be the mechanism of PVA adsorption (physical adsorption or chemical reaction), all pegylated polymers decreased surface PVA adsorption almost by 50% as compared to PLA. This is attributed to the enhanced surface hydrophilicity. This is consistent with Shakesheff et al²⁷, who reported reduced PVA adsorption for more hydrophilic PLGA microspheres than PLA microspheres.

XPS analysis also revealed that PEG surface concentration for PEG_{1%}-g-PLA and PEG_{5%}-g-PLA NPs was 5.5 and 9.1% respectively, whereas multiblock copolymer NPs showed only 3.7% surface composed of PEG despite of high PEG content in the copolymer (17.8 mol% for multiblock copolymer as against 1-7 mol% for grafted copolymers, Table 5.1 and Table 5.4). This was attributed to the polymer architecture. Peculiar architecture of grafted polymers allowed easy migration of PEG on the surface of NPs whereas covalent linkage of PEG with two PLA blocks hampered this process in multiblock copolymer, thus reducing its surface coverage. Indeed, Rieger et al⁹ have recently observed that grafted copolymers of poly(ϵ -caprolactone) (PCL) and PEG resulted in 70 % PEG available at NP surface, compared to 25% in case of diblock copolymer. They proposed grafted copolymer to have palm tree like structure where hydrophobic PCL trunk served as anchoring block while hydrophilic PEG palms formed denser hydrophilic brush. On the other hand, diblock copolymer consisted of only one PEG block resulting in less surface packing in this case.

Table 5.4. Relative percentage of monomer from area under the curves from respective C1s peaks

Nanoparticles	Lactide	Vinyl alcohol	PEG
PLA	20.4	56.4	-
PEG1%	42.1	30.5	5.5
PEG5%	67.0	17.5	9.1
Multi + PLA (50:50)	67.6	28.7	3.7

In a nutshell, it can be seen that PLA NPs had more hydrophilic surface (56% surface covered with PVA), followed by PEG_{1%}-g-PLA and PEG_{5%}-g-PLA NPs whereas multiblock copolymer NPs had highest proportion of PLA on the surface (Table 5.4). The absence of chemical reaction with PVA and low surface PEG coverage of multiblock copolymer NPs supports higher negative potential of multiblock copolymer NPs due to delocalization of negative charge.

5.4.5 Plasma protein binding

Surface properties of a carrier decide the extent and specificity of protein adsorption. With constant research in this area a general assumption was put forth that more

protein adsorbs on to poorly water wettable (hydrophobic) surfaces⁴². Nagahama et al⁴³ have recently shown that 8-armed pegylated polymer had improved resistance to protein adsorption and cell adhesion than 2-armed linear polymer due to their lower water absorption capacity. Similarly, Rieger et al⁹ have shown that PCL-*g*-PEO copolymers were more effective in preventing protein adsorption as compared to PEO-*b*-PCL diblock copolymers. These results are directly correlated to the effective PEG surface density on NPs as a consequence of polymer architecture. In accordance with XPS results, multiblock copolymer NPs displayed less amount of PEG and more amount of PLA on the surface and hence, they would be less wettable. Indeed, the silver-stained SDS-PAGE profiles in Fig. 5.3 reveal that PLA and multiblock copolymer NPs adsorbed higher amounts of proteins, compared with grafted copolymer NPs. It is worthy to note that only few protein bands are visible in grafted copolymer NPs as against PLA and multiblock copolymer NPs. This puts forward the fact that surface PEG concentration of any colloidal drug delivery system is more important than total polymer PEG concentration in determining their protein resistant ability.

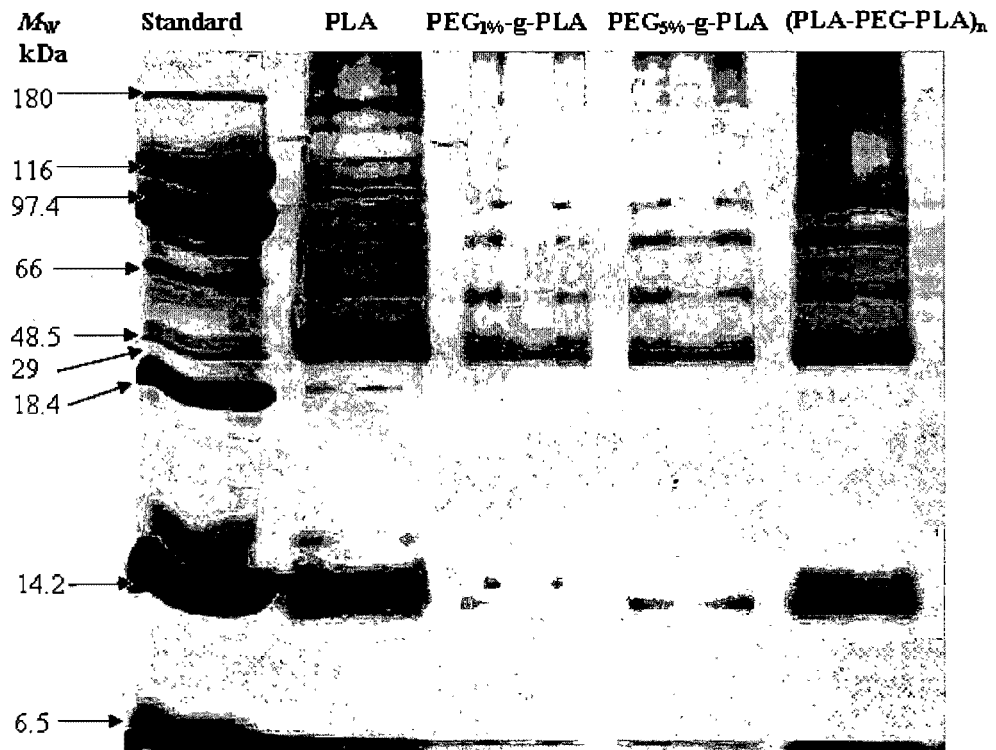


Figure 5.3. Plasma protein adsorption of different NPs by SDS-PAGE gel electrophoresis

5.4.6 Cellular toxicity and uptake studies

PLA is a well-known biodegradable and biocompatible polymer. In our study, NPs of all the polymers were well tolerated and exhibited no adverse effects on the cell viability as shown by cell proliferation assays (Fig. 5.4).

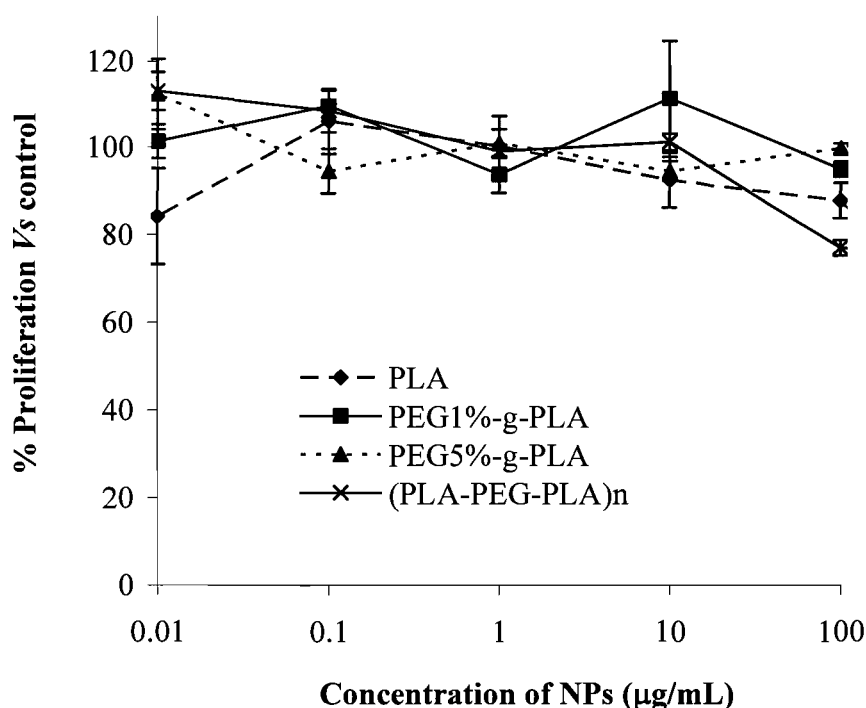


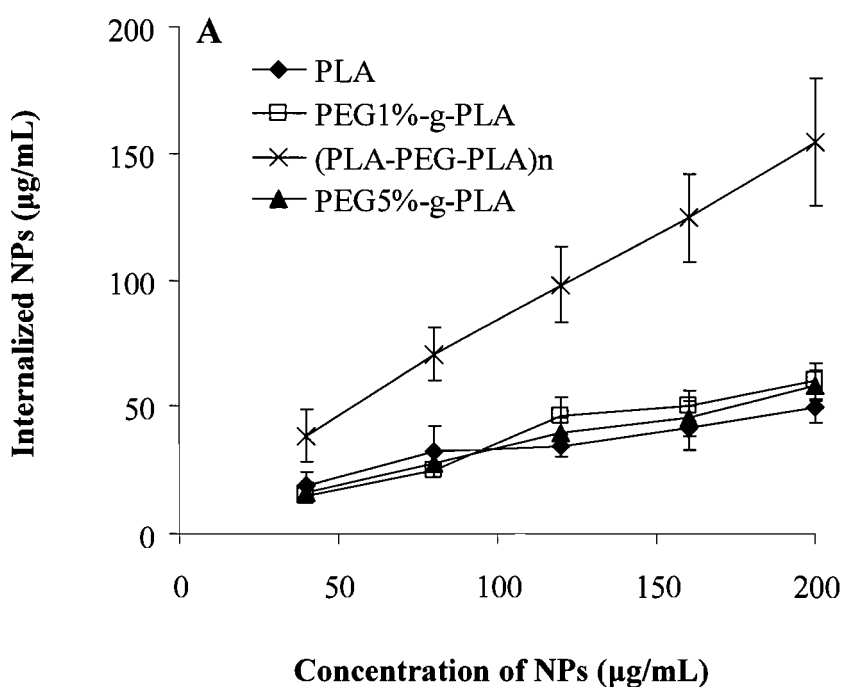
Figure 5.4. Cytotoxicity of NPs in RAW 264.7 cells by MTT assay. PLA (◆); PEG_{1%}-g-PLA (■); PEG_{5%}-g-PLA (▲); (PLA-PEG-PLA)_n (×)

In the uptake study by RAW 264.7 cells, reduced uptake was observed for PLA NPs. This is the result of high and uniform adsorption of residual PVA on PLA NPs. These results are in accordance with Sahoo et al⁴⁰ and Prabha et al⁴⁴ who have reported decreased cellular uptake and decreased gene transfection efficiency due to presence of PVA on the surface of NPs. Thus, the uptake results of pegylated NPs cannot actually be compared with PLA NPs as a positive control. It is interesting to note that grafted polymer NPs resulted in lower degree of internalization in macrophages compared to multiblock copolymers NPs. This may be ascribed to surface hydrophobicity and charge of the multiblock copolymer NPs. Highly anionic surface charge and presence of less PEG (thus, more hydrophobic surface) was thought to be the reason for this increased uptake of multiblock copolymer

NPs. Indeed, it has been previously found that macrophage uptake of NPs increases with surface charge^{45,46} and surface hydrophobicity⁴⁷. Roser et al⁴⁶ have studied phagocytosis of albumin NPs in U-937 cells as well as activated mouse peritoneal macrophages. Their results showed that higher negative or positive surface charge of albumin particles significantly increased their cellular uptake. Fang et al¹⁸ have also shown increased uptake of negatively charged poly(hexadecyl cyanoacrylate) NPs in macrophages as compared to their less negative pegylated NPs. It has also been reported that negatively charged particles are taken up by Kupffer cells by non-specific scavenger receptor-mediated endocytosis⁴⁵. These results suggest the possibility of use of negatively charged multiblock copolymer NPs for their potential application in liver targeting whereas grafted copolymer NPs can be used as long-circulating drug carriers for intravenous administration.

It was further interesting to find out whether this difference in the uptake was related to different mechanisms operating at cellular level for different polymer types. Hence, cell monolayers were incubated with various metabolic and endocytic inhibitors in addition to the NPs. As shown in Fig. 5.5 A and B, the cellular uptake was concentration and temperature dependent as reported for poly(lactide-co-glycolide) NPs⁴⁸. Further, significant inhibition of uptake (35-62%, $p < 0.01$) of all NPs by metabolic inhibitor (sodium azide, 0.1%w/v) confirmed active endocytic mechanism of their uptake⁴⁴. It could be seen that grafted polymer NPs showed greater extent of inhibition with sodium azide than PLA and multiblock copolymer NPs (Fig. 5.6). Hyperosmotic sucrose (450 mM) inhibits fluid phase and receptor-mediated endocytosis⁴⁹. A 1 h pretreatment with sucrose resulted in drastic decrease in the uptake of all the NPs, especially pegylated NPs (50 to 90 % inhibition), further confirming fluid phase endocytosis as the major uptake pathway for these NPs. Chlorpromazine (10 $\mu\text{g}/\text{mL}$) is known to disrupt the assembly and disassembly of clathrin by reducing the number of coated pit-associated receptors⁵⁰ and it was found to reduce uptake of all NPs by 68 to 92%. Thus, all NPs showed fluid phase and clathrin-dependent endocytosis for their uptake. Interestingly, incubation of NPs with cytochalasin B (10 $\mu\text{g}/\text{mL}$), maneuver known to restrict actin polymerization surrounding endocytic vesicle in macropinocytosis⁵¹, did not affect uptake of PLA, PEG_{5%}-g-PLA and multiblock copolymer NPs significantly (6-9% inhibition) whereas PEG_{1%}-g-PLA showed significant inhibition (42%; $p < 0.01$) with cytochalasin B treatment. This difference in the results is not understood, but may be attributed to the different core/shell structure of NPs. Indeed,

Mahmud et al⁵² have reported similar discrepancy in internalization mechanism for PEO-*b*-PCL micelles having different block length finally affecting their core/shell structure. The authors have reported that cytochalasin B inhibited internalization of 5000-5000 and 5000-13000 PEO-*b*-PCL micelles without having any effect on the internalization of 2000-5000 and 5000-24000 PEO-*b*-PCL micelles. They assigned this to the difference in core/shell structure⁵². The reason for inconsistency in our results is not clear at this moment and needs further investigation. However, it is evident that uptake of pegylated NPs involved different endocytic routes and was not by phagocytosis. Also, polymer architecture resulted in change in the surface properties and hence, differences in the uptake of these NPs.



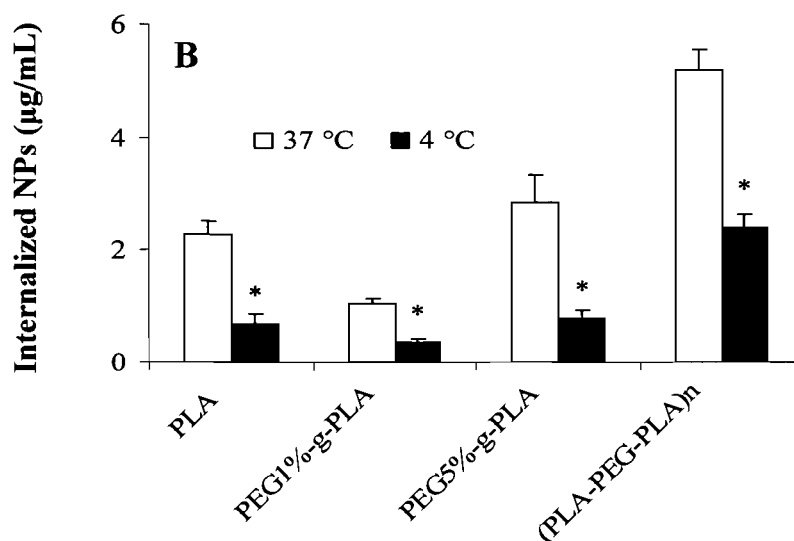


Figure 5.5. **A.** Effect of NP concentration on cellular uptake by RAW 264.7 cells. Cells were incubated with NPs at concentrations 40, 80, 120, 160 and 200 $\mu\text{g/mL}$ at 37 °C for 3 h. Mean \pm SD, $n = 5$; PLA (\blacklozenge); PEG_{1%}-g-PLA (\square); PEG_{5%}-g-PLA (\blacktriangle); (PLA-PEG-PLA)_n (\times); **B.** Effect of temperature on cellular uptake of NPs by RAW 264.7 cells. Cells were incubated with NPs at 37 °C (open bar) and 4 °C (filled bar) at a dose of 20 $\mu\text{g/mL}$

5.5 Conclusion

NPs were formulated using novel copolymers of PEG and PLA with different molecular architecture. AFM phase imaging studies successfully showed presence of PEG on the surface of pegylated NPs irrespective of their chemistry. Systematic study of surface characterization showed that multiblock copolymer displayed less amount of PEG on the surface due to interpenetration of PEG chains inside the core of NPs. This resulted in higher negative charge, surface hydrophobicity and less resistance to protein adsorption of multiblock copolymer NPs irrespective of its higher total PEG content. On the contrary, chemical structure of grafted copolymer favored easy migration of PEG chains on the surface of NPs improving their protein resistance despite of low total PEG content of these polymers. Covalently linked PEG was always more efficient in preventing protein binding as compared to homogeneously adsorbed PVA on PLA NPs. Further, cellular uptake studies clearly revealed clathrin dependent active endocytic pathways involved in their internalization. In a nutshell, molecular architecture of the polymer is an important

parameter controlling surface characteristics of NPs which in turn determine their protein resistant capabilities and cellular interactions.

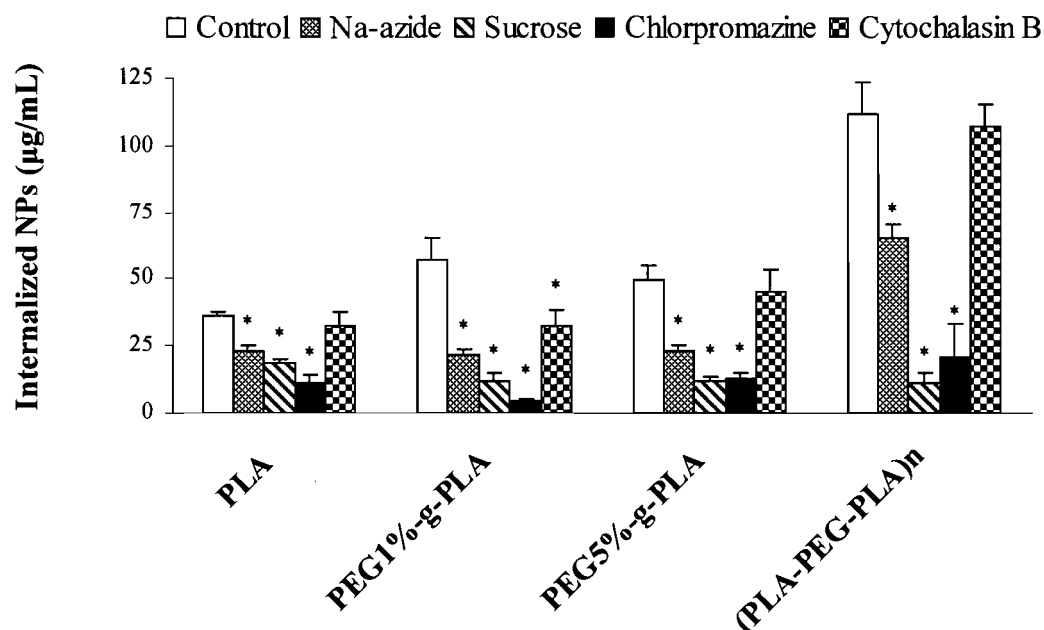


Figure 5.6. Uptake of fluorescent NPs of different polymers by RAW 264.7 cells at 37 °C in the presence of sodium azide (0.1% w/v), hyperosmolar sucrose (0.45 M), Chlorpromazine (10 µg/mL), and Cytochalasin B (10 µg/mL) (B). Cells were pretreated with the inhibitors for 1 h followed by NPs (160 µg/mL) for another 3 h. Mean ± SD, n ≥ 4; *: values significantly different at P > 0.01.

5.6 Acknowledgements

Authors are thankful to Natural Sciences and Engineering Council (NSERC), Canada for funding this work and Postgraduate Scholarship awarded to Shilpa Sant.

5.7 References

1. Deschamps AA, Grijpma DW, Feijen J. Poly(ethylene oxide)/poly(butylene terephthalate) segmented block copolymers: the effect of copolymer composition on physical properties and degradation behavior. *Polymer* 2001;42(23):9335-9345.

2. Owens DE, Peppas NA. Opsonization, biodistribution, and pharmacokinetics of polymeric nanoparticles. *Int J Pharm* 2006;307(1):93-102.
3. Moghimi SM, Hunter AC, Murray JC. Long-circulating and target-specific nanoparticles: theory to practice. *Pharmacol Rev* 2001;53(2):283-318.
4. Moghimi SM, Szebeni J. Stealth liposomes and long circulating nanoparticles: critical issues in pharmacokinetics, opsonization and protein-binding properties. *Prog Lipid Res* 2003;42(6):463-78.
5. Quellec P, Gref R, Perrin L, Dellacherie E, Sommer F, Verbavatz JM, Alonso MJ. Protein encapsulation within polyethylene glycol-coated nanospheres. I. Physicochemical characterization. *J Biomed Mater Res* 1998;42(1):45-54.
6. Li Y, Pei Y, Zhang X, Gu Z, Zhou Z, Yuan W, Zhou J, Zhu J, Gao X. PEGylated PLGA nanoparticles as protein carriers: synthesis, preparation and biodistribution in rats. *J Control Release* 2001;71(2):203-11.
7. Moghimi SM, Hunter AC, Murray JC. Nanomedicine: current status and future prospects. *Faseb J* 2005;19(3):311-330.
8. Qiu LY, Bae YH. Polymer architecture and drug delivery. *Pharm Res* 2006;23(1):1-30.
9. Rieger J, Passirani C, Benoit JP, Van Butsele K, Jerome R, Jerome C. Synthesis of amphiphilic copolymers of poly(ethylene oxide) and poly(epsilon-caprolactone) with different architectures, and their role in the preparation of stealthy nanoparticles. *Adv Funct Mater* 2006;16(11):1506-1514.
10. Mosqueira VCF, Legrand P, Gulik A, Bourdon O, Gref R, Labarre D, Barratt G. Relationship between complement activation, cellular uptake and surface physicochemical aspects of novel PEG-modified nanocapsules. *Biomaterials* 2001;22(22):2967-2979.
11. Woodle MC. Controlling liposome blood clearance by surface-grafted polymers. *Adv Drug Deliv Rev* 1998;32(1-2):139-152.
12. Papisov MI. Theoretical considerations of RES-avoiding liposomes: Molecular mechanics and chemistry of liposome interactions *Adv Drug Deliv Rev* 1998;32(1-2):119-138.
13. Omidi Y, Gumbleton M. Biological Membranes and Barriers. In: Mahato R, editor. *Biomaterials for Delivery and Targeting of Proteins and Nucleic Acids*. Boca Raton: CRC Press; 2005. p 232-273.

14. Zahr AS, Davis CA, Pishko MV. Macrophage uptake of core-shell nanoparticles surface modified with poly(ethylene glycol). *Langmuir* 2006;22(19):8178-8185.
15. Gbadamosi JK, Hunter AC, Moghimi SM. PEGylation of microspheres generates a heterogeneous population of particles with differential surface characteristics and biological performance. *FEBS Lett* 2002;532(3):338-44.
16. Gref R, Luck M, Quellec P, Marchand M, Dellacherie E, Harnisch S, Blunk T, Muller RH. 'Stealth' corona-core nanoparticles surface modified by polyethylene glycol (PEG): influences of the corona (PEG chain length and surface density) and of the core composition on phagocytic uptake and plasma protein adsorption. *Colloids Surf B Biointerfaces* 2000;18(3-4):301-313.
17. Vonarbourg A, Passirani C, Saulnier P, Simard P, Leroux JC, Benoit JP. Evaluation of pegylated lipid nanocapsules versus complement system activation and macrophage uptake. *J Biomed Mater Res A* 2006;78A(3):620-628.
18. Fang C, Shi B, Pei YY, Hong MH, Wu J, Chen HZ. In vivo tumor targeting of tumor necrosis factor-alpha-loaded stealth nanoparticles: Effect of MePEG molecular weight and particle size. *Eur J Pharm Sci* 2006;27(1):27-36.
19. Deshpande MC, Davies MC, Garnett MC, Williams PM, Armitage D, Bailey L, Vamvakaki M, Armes SP, Stolnik S. The effect of poly(ethylene glycol) molecular architecture on cellular interaction and uptake of DNA complexes. *J Control Release* 2004;97(1):143-156.
20. Behrens I, Pena AIV, Alonso MJ, Kissel T. Comparative uptake studies of bioadhesive and non-bioadhesive nanoparticles in human intestinal cell lines and rats: The effect of mucus on particle adsorption and transport. *Pharm Res* 2002;19(8):1185-1193.
21. Kaul G, Amiji M. Long-circulating poly(ethylene glycol)-modified gelatin nanoparticles for intracellular delivery. *Pharm Res* 2002;19(7):1061-1067.
22. Zhang Y, Kohler N, Zhang MQ. Surface modification of superparamagnetic magnetite nanoparticles and their intracellular uptake. *Biomaterials* 2002;23(7):1553-1561.
23. Hatakeyama H, Akita H, Kogure K, Oishi M, Nagasaki Y, Kihira Y, Ueno M, Kobayashi H, Kikuchi H, Harashima H. Development of a novel systemic gene delivery system for cancer therapy with a tumor-specific cleavable PEG-lipid. *Gene Ther* 2006;14(1):68-77.

24. Nadeau V, Leclair G, Sant S, Rabanel J-M, Quesnel R, Hildgen P. Synthesis of new versatile functionalized polyesters for biomedical applications. *Polymer* 2005;46(25):11263-11272.
25. Sant S, Nadeau V, Hildgen P. Effect of porosity on the release kinetics of propafenone-loaded PEG-g-PLA nanoparticles. *J Control Release* 2005;107(2):203-214.
26. Quesnel R, Hildgen P. Synthesis of PLA-b-PEG multiblock copolymers for stealth drug carrier preparation. *Molecules* 2005;10(1):98-104.
27. Shakesheff KM, Evora C, Soriano I, Langer R. The Adsorption of Poly(vinyl alcohol) to Biodegradable Microparticles Studied by X-Ray Photoelectron Spectroscopy (XPS). *J Colloid Interface Sci* 1997;185(2):538.
28. Huang M, Ma ZS, Khor E, Lim LY. Uptake of FITC-chitosan nanoparticles by A549 cells. *Pharm Res* 2002;19(10):1488-1494.
29. Zambaux MF, Bonneaux F, Gref R, Maincent P, Dellacherie E, Alonso MJ, Labrude P, Vigneron C. Influence of experimental parameters on the characteristics of poly(lactic acid) nanoparticles prepared by a double emulsion method. *J Control Release* 1998;50(1-3):31-40.
30. Quaglia F, Ostacolo L, De Rosa G, La Rotonda MI, Ammendola M, Nese G, Maglio G, Palumbo R, Vauthier C. Nanoscopic core-shell drug carriers made of amphiphilic triblock and star-diblock copolymers. *Int J Pharm* 2006;324(1):56-66.
31. Raghavan D, Gu X, Nguyen T, VanLandingham M, Karim A. Mapping Polymer Heterogeneity Using Atomic Force Microscopy Phase Imaging and Nanoscale Indentation. *Macromolecules* 2000;33(7):2573-2583.
32. Kopp-Marsaudon S, Leclere P, Dubourg F, Lazzaroni R, Aime JP. Quantitative Measurement of the Mechanical Contribution to Tapping-Mode Atomic Force Microscopy Images of Soft Materials. *Langmuir* 2000;16(22):8432-8437.
33. Magonov SN, Elings V, Whangbo MH. Phase imaging and stiffness in tapping-mode atomic force microscopy. *Surf Sci* 1997;375(2-3):L385-L391.
34. Paredes JI, Gracia M, Martinez-Alonso A, Tascon JMD. Nanoscale investigation of the structural and chemical changes induced by oxidation on carbon black surfaces: A scanning probe microscopy approach. *J Colloid Interface Sci* 2005;288(1):190-199.

35. Mu L, Feng SS. A novel controlled release formulation for the anticancer drug paclitaxel (Taxol): PLGA nanoparticles containing vitamin E TPGS. *J Control Release* 2003;86(1):33-48.
36. Zhang Y, Zhang J. Surface modification of monodisperse magnetite nanoparticles for improved intracellular uptake to breast cancer cells. *J Colloid Interface Sci* 2005;283(2):352-7.
37. Matejicek P, Stepanek M, Uchman M, Prochazka K, Spirkova M. Atomic force microscopy and light scattering study of onion-type micelles formed by polystyrene-block-poly(2-vinylpyridine) and poly(2-vinylpyridine)-block-poly(ethylene oxide) copolymers in aqueous solutions. *Collection of Czechoslovak Chemical Communications* 2006;71(5):723-738.
38. Garlotta D, Doane W, Shogren R, Lawton J, Willett JL. Mechanical and thermal properties of starch-filled poly(D,L-lactic acid)/poly(hydroxy ester ether) biodegradable blends. *J Appl Polym Sci* 2003;88(7):1775-1786.
39. Wang H, Djuricic AB, Chan WK, Xie MH. Factors affecting phase and height contrast of diblock copolymer PS-b-PEO thin films in dynamic force mode atomic force microscopy. *Appl Surf Sci* 2005;252(4):1092-1100.
40. Sahoo SK, Panyam J, Prabha S, Labhasetwar V. Residual polyvinyl alcohol associated with poly (D,L-lactide-co-glycolide) nanoparticles affects their physical properties and cellular uptake. *J Control Release* 2002;82(1):105-114.
41. Scholes PD, Coombes AG, Illum L, Davis SS, Watts JF, Ustariz C, Vert M, Davies MC. Detection and determination of surface levels of poloxamer and PVA surfactant on biodegradable nanospheres using SSIMS and XPS. *J Control Release* 1999;59(3):261-78.
42. Noh H, Vogler EA. Volumetric interpretation of protein adsorption: Mass and energy balance for albumin adsorption to particulate adsorbents with incrementally increasing hydrophilicity. *Biomaterials* 2006;27(34):5801-5812.
43. Nagahama K, Ohya Y, Ouchi T. Suppression of cell and platelet adhesion to star-shaped 8-armed poly(ethylene glycol)-poly(L-lactide) block copolymer films. *Macromol Biosci* 2006;6(6):412-419.
44. Prabha S, Labhasetwar V. Critical Determinants in PLGA/PLA Nanoparticle-Mediated Gene Expression. *Pharm Res* 2004;21(2):354.

45. Popielarski SR, Pun SH, Davis ME. A nanoparticle-based model delivery system to guide the rational design of gene delivery to the liver. 1. Synthesis and characterization. *Bioconjug Chem* 2005;16(5):1063-1070.
46. Roser M, Fischer D, Kissel T. Surface-modified biodegradable albumin nano- and microspheres. II: effect of surface charges on in vitro phagocytosis and biodistribution in rats. *Eur J Pharm Biopharm* 1998;46(3):255-263.
47. Prior S, Gander B, Blarer N, Merkle HP, Subira ML, Irache JM, Gamazo C. In vitro phagocytosis and monocyte-macrophage activation with poly(lactide) and poly(lactide-co-glycolide) microspheres. *Eur J Pharm Sci* 2002;15(2):197-207.
48. Panyam J, Labhasetwar V. Dynamics of endocytosis and exocytosis of poly(D,L-lactide-co-glycolide) nanoparticles in vascular smooth muscle cells. *Pharm Res* 2003;20(2):212-220.
49. Zastre J, Jackson J, Burt H. Evidence for modulation of P-glycoprotein-mediated efflux by methoxypolyethylene glycol-block-polycaprolactone amphiphilic diblock copolymers. *Pharm Res* 2004;21(8):1489-1497.
50. Ma ZS, Lim LY. Uptake of chitosan and associated insulin in Caco-2 cell monolayers: A comparison between chitosan molecules and chitosan nanoparticles. *Pharm Res* 2003;20(11):1812-1819.
51. Geiser M, Rothen-Rutishauser B, Kapp N, Schurch S, Kreyling W, Schulz H, Semmler M, Hof VI, Heyder J, Gehr P. Ultrafine particles cross cellular membranes by nonphagocytic mechanisms in lungs and in cultured cells. *Environmental Health Perspectives* 2005;113(11):1555-1560.
52. Mahmud A, Lavasanifar A. The effect of block copolymer structure on the internalization of polymeric micelles by human breast cancer cells. *Colloids Surf B Biointerfaces* 2005;45(2):82-89.

CHAPTER 6.

GENERAL DISCUSSION

Introduction

First part of this chapter will focus on the synthesis and characterization of biodegradable polymers. Feasibility of use of gas adsorption technique for analysis of micropores and effect of formulation factors, especially drug loading on the microporosity of formulated NPs will be discussed in the next section. Third section will discuss the impact of molecular architecture of polymer in deciding the microstructure of NPs and in turn, the release kinetics. Finally, this work will bring about the importance of a comprehensive study of various physicochemical surface properties in relation to their biological properties like protein resistance, macrophage uptake and its mechanism.

6.1 Synthesis and characterization of pegylated polymers

We have developed a rapid synthetic method with high yields for PLA grafted with allyl, hydroxy and carboxylic pendant functional groups in our laboratory [1]. Using this synthesis method, methoxyPEG was grafted on the hydrophobic PLA backbone at two different densities; 1 and 5 mole % of lactic acid monomer, referred henceforth as PEG_{1%}-g-PLA and PEG_{5%}-g-PLA, respectively. Multiblock copolymer, (PLA-PEG-PLA)_n was utilized as synthesized in our laboratory [2]. These polymers were characterized for their structural elucidation (¹H NMR), molecular weight and polydispersity by gel permeation chromatography (GPC) (Table 4.1, Fig. 4.1) and thermal properties (Differential scanning calorimetry, DSC) (Table 4.1, Fig. 4.2).

6.1.1 Chemical structure by ¹H NMR

Typical spectra were obtained with peaks at 5.2 ppm corresponding to the tertiary PLA proton, peak at 3.6 ppm for the protons of the repeating units in PEG chain, peak at 4.3 ppm for the PEG connecting unit to the PLA block, and peak at 1.5 ppm for the pendant methyl group of the PLA chain. For the multiblock copolymer, additional peak could be seen at around 2.7 ppm corresponding to the succinic acid moiety as reported earlier [2]. Actual PEG grafting percentage was close to the feed ratio as shown in Table 4.1. Also, as shown in fig. 4.1, peak intensity at 3.6 ppm increased with increase in PEG grafting density in case of grafted polymers, while multiblock copolymer showed highest PEG content

(17.8 % of lactic acid monomer) when calculated by the ratio of peak intensity at 3.6 ppm and 5.2 ppm. Also, synthesized polymers showed very narrow polydispersities as determined by GPC results.

6.1.2 Thermal properties by DSC

In addition to molar mass and polydispersity, thermal properties of polymers are influenced by their molecular structure. It was clearly seen that changing the percentage of grafting resulted in change in the thermal behavior of polymers. Also, block copolymer showed good phase mixing between PLA and PEG blocks with ability to form PEG microdomains rapidly on cooling (Fig. 4.2).

Thus, we could successfully synthesize pegylated polymers with different PEG concentrations and different polymer architectures (linear multiblock versus branched graft copolymer). Polymer architecture defines the shape of a single polymer molecule, which often determines its physicochemical properties [3]. As we see from DSC results, it is clear that addition of PEG at 5 mole% of lactic acid monomer, resulted in plasticization effect leading to decrease in T_g of the polymer. However, it should be noted that at very low grafting PEG concentration, effect of branching predominated with subsequent increase in T_g of the PEG_{1%}-g-PLA polymer. Although PEG_{5%}-g-PLA and (PLA-PEG-PLA)_n, both showed decrease in T_g suggesting improved phase mixing, they also exhibited PEG melting endotherm, further stressing the existence of crystalline PEG microdomains (Fig. 4.2). This has already been reported for polyanhydride copolymers of poly(1,3-bis-*p*-carboxyphenoxy propane-*co*-sebacic anhydride) [4]. When concentration of one of the block exceeds that of other, clear microphase separation could be observed, however, at equal concentration of both blocks, there was complete phase mixing. This type of phase mixing or phase separation has been reported for various polymer blends or copolymer films. However, it is questionable whether these phenomena would occur reproducibly during NP formation. If yes, how these polymer chains reorganize during the process of NP formation will further decide microstructure of the core as well as surface properties of these NPs.

6.2 NP preparation and impact of formulation factors on their microporosity

In this study, NPs were prepared using same polymer, PEG_{1%}-g-PLA and the Propafenone hydrochloride (Prop) as a model drug. The amount of triethylamine (TEA) added to solubilize hydrochloride salt and drug loading levels were varied.

6.2.1 Physicochemical properties of NPs

It can be clearly seen that monodispersed and smooth spherical particles in the size range of 178-192 nm were obtained by high-pressure homogenization technique (Table 3.1 and Fig. 3.1). There was no effect of the amount of TEA or drug loading on the size and morphology of these NPs, suggesting complete control of homogenization technique on their size. As reported by Kohori and co-workers [5], TEA successfully served the purpose of increasing the encapsulation efficiency of Prop. It was proposed that TEA scavenges hydrochloride of the salt, thus setting free more hydrophobic Prop base. This led to increased encapsulation of Prop base into PLA core, probably due to enhanced hydrophobic and/or ionic interactions between the carboxylic groups of PLA and amino groups of Prop. To further confirm this mechanism, free base generated using TEA was used for drug loading experiments. Increase in drug loading of base as compared to hydrochloride salt without use of TEA confirmed our hypothesis of hydrophobic and/or ionic interaction between the drug and polymer playing role in their encapsulation. It is clear that addition of 1:2 M TEA *in situ* was more effective in setting free the basic form of the drug than 1:1 M TEA, favoring its interaction with the polymer, thus further increasing its encapsulation efficiency (Table 3.1).

These results are further confirmed by thermal analysis of pure drug (both salt and basic forms), pure polymer, their physical mixtures and Prop-loaded NPs (Fig. 3.3). Retention of the melting endotherms (T_m) of the salt as well as base in both the physical mixtures is evident from DSC results. Although encapsulation of Prop in the NPs resulted in the disappearance of T_m , shift of T_g of the polymer towards higher temperatures clearly supported the interaction between the polymer and drug (Fig. 3.3). Indeed, DSC has been successfully used to study the interaction between the drug and the polymer [6, 7]. Okada and co-workers [6] have already suggested interaction between carboxylic acid residues of

PLA and amine groups of basic drug, resulting in increase in T_g of the formulated microspheres. They attributed this to the formation of rigid structures inside the matrix due to ionic interaction between the drug and polymer. Similarly, Miyajima et al reported increase in T_g of copoly(lactic/glycolic acid) after incorporation of basic drugs [7].

6.2.2 *In vitro* release kinetics

Although TEA increased the drug loading significantly, it did not have any apparent effect on drug release (Table 3.1, Fig. 3.5). On the other hand, initial drug loading affected both, the real loading inside the NPs as well as drug release kinetics (Table 3.1, Fig. 3.6). Higher drug loading resulted in slower drug release kinetics, irrespective of amount of TEA used. This could not be explained just based on the physicochemical properties of the NPs as all of them have been prepared from the same drug and the polymer as well as they showed comparable particle size distribution (178-192 nm; Table 3.1). Also, increased drug loading did not lead to any evidence of crystallization of Prop inside the polymeric matrix. In fact, DSC results confirmed amorphous or disordered crystalline phase of molecular dispersion of Prop inside NPs (Fig. 3.3). This implies that release kinetics is controlled by the drug diffusivity in the matrix.

The porous structure of a material is important in both natural phenomena and practical applications such as dissolution, adsorption and diffusion of drugs [8]. Lemaire et al [9] suggested that, during release, a drug molecule located inside a pore would naturally diffuse towards one of the end-points of the pore and eventually reach outside. If a drug molecule is present within the network of micro pores, it will have to diffuse towards the closest pore to be released outside. The movement of such molecule in the micropore network is highly restricted due to the limited space available and due to more important interaction between drug molecule present in the micropore and wall of micropore. Microporosity also hampers water flux inside such matrix affecting its hydration. Thus, in other words, the effective pore diffusion coefficient of drug in microporous network will be smaller than the diffusivity in a straight cylindrical/slit-like pore as a result of the random orientation of pores leading to longer diffusion path. This effective restricted diffusion coefficient of the drug in the porous media is a function of the diffusivity of drug, porosity (ϵ) and tortuosity (τ) of the matrix. The tortuosity in turn depends on the pore structure, pore size and shape distributions [10]. Thus, study of microstructure of NPs was undertaken

to see whether this porous microstructure was responsible for these differences in the release kinetics of Prop. To this end, we applied nitrogen gas adsorption technique to calculate BET surface area, total pore volume, pore size distribution (PSD) and microporosity. Microporosity was studied by Horvath-Kawazoe [11, 12] known as HK method. The HK method is based on slit-shaped pore model. Even though this pore model may not be appropriate for NPs, it was applied in this thesis accepting the limitation that it will still allow comparison between samples, since the analysis were carried out under identical conditions.

All the parameters, viz., BET surface area, total pore volume, PSD showed no significant difference for the formulations tested (Table 3.2). A closer look at microporosity of formulations prepared with different amounts of TEA revealed similar microporosity and drug release profiles even though they had different drug loading efficiencies (Fig. 3.4 & 3.5). Hence, TEA affected neither microporosity nor drug release. However, formulations prepared with same TEA but different initial drug loading clearly exhibited differences in their microporosities and subsequently, drug release profiles (Fig. 3.4 & 3.6). These results revealed that formulations having less microporosity (5_0 and $5_{1:2}$) always had higher release rate than those with higher microporosity (10_0 and $10_{1:2}$, respectively). Both these formulations with 10% initial loading had comparable encapsulation efficiencies, but higher real loading (% w/w) and higher microporosities (Table 3.2). So, question was asked if the real loading (amount of drug present in the matrix at $t = 0$) was responsible for determining the release kinetics. Indeed, formulations 5_0 and $5_{1:1}$ as well as 10_0 and $10_{1:1}$ showed no significant differences in real loading and consequently, drug release kinetics. However, it is worthwhile to note that formulations, $5_{1:2}$ and 10_0 or $10_{1:1}$ also showed comparable real drug loading, but different release kinetics. Why? Answer lies in their different microporosities (Fig 6.1). This strongly points out to the fact that real loading inside the matrix is not the actual factor determining the drug release rate. Thus, microporosity seems to be more important and predictable in determining release profiles than other factors. As previously discussed by Lemaire et al [9], more microporosity hindered the movement of drug and changed medium flux thereby reducing effective prop diffusion coefficient. This in turn slowed down the release phenomena.

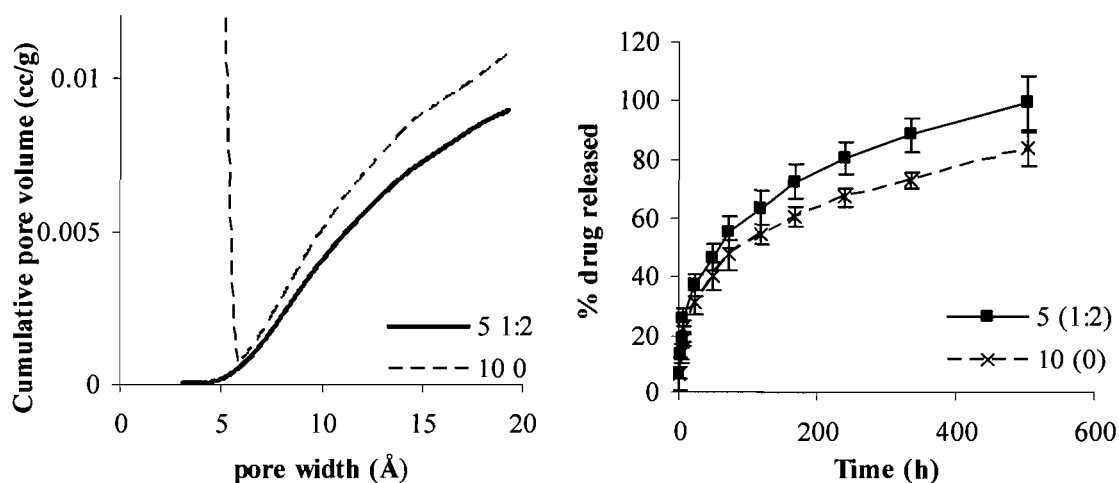


Figure 6.1. Microporosity determines the release; Formulations ($5_{1:2}$, 10_0) having same real loading (% w/w), but different microporosity resulted in different release kinetics; higher the microporosity (100), slower the release is.

In conclusion, these studies clearly supported the hypothesis that formulation factors affect the internal structure as well as microporosity, influencing drug release kinetics from NPs. Also, gas adsorption technique could be successfully used to probe into the microporosity of NPs.

6.3 Role of polymer architecture: Study on Blank NPs

As can be seen from the preceding discussion, formulation factors resulted in very marginal changes in the microporosities of prepared NPs. It was thought that this microporosity of NPs may be the result of cavities/void spaces between the same or different polymer chains created during the NP formation. Further, the question was asked if changes in the polymer architecture would be able to magnify such differences. In other words, it is quite possible that formulation factors considered in the previous study might not be able to create big differences in the polymer chain folding. However, if the basic molecular architecture is changed, it might create big differences in the free volume as well as wriggling of polymer chains and probably, microporous structure of their NPs. To confirm this hypothesis, homopolymer, PLA and its pegylated copolymers with different molecular architecture (graft or linear block copolymer) were used to prepare NPs. It was hypothesized that polymers would rearrange differently during NP formation depending on

their architecture, leading to change in the internal NP structure. Hence, blank NPs were prepared under identical formulation conditions to rule out any effect of drug loading or formulation factors on their internal structure.

Nitrogen adsorption studies revealed differences in the microporosity of these NPs (Fig. 4.4, Table 4.2). NPs of grafted polymer, PEG_{1%}-g-PLA showed highest nitrogen adsorption capacity, microporosity and BET surface area while that of multiblock copolymer, (PLA-PEG-PLA)_n showed the reverse trend (Fig. 4.4, Table 4.2). Changes in BET surface area have been suggested to be due to differences in the particle size, texture, structural differences, surface irregularities or presence of impurities [13]. Interestingly, all the NPs exhibited same particle size and size distribution. Thus, change in BET was attributed to the microporosity and structural differences in NPs as both these parameters followed the same trend.

To explain this, we proposed a model of polymer chain reorganization inside NPs (Fig. 4.6). PLA being hydrophobic will undergo precipitation and NP formation once the organic solvent is extracted into the external aqueous phase. When hydrophobic PLA and hydrophilic PEG chains coexist in the polymer structure, microphase separation is expected to take place depending on the concentration of each block and their molecular architecture [14, 15]. We proposed that it would be easy for PEG chains to migrate to the surface of NPs in case of grafted copolymer as hydrophobic PLA backbone can easily collapse in aqueous external phase leaving PEG on the external surface of emulsion droplet during NP formation. However, this phase separation would be difficult in case of multiblock copolymer because each PEG chain is covalently linked to two blocks of PLA. During NP formation, there would be competition between gelation of hydrophobic polymeric phase and microphase separation between PLA and PEG chains. Faster gelation will lead to some of the PEG chains being entrapped inside the hydrophobic domain, allowing only few PEG chains to be migrated at the external surface of NPs. This will result in NPs of both types with hydrophobic PLA core surrounded by hydrophilic PEG corona, except with different PEG conformation on the surface. In case of grafted polymer, NPs will have PEG with one end free to move (extended brush) whereas multiblock copolymer will result in mushroom conformation (Fig. 4.6). In addition, multiblock copolymer NPs will have hydrophilic core due to entrapment of some of the PEG chains inside the NPs. This hypothesis seems quite

logical as interpenetration of PEG inside the core would result in blocking of some of the pores reducing overall microporosity of these NPs as observed with multiblock copolymer NPs.

XPS results further supported this proposed model (Table 4.2). Multiblock copolymer NPs showed very less PEG surface concentration even though copolymer itself had higher PEG content compared to grafted copolymer. Thus, polymer architecture seems to have affected reorganization of polymer chains during NP formation leading to change in their microporous structure. It was further interesting to see how this would affect the drug release kinetics from NPs.

6.4 Release kinetics

6.4.1 Considering conventional factors in the literature

After addressing the role of polymer architecture in determining the microporosity of NPs, Prop-loaded NPs were prepared using PEG_{1%}-g-PLA and (PLA-PEG-PLA)_n. Drug release kinetics from these NPs was studied along with their microporosity. As discussed in the previous chapter, drug release mechanisms from polymeric NPs include diffusion or degradation or combination of both. The release profiles of Prop from grafted and multiblock copolymers exhibited an initial burst effect followed by slow and sustained release over 40 days. The release pattern showed good correlation coefficient ($R^2 \geq 0.99$) when fitted to Higuchi equation of diffusion. For grafted copolymer NPs, Higuchi equation was $Q = 5.33t + 20.62$, $r = 0.996$ and that for multiblock copolymer NPs was $Q = 8.48t + 28.94$, $r = 0.994$, where Q is the percent amount released in time t . The initial fast release (28% and 35% respectively for grafted and multiblock copolymer NPs) can be attributed to the prop adsorbed on or present near the surface, or even easily accessible to the bigger pores open at the surface. After this phase, the release was diffusion controlled.

Conventional factors affecting release discussed so far in the literature include particle size [16, 17], physical state of drug inside the matrix [18], porosity of the matrix [19, 20] etc. Both the nanoparticulate systems studied here showed monodispersed size distribution (Supporting information, Fig. S3, Chapter 4) and similar particle sizes viz. 205 ± 10 nm for PEG_{1%}-g-PLA and 211 ± 6 nm for (PLA-PEG-PLA)_n (Table 4.3). This

completely rules out any possible role played by size in determining the release kinetics. From DSC thermograms, T_g of blank NPs was found to be higher than respective polymers (Table 4.1 & 4.2). This seems logical as formation of NPs will lead to more rigid structure restricting the movement of polymer molecules. Prop incorporation inside PEG_{1%}-g-PLA NPs led to decrease in T_g compared to blank NPs suggesting plasticizer effect of drug. However, Prop-loaded NPs of (PLA-PEG-PLA)_n showed further increase in their T_g signifying formation of more rigid structure [6]. It is interesting that melting endotherm of Prop was absent in any of these NPs suggesting that Prop is molecularly dispersed or in the amorphous state in the NPs as discussed previously. It is evident from T_g values of prop-loaded PEG_{1%}-g-PLA and (PLA-PEG-PLA)_n NPs that the former has higher T_g than latter. This partly explains higher rate of release from (PLA-PEG-PLA)_n NPs. Indeed, Frank et al [21] have proved that the magnitude of diffusion coefficient of drug through PLA and PLGA polymers correlated inversely with the magnitude of measured T_g . Therefore, they suggested that polymeric system with lower T_g would exhibit increased release rates when the release is controlled solely by diffusion. This seems logical as lower T_g means increased plasticity, better hydration and hence, higher release kinetics [22].

Now coming to the overall porosity of the matrix, it was highly surprising that (PLA-PEG-PLA)_n NPs had lower total pore volume (0.048 cc/g ± 0.002) as against PEG_{1%}-g-PLA NPs (0.28 cc/g ± 0.002). Also, it is well known that specific surface area plays an important role in release kinetics. BET surface areas obtained from nitrogen gas adsorption for these Prop-loaded NPs were 3.79±0.62 and 20.4±1.10 m²/g for (PLA-PEG-PLA)_n and PEG_{1%}-g-PLA NPs respectively. These values were confirmed by krypton gas adsorption (Table 4.3). These results would suggest faster Prop release for PEG_{1%}-g-PLA NPs due to its higher BET and higher total pore volume which is contradictory to *in vitro* release results (Fig. 4.7).

6.4.2 Significance of microporosity

Given the fact that both these systems have similar size and size distribution (Supporting information, Fig. S3, Chapter 4), changes in the BET can be attributed to their structural and microporosity differences as discussed for blank NPs. It is clear from Fig. S2 (Supporting information, Chapter 4) that (PLA-PEG-PLA)_n exhibited much less microporosity than PEG_{1%}-g-PLA NPs. These studies again confirmed the results

corroborated in our first article (Chapter 3) that microporosity really plays an important role in drug release kinetics. Here, size of diffusing molecule like propafenone (16 Å as calculated from Chemoffice 8.0) is not at all negligible as compared to size of micropores, which more logically presents the distance between the closest polymer chains. Probably, prop molecules are entrapped / sandwiched between polymer chains during NP formation. Release of such drug outside NPs will then depend on its interaction with the pore wall as well as swelling and/or relaxation of polymer chains to create sufficient space for movement of drug molecules as suggested very recently by Zhao et al [23]. This will slow down the process of diffusion. Thus, higher microporosity will pose more restrictions for movement of drug through the aqueous channels reducing its effective diffusion coefficient and thus, the final rate of release [9].

6.4.3 Role of polymer chain organization

It is also important to think why higher total pore volume or higher surface area of PEG_{1%}-g-PLA NPs did not result in faster release from these NPs? As discussed before, higher BET surface area of PEG_{1%}-g-PLA NPs was a result of higher microporosity, which worked against faster release. As far as total pore volume is concerned, it should be remembered that nitrogen adsorption studies are carried out in the dry state. What will happen when both these systems are put in the aqueous system? Answer lies in the internal structure or polymer chain organization inside NPs. Going back to the hypothesis of polymer chain organization (Fig 4.6), (PLA-PEG-PLA)_n NPs have hydrophilic core due to PEG chain interpenetration. This resulted in pore blocking and reduced microporosity in dry state as seen by gas adsorption. However, PEG chains of these NPs would take up release medium efficiently when introduced in aqueous environment, reversing the pore blocking and in turn, creating more aqueous channels for diffusion of drug molecules. This would not be the case with PEG_{1%}-g-PLA NPs where the core is composed of hydrophobic PLA chains. The diffusion of drug through this system will then depend on the amount and accessibility of surface pores as well as restricted diffusion through the micropores. Thus, release kinetics also supports the hypothesis about chain organization or self-assembly of polymers during NP formation.

This research clearly indicated significance of the microporosity, internal structure and polymer self assembly for release properties of NPs. This would definitely serve as a

guideline for drug delivery of not only small molecule but also large molecules like proteins. Indeed, it has been suggested that high internal porosity is essential for release of high molecular weight proteins and also, control of internal morphology might be indispensable to adjust the release rates from any carrier [24]. In our opinion, preceding research in this dissertation has attempted to address this issue, pertaining more to the microporosity as well as internal morphology of NPs by gas adsorption technique. Further, it can not be any more assumed that higher surface area leads to faster drug release; in fact, the underlying cause of the increased surface area should always be taken into account before any such conclusion. Also, even if it is seen as drug-polymer interaction, and/or individual polymer or drug properties affecting the release kinetics, these macroscopic properties may lead to changes in microporosity at a molecular scale and finally, affect the drug release rate. Thus, by studying effect of other factors like molecular weight or solvent evaporation kinetics on microporosity, we can gain further insight into the molecular arrangement of polymer chains inside NPs and then, polymers can be tailor-made to achieve more precise drug release kinetics.

6.5 Characterization of surface properties and Cellular interaction of NPs

In the preceding section of this thesis, we have already seen the effect of polymer architecture on the internal structure and release properties of the NPs. It was further interesting to study how polymer architecture affected the surface properties and cellular interaction of NPs. Hence, systematic investigation was undertaken to study surface structure of NPs using various techniques like ^1H NMR, AFM and XPS. Also, efforts were made to correlate the results of surface characteristics with protein binding and cellular internalization capacity of these NPs.

6.5.1 Surface structure

6.5.1.1 ^1H NMR of NPs in D_2O

^1H NMR studies of NPs in D_2O showed presence of methylene protons of PEG chains at 3.7 ppm (Fig. 6.2). Signals from PLA methyl or methyne protons were absent.

This indicates that PLA protons are in solid environment and cannot be detected whereas PEG chains must be in mobile state. Similar results have been reported for PLA-PEG diblock NPs to confirm their core-shell structure [25]. Similarly, Breitenbach et al [26, 27] have found that NPs of comb polyesters of PVA-g-PLGA in water exhibited reduced signal intensity of the more hydrophobic PLGA chain compared to hydroxyl terminated end groups. They proposed that hydrophilic polymer parts are oriented towards the outer water phase during precipitation and NP hardening whereas the more lipophilic polyester residues form the inner core. Our results are in accordance with the above-cited references suggesting NPs made of PLA core and PEG corona. However, these studies are not quantitative to comment whether all the PEG chains constitute the corona.

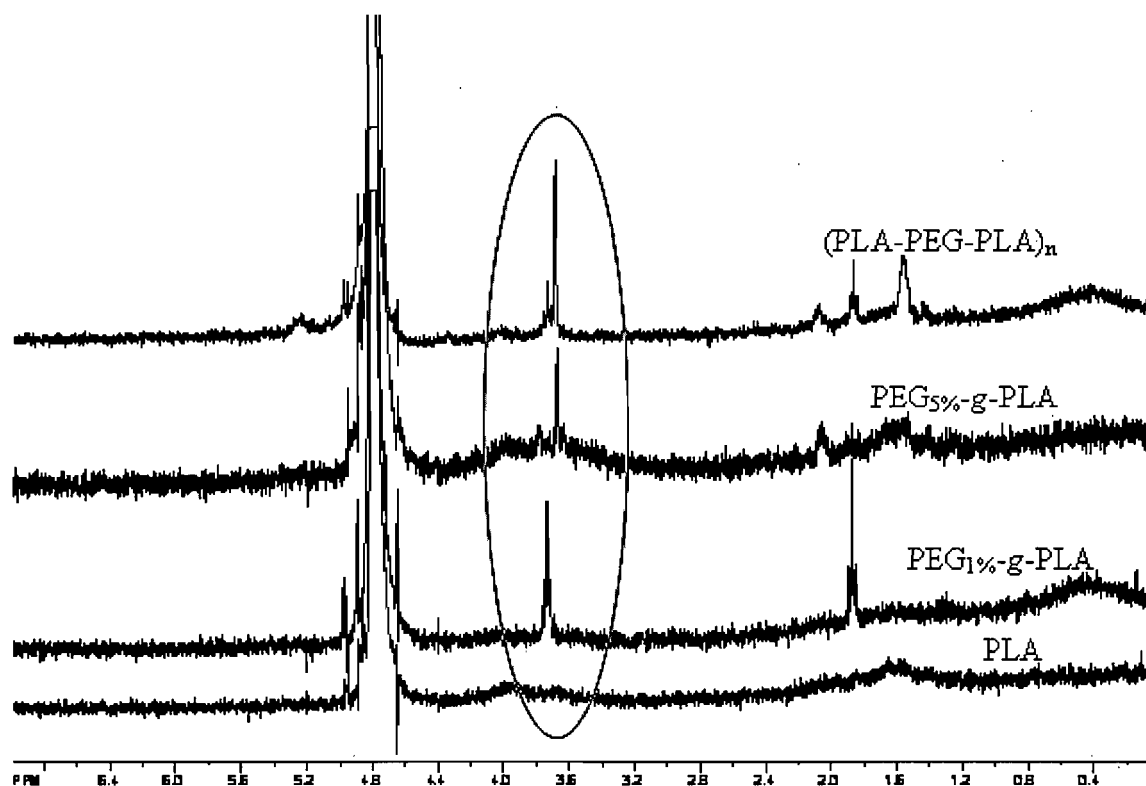


Figure 6.2. ^1H NMR of blank NPs of PLA, $\text{PEG}_{1\%}\text{-g-PLA}$, $\text{PEG}_{5\%}\text{-g-PLA}$, and $(\text{PLA-PEG-PLA})_n$ in D_2O . PEG peaks at 3.6 ppm are encircled.

6.5.1.2 AFM image analysis of NPs

Phase image AFM studies provided additional visual support to ^1H NMR studies. Two separate phases were clearly present in the phase images of pegylated NPs as against homogenous surface of PLA NPs (Fig. 5.2). This demonstrates presence of softer (dark regions in the phase) PEG segments on the surface of rigid (light regions in phase) PLA segments. This has been previously reported for polymer films [28], however, not for NPs to the best of our knowledge.

6.5.1.3 XPS analysis

Results of XPS brought forward some interesting results (Table 5.3). First of all, PVA was found associated with all the NPs as found by others [29, 30] and amount of adsorbed PVA decreased with increased surface PEG concentration [31]. Secondly, XPS results confirmed that PEG chains of multiblock copolymer penetrate inside the PLA core resulting in reduced surface PEG concentration. On the other hand, grafted copolymer NPs exhibited higher surface PEG concentration suggesting ease of PEG migration on the surface due to peculiar polymer architecture. This was consistent with the results of Rieger et al [32] who found higher surface PEG for grafted copolymer than diblock copolymer.

From the appearance of two additional peaks, XPS results also revealed the possibility of interaction between PLA-COOH and PVA-OH end groups in case of PLA homopolymer and grafted copolymers. This reaction was absent in multiblock copolymer $(\text{PLA-PEG-PLA})_n$ NPs, probably due to unavailability of end -COOH groups in this polymer structure. In our opinion, these results partly explain the failure of extensive washing procedures for removal of NP associated PVA and also effective zeta potential reduction of PLA NPs [29-31, 33, 34]. These results also emphasized that association of PVA with NPs may not be just due to the hydrophobic interaction between acetate group of PVA and hydrophobic polymer chains as suggested previously [29, 30].

6.5.2 Plasma protein binding

From the above surface structure studies, it was clear that grafted copolymers had more surface PEG concentration even though $(\text{PLA-PEG-PLA})_n$ had higher total PEG concentration (surface as well as core). Protein binding studies revealed trends in

accordance with these results. As a general rule, highly hydrophobic or poorly wettable surface adsorbs higher proteins [35]. Hence, PLA and (PLA-PEG-PLA)_n exhibited higher protein binding than grafted copolymer NPs (Fig. 5.3). This can again be attributed to polymer architecture as suggested by Nagahama et al [36] where they found 8-armed copolymer structure more protein resistant than its linear copolymer. Similar results have been reported by Rieger et al [32] for grafted and diblock copolymers of PCL and PEG; where grafted copolymers adsorbed less proteins.

6.5.3 Cellular uptake studies

Uptake of all NPs in RAW 264.7 cells was concentration and temperature dependent (Fig. 5.5) as shown earlier for poly(lactide-co-glycolide) NPs [37]. Further, differences in their uptake can be explained based on the surface characteristics. In general, adsorbed PVA reduced internalization of PLA NPs as reported previously [29, 38] either due to masking the surface charge or rendering the surface more hydrophilic. Interestingly, among the pegylated NPs, multiblock copolymer NPs showed highest uptake which can be attributed to reduced surface PEG concentration (and hence, more surface hydrophobicity) as seen by XPS. Indeed, there are various reports in the literature signifying role of surface charge and hydrophobicity in the cellular uptake of particles [39-42].

Further mechanistic evaluation of cellular uptake revealed active, fluid phase and clathrin- dependent endocytosis for all NPs. Their uptake was significantly inhibited by sodium azide (metabolic inhibitor), hyperosmotic sucrose (fluid phase endocytosis inhibitor) and chlorpromazine (reduces clathrin-coated pits) (Fig. 5.6). Cytochalasin B, inhibitor of actin polymerization in macropinocytosis affected uptake of only PEG_{1%}-g-PLA NPs. The exact reason for this discrepancy could not be explained. In fact, Mahmud et al [43] have found similar inconsistency in PEO-*b*-PCL micelles prepared with varying length of two blocks, which they ascribed to the different core-shell structure. Further studies are needed to explore the exact reason of this effect.

Thus, this systematic and complete investigation proved that polymer architecture plays a definite role in determining the surface chemistry of formulated NPs. Further, these surface properties are critical in deciding protein binding and cellular uptake

of NPs, which in turn will determine their *in vivo* stability and biodistribution and therapeutic success.

6.6 References

1. Nadeau V, Leclair G, Sant S, Rabanel J-M, Quesnel R, Hildgen P. Synthesis of new versatile functionalized polyesters for biomedical applications. *Polymer* 2005;46:11263-11272.
2. Quesnel R, Hildgen P. Synthesis of PLA-b-PEG multiblock copolymers for stealth drug carrier preparation. *Molecules* 2005;10:98-104.
3. Qiu LY, Bae YH. Polymer architecture and drug delivery. *Pharm Res* 2006;23:1-30.
4. Shen E, Pizszczek R, Dziadul B, Narasimhan B. Microphase separation in bioerodible copolymers for drug delivery. *Biomaterials* 2001;22:201-210.
5. Kohori F, Yokoyama M, Sakai K, Okano T. Process design for efficient and controlled drug incorporation into polymeric micelle carrier systems. *J Control Release* 2002;78:155-163.
6. Okada H, Doken Y, Ogawa Y, Toguchi H. Preparation of three-month depot injectable microspheres of leuporelin acetate using biodegradable polymers. *Pharm Res* 1994;11:1143-1147.
7. Miyajima M, Koshika A, Okada J, Kusai A, Ikeda M. The effects of drug physico-chemical properties on release from copoly (lactic/glycolic acid) matrix. *Int J Pharm* 1998;169:255-263.
8. Mehta KA, Kislalioglu MS, Phuapradit W, Malick AW, Shah NH. Effect of formulation and process variables on porosity parameters and release rates from a multi unit erosion matrix of a poorly soluble drug. *J Control Release* 2000;63:201-211.
9. Lemaire V, Belair J, Hildgen P. Structural modeling of drug release from biodegradable porous matrices based on a combined diffusion/erosion process. *Int J Pharm* 2003;258:95-107.
10. Veith SR, Hughes E, Vuataz G, Pratsinis SE. Restricted diffusion in silica particles measured by pulsed field gradient NMR. *J Colloid Interface Sci* 2004;274:216-228.
11. Horvath G, Kawazoe K. Method for the calculation of effective pore size distribution in molecular sieve carbon. *J Chem Eng Japan* 1983;16:470-475.

12. Dombrowski RJ, Lastoskie CM, Hyduke DR. The Horvath-Kawazoe method revisited. *Colloid Surf A Physicochem Eng Asp* 2001;187:23-39.
13. Cejka J, Zilkova N, Rathousky J, Zukal A, Jagiello J. High-resolution adsorption of nitrogen on mesoporous alumina. *Langmuir* 2004;20:7532-7539.
14. Shin D, Shin K, Aamer KA, Tew GN, Russell TP, Lee JH, et al. A morphological study of a semicrystalline poly(L-lactic acid-b-ethylene oxide-b-L-lactic acid) triblock copolymer. *Macromolecules* 2005;38:104-109.
15. Wang S, Cui W, Bei J. Bulk and surface modifications of polylactide. *Anal Bioanal Chem* 2005;381:547-556.
16. Gorner T, Gref R, Michenot D, Sommer F, Tran MN, Dellacherie E. Lidocaine-loaded biodegradable nanospheres. I. Optimization Of the drug incorporation into the polymer matrix. *J Control Release* 1999;57:259-268.
17. Chorny M, Fishbein I, Danenberg HD, Golomb G. Lipophilic drug loaded nanospheres prepared by nanoprecipitation: effect of formulation variables on size, drug recovery and release kinetics. *J Control Release* 2002;83:389-400.
18. Sant S, Nadeau V, Hildgen P. Effect of porosity on the release kinetics of propafenone-loaded PEG-g-PLA nanoparticles. *J Control Release* 2005;107:203-214.
19. Petrov O, Furo I, Schuleit M, Domanig R, Plunkett M, Daicic J. Pore size distributions of biodegradable polymer microparticles in aqueous environments measured by NMR cryoporometry. *Int J Pharm* 2006;309:157-162.
20. Yang Y-Y, Chung T-S, Bai X-L, Chan W-K. Effect of preparation conditions on morphology and release profiles of biodegradable polymeric microspheres containing protein fabricated by double-emulsion method. *Chem Eng Sci* 2000;55:2223-2236.
21. Frank A, Rath SK, Venkatraman SS. Controlled release from bioerodible polymers: effect of drug type and polymer composition. *J Control Release* 2005;102:333-344.
22. Dailey LA. The role of branched polyesters and their modifications in the development of modern drug delivery vehicles. *J Control Release* 2005;101:137-149.
23. Zhao ZJ, Wang Q, Zhang L, Liu YC. A different diffusion mechanism for drug molecules in amorphous polymers. *J Phys Chem B* 2007;111:4411-4416.

24. Ruan G, Feng SS, Li QT. Effects of material hydrophobicity on physical properties of polymeric microspheres formed by double emulsion process. *J Control Release* 2002;84:151-160.
25. Riley T, Stolnik S, Heald CR, Xiong CD, Garnett MC, Illum L, et al. Physicochemical evaluation of nanoparticles assembled from poly(lactic acid)-poly(ethylene glycol) (PLA-PEG) block copolymers as drug delivery vehicles. *Langmuir* 2001;17:3168-3174.
26. Jung T, Breitenbach A, Kissel T. Sulfobutylated poly(vinyl alcohol)-graft-poly(lactide-co-glycolide)s facilitate the preparation of small negatively charged biodegradable nanospheres. *J Control Release* 2000;67:157-169.
27. Kim Y, Pyun J, Frechet JMJ, Hawker CJ, Frank CW. The dramatic effect of architecture on the self-assembly of block copolymers at interfaces. *Langmuir* 2005;21:10444-10458.
28. Wang H, Djurisic AB, Chan WK, Xie MH. Factors affecting phase and height contrast of diblock copolymer PS-b-PEO thin films in dynamic force mode atomic force microscopy. *Appl Surf Sci* 2005;252:1092-1100.
29. Sahoo SK, Panyam J, Prabha S, Labhasetwar V. Residual polyvinyl alcohol associated with poly (D,L-lactide-co-glycolide) nanoparticles affects their physical properties and cellular uptake. *J Control Release* 2002;82:105-114.
30. Scholes PD, Coombes AG, Illum L, Davis SS, Watts JF, Ustariz C, et al. Detection and determination of surface levels of poloxamer and PVA surfactant on biodegradable nanospheres using SSIMS and XPS. *J Control Release* 1999;59:261-278.
31. Shakesheff KM, Evora C, Soriano I, Langer R. The Adsorption of Poly(vinyl alcohol) to Biodegradable Microparticles Studied by X-Ray Photoelectron Spectroscopy (XPS). *J Colloid Interface Sci* 1997;185:538.
32. Rieger J, Passirani C, Benoit JP, Van Butsele K, Jerome R, Jerome C. Synthesis of amphiphilic copolymers of poly(ethylene oxide) and poly(epsilon-caprolactone) with different architectures, and their role in the preparation of stealthy nanoparticles. *Adv Funct Mater* 2006;16:1506-1514.
33. Mu L, Feng SS. Vitamin E TPGS used as emulsifier in the solvent evaporation/extraction technique for fabrication of polymeric nanospheres for controlled release of paclitaxel (Taxol). *J Control Release* 2002;80:129-144.

34. Zambaux MF, Bonneaux F, Gref R, Maincent P, Dellacherie E, Alonso MJ, et al. Influence of experimental parameters on the characteristics of poly(lactic acid) nanoparticles prepared by a double emulsion method. *J Control Release* 1998;50:31-40.
35. Noh H, Vogler EA. Volumetric interpretation of protein adsorption: Mass and energy balance for albumin adsorption to particulate adsorbents with incrementally increasing hydrophilicity. *Biomaterials* 2006;27:5801-5812.
36. Nagahama K, Ohya Y, Ouchi T. Suppression of cell and platelet adhesion to star-shaped 8-armed poly(ethylene glycol)-poly(L-lactide) block copolymer films. *Macromol Biosci* 2006;6:412-419.
37. Panyam J, Labhasetwar V. Dynamics of endocytosis and exocytosis of poly(D,L-lactide-co-glycolide) nanoparticles in vascular smooth muscle cells. *Pharm Res* 2003;20:212-220.
38. Prabha S, Labhasetwar V. Critical Determinants in PLGA/PLA Nanoparticle-Mediated Gene Expression. *Pharm Res* 2004;21:354.
39. Roser M, Fischer D, Kissel T. Surface-modified biodegradable albumin nano- and microspheres. II: effect of surface charges on in vitro phagocytosis and biodistribution in rats. *Eur J Pharm Biopharm* 1998;46:255-263.
40. Prior S, Gander B, Blarer N, Merkle HP, Subira ML, Irache JM, et al. In vitro phagocytosis and monocyte-macrophage activation with poly(lactide) and poly(lactide-co-glycolide) microspheres. *Eur J Pharm Sci* 2002;15:197-207.
41. Popielarski SR, Pun SH, Davis ME. A nanoparticle-based model delivery system to guide the rational design of gene delivery to the liver. 1. Synthesis and characterization. *Bioconj Chem* 2005;16:1063-1070.
42. Fang C, Shi B, Pei YY, Hong MH, Wu J, Chen HZ. In vivo tumor targeting of tumor necrosis factor-alpha-loaded stealth nanoparticles: Effect of MePEG molecular weight and particle size. *Eur J Pharm Sci* 2006;27:27-36.
43. Mahmud A, Lavasanifar A. The effect of block copolymer structure on the internalization of polymeric micelles by human breast cancer cells. *Colloids Surf B Biointerfaces* 2005;45:82-89.

CHAPTER 7.
CONCLUSION

Conclusion

Although introduction of nanotechnology obviously permitted to step over numerous milestones towards the development of the “magic bullet”, there are unresolved delivery problems to be still addressed. For instance, with the advent of versatile nanoscale delivery approaches like nanoparticles, micelles and dendrimers, various polymeric architectures are being synthesized for controlled drug delivery applications. Such large number of newly synthesized polymers brings a new problem of quickly selecting a suitable polymer for a specified drug as its controlled release material. Although drug release properties of nanoscale drug delivery systems have been studied in the past as a function of various formulation parameters, the experiments in this field has addressed only the macroscopic behavior of drug release. A paradigm shift of current research from ‘micro’ to ‘nano’ scale needs more information on the molecular level diffusion mechanisms of drug molecules in polymer matrix. This thesis is an endeavor to probe into such mechanisms by correlating differences in microporosity to the drug release kinetics and surface properties of polymeric nanoparticles.

This thesis first puts forward following hypotheses:

1. Polymer architecture markedly influences polymer chains reorganization in the bulk of NPs, thus deciding the internal structure as well as surface properties of NPs.
2. Microporosity plays vital role in determining the drug release kinetics from polymeric NPs.
3. Polymer architecture also affects surface properties of NPs, thus determining their protein resistance as well as cellular interaction abilities. This in turn, will determine their *in vivo* stability and therapeutic efficacy as drug delivery systems.

The importance of microporosity and internal structure of these nanosized polymeric particles has always been overlooked in the past. The first study reported herein proposes use of gas adsorption for unraveling microstructure and mechanism of drug

release kinetics of nanoparticles at molecular scale. Investigations undertaken thereafter with different polymer architectures confirm the results obtained in the first study with PEG_{1%}-g-PLA NPs, and also support the importance of microporosity in determining drug release kinetics. Not only this, both these studies clearly question the universally accepted common notion that increased specific surface area leads to enhanced drug release kinetics. It urges scientists to reconsider the reason of this increase in specific surface area before drawing any such conclusion. Higher microporosity can be one of the reasons contributing to higher surface area. It reduces effective diffusion coefficient of drug in the polymer matrix, decreasing its release rate as in case of PEG_{1%}-g-PLA NPs.

According to best of our knowledge, polymer chain organization inside the polymeric nanoparticles has been studied for the first time and validated successfully using gas adsorption technique as well as other surface analysis techniques like XPS. This also demonstrated the importance of polymer architecture on the chain arrangement inside NPs. Polymer chain arrangement affected not only the internal structure of the NPs but also their surface properties. Multiblock copolymer NPs resulted in hydrophilic internal core due to PEG entrapment inside PLA core. This led to lower glass transition temperature of multiblock copolymer NPs as compared to other NPs and faster drug release kinetics. At the same time, PEG entrapment inside the core of multiblock copolymer NPs resulted in less PEG surface density. This affected their surface properties leading to enhanced protein binding and endocytic uptake by macrophages. On the contrary, chemistry of grafted copolymers allowed most of PEG chains to easily migrate to surface covering more NP surface despite of low initial PEG content in the polymers. This resulted in higher PEG surface density leading to low protein binding and less macrophage uptake.

This dissertation also brings about some of the novel aspects of pegylated NPs in the course of various studies. For instance, direct visible evidence of presence of PEG on the surface of NPs has not been provided till date, despite of lot of work in the area of pegylated systems. This is due to the difficulty in imaging such small size particles and probably, the damage caused to the NPs leading to their deformation. However, we successfully used tapping mode AFM phase image analysis of NP surface by carefully controlling set point ratio. Pegylated NPs clearly showed presence of PEG on the surface of NPs. Although this data can be regarded as more qualitative than quantitative, clear phase

separation between rigid PLA domains and soft PEG domains on the surface of NPs was reported for the first time through these studies.

Another point brought to notice in this dissertation is the mechanism of PVA adsorption on PLA NPs. Till now, it has been reported that vinyl acetate segment interpenetrated PLA/PLGA core through hydrophobic interactions/hydrogen bonding and hence, it was difficult to completely remove surface adsorbed PVA. However, from XPS results reported here, we strongly suggest possibility of chemical interaction between PLA –COOH end groups and PVA –OH groups. It seems logical to assume that such a chemical reaction would hamper any attempt of complete removal of adsorbed PVA from surface of NPs even after several washings.

All the hypotheses put forward have been successfully converted into results through systematic design of various experiments. Nonetheless, in our opinion, this work has opened a completely new avenue of fine-tuning polymer architecture to get the desired pharmaceutical and targeting properties of nanoscale drug delivery systems. Very small size of such delivery systems urges us to probe at the molecular level. The importance of studying molecular drug diffusion mechanisms in polymer matrix is clearly evident by the work done on microporosity of nanoparticles in this thesis. There are many questions which are generated from this work and need to be answered. For instance, effect of various formulation factors like method of NP preparation, rate of solvent evaporation, ratio of external to internal phase of emulsion, effect of different drugs on the microporosity of given polymeric system will shed more light on their internal structure and release kinetics. Although this study shows definite polymer chain rearrangement inside NPs, various diverse and novel polymeric architectures such as dendrimers, star block copolymers, stimuli-responsive polymers should be studied to gain more insight into polymer self assembly. Such studies will also provide in-depth understanding of the factors to control bulk and surface orientation of polymeric nanostructures precisely, thus controlling both their release as well as site-specific intracellular delivery. Once such fine control is achieved, the dream of converting these smart drug delivery systems into “magic bullets” will soon turn into a reality!

ANNEX-I
CURRICULUM VITAE

Sant Shilpa

Montreal, Quebec,

E-mail address

Status in Canada: Citizen

Languages spoken: bilingual

Educational qualification

M. Pharm.: Bombay College of Pharmacy, India; August 1997 to June 1999

Dissertation: Optimization and characterization of pentoxifylline-loaded niosomal formulation and their *in vivo* efficacy

Scholarships, Fellowships and Awards

1. Post-doctoral fellowship, FQRNT, Quebec, Canada, Jan 2008- 2010
2. Post-Graduate Scholarship, NSERC, University of Montréal, May 2005-April 2007
3. Recipient of grant for presenting the poster at 33rd International symposium of Controlled Release of Bioactive Materials, 2006, Vienna, Austria
4. Recipient of Travel fellowship for presenting the poster at 3rd International Nanomedicine and Drug Delivery Symposium, USA, 2005
5. Bourse de Recruitment, University of Montréal, Canada, Feb 2003 –December 2003
6. Bourse d'excellence, University of Montréal, Canada, for 2002 and 2003
7. Bourse de Maternité, University of Montréal, Canada, May 2003

Experience

Research: Since 1998-till date

1. Formulation and *in vitro* characterization of particulate delivery systems
2. Synthesis and characterization of biodegradable polyester-based polymers
3. Hands on *Epifluorescence & Confocal* microscopy (Cells) and AFM (polymers and particles)
4. Well-versed with cell culture and PAGE electrophoresis
5. Confident in Animal handling
6. Multidisciplinary experience in various fields like *polymer chemistry, particle physics* (microporosity by gas adsorption), *material science and technology, physical chemistry, molecular and cellular biology and drug targeting*

Academic: Since 1999-Winter 2007

1. **Lecturer:** Bharati Vidyapeeth College of Pharmacy, Navi Mumbai, India; July 1999 to May 2000. Conducted theory and practical courses for undergraduate students in **Anatomy, Physiology and Health Education, Pharmacology, Biopharmaceutics and pharmacokinetics**, and evaluate their performance
2. **Teaching Assistant:**
 1. University of Montréal, Montréal, Quebec, May 2005-till date
 - Supervised and guided 2 apprentice for 2 different research projects
 - Worked as lab demonstrator for Galenic II practicals, Evaluated undergraduate students for the course of Physical chemistry, Medicinal chemistry
 2. C. U. Shah College of Pharmacy, SNTD Women's university, Bombay, India
 - Given the course on 'Sutures and Ligatures' to graduate students

3. Bombay College of Pharmacy, India; August 1998 to March 1999
 - Worked as a teaching assistant for undergraduate pharmacology laboratories

SYNOPSIS OF PUBLICATIONS

No.	No. of publications	Type of publications
A	5	Articles in refereed journals
B	2	Accepted Manuscripts
C	1	Manuscripts in preparation
D	8	Refereed Symposium abstracts published
E	4	Refereed conference presentations
F	1	Podium presentation
G	1	Book Chapter

Publications

1. **Sant S.**, and Thommes, M. and Hildgen P., (2007), Drug release kinetics and microporous structure of polymeric nanoparticles, manuscript received for minor revision, **Langmuir**
2. **Sant S.**, Poulin, S. and Hildgen P., (2007), Effect of polymer chemistry of pegylated nanoparticles on their surface properties, plasma protein adsorption and cellular interactions, manuscript accepted with minor revision, **J Biomed Mater Res A**
3. **Sant S.**, and Hildgen P., (2007), Nuclear targeting potential of doxorubicin nanoparticles of pegylated polymers of different architectures, **manuscript in preparation**
4. Véronique Nadeau, Jean-Michel Rabanel, **Shilpa Sant**, Roula Chahwan, Sophie-Dorothée Clas and Patrice Hildgen, Synthesis and characterization of biodegradable and charged salen-based polymers, **J. Appl. Polymer Sci.**, 2006, 102 (3), 2568-2577.
5. **Sant S.**, Nadeau, V. and Hildgen P., Effect of Porosity on the Release Kinetics of Propafenone-loaded PEG-g-PLA Nanoparticles, **J Control Release**, 2005, 107(2): 203-214.
6. Nadeau, V., Leclair, G., **Sant, S.**, Rabanel J-M., Quesnel R., and Hildgen P., Synthesis of new versatile functionalized polyesters for biomedical applications, **Polymer**, 2005, 46(25): 11263-11272.
7. **S. Y. Gaikwad**, A. G. Jagtap, A. D. Ingle, S. G. A. Rao, R. P. Gude, Antimetastatic Activity of Niosomal Pentoxifylline and Its Combination with Activated Macrophages in Murine B16F10 Melanoma Model, **Cancer Biotherapy and Radiopharmaceuticals**, 2000, 15 (6), 605-615.
8. Jagtap, A. G. and **Gaikwad S. Y.**, Applications of Genomic Pharmacology in Cancer Treatment, **Indian Drugs**, 2000, 37 (1), 22.

Book Chapter

Jean-Michel Rabanel, Nicolas Bertrand, **Shilpa Sant**, Salma Louati and Patrice Hildgen, "Polysaccharide Hydrogels for the Preparation of Immunoisolated Cell

Delivery Systems” In: **Polysacchararides for drug delivery and pharmaceutical applications**, Robert H. Marchessault, François Raveneelle And Xiao Xia Zhu Eds., American Chemical Society, Washington, ACS Symposium series no. 934, , 2006, pp. 305-339.

Presentations

Podium: 1

1. **Sant, S.** and Hildgen, P., (2006) In “Biological Challenges” session; 33rd International Symposium on Controlled Release of Bioactive Materials, Austria,

Posters: 12

1. **Sant, S.** and Hildgen, P., (2006) 33rd International Symposium on Controlled Release of Bioactive Materials, Vienna, Austria, abstract no. 958, ***Grant winner***.
2. **Sant, S.** and Hildgen, P., (2006) 33rd International Symposium on Controlled Release of Bioactive Materials, Vienna, Austria, Abstract no. 214.
3. **Sant, S.** and Hildgen, P., (2006) 33rd International Symposium on Controlled Release of Bioactive Materials, Vienna, Austria, Abstract no.969.
4. **Sant, S.** and Hildgen, P., (2005) 3rd International Nanomedicine and Drug Delivery Symposium, organized by Controlled Release Society, Baltimore, ***Awarded Travel grant***
5. **Sant, S.** and Hildgen, P., (2005) Pharmaceutical Sciences Fair & Exhibition, 2005, Nice, France.
6. **S. Sant**, Hildgen P., (2004) American Association of Pharmaceutical Scientists, Baltimore, USA, Abstract no. T2148.
7. **Shilpa Sant**, Patrice Hildgen, (2004) 2nd World Congress of the board of Pharmaceutical Sciences of FIP, Kyoto, Japan, Abstract no. P3A-IV-030.
8. T. Hammady, **S. Sant** and P. Hildgen, (2003) 30th International Symposium on Controlled Release of Bioactive Materials, Glasgow, England, Abstract no. 582.
9. **Shilpa Sant**, K. K. Singh, Sukhjeet Singh and Amarjit Singh, (2002), 9th International Symposium on Controlled Release of Bioactive Materials, Seoul, Korea, Abstract no. 298.
10. **Shilpa Sant**, K. K. Singh, Sukhjeet Singh and Amarjit Singh, (2002) 4th International symposium on Advances in Technology and Business Potential of New Drug Delivery Systems, Controlled Release Society-Indian Local Chapter at Mumbai, India.
11. **Shilpa Sant**, K. K. Singh, Sukhjeet Singh and Amarjit Singh (2001) 53rd Indian Pharmaceutical Congress, Delhi, India.
12. **S. Y. Gaikwad**, A. G. Jagtap, A. D. Ingle, S. G. A. Rao and R. P. Gude (1998) 50th Indian Pharmaceutical Congress, Mumbai, India.